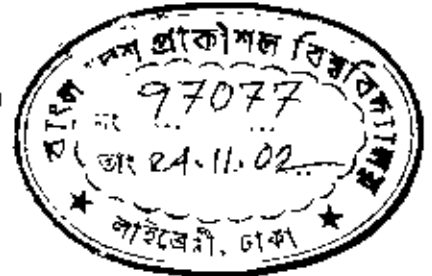




# DEVELOPMENT AND STUDY OF NANOCRYSTALLINE SOFT MAGNETIC MATERIAL

MD. SULTAN MAHMUD



A DISSERTATION SUBMITTED TO THE DEPARTMENT OF PHYSICS,  
BANGLADESH UNIVERSITY OF ENGINEERING AND TECHNOLOGY, DHAKA  
IN PARTIAL FULFILMENT FOR THE DEGREE OF  
MASTER OF PHILOSOPHY

DEPARTMENT OF PHYSICS  
BANGLADESH UNIVERSITY OF ENGINEERING AND TECHNOLOGY  
DHAKA-1000, BANGLADESH

OCTOBER 2002



#97077#

**BANGLADESH UNIVERSITY OF ENGINEERING AND TECHNOLOGY**

**DEPARTMENT OF PHYSICS, DHAKA-1000, BANGLADESH**

**CERTIFICATION OF THESIS**

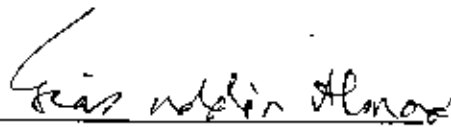
The Thesis titled *Development and Study of Nanocrystalline Soft Magnetic Material* submitted by Md. Sultan Mahmud, Roll No. 040014014F, Session April 2000, has been accepted as satisfactory in partial fulfillment of the requirement for the degree of Master of Philosophy on October 30, 2002.

**Board of Examiners**

1 Prof. M. Ali Asgar (Supervisor)  
Professor  
Department of Physics, BUET, Dhaka

  
Chairman

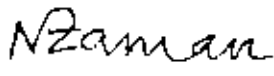
2 Dr. Gias Uddin Ahmad  
Professor  
Department of Physics, BUET, Dhaka

  
Member

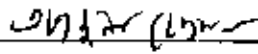
3 Dr. Md. Feroz Alam Khan  
Associate Professor  
Department of Physics, BUET, Dhaka

  
Member

4 Dr. Nazma Zaman  
Professor & Head  
Department of Physics, BUET, Dhaka

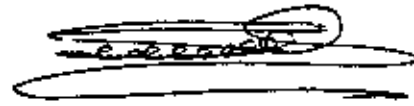
  
Member  
(Ex-Officio)

5 Dr. Tafazzal Hussain  
Professor  
Department of Physics  
Dhaka University, Dhaka

  
Member  
(External)

# CANDIDATE'S DECLARATION

It is hereby declared that this thesis or any part of it has not been submitted elsewhere for the award of any degree or diploma.

A handwritten signature in black ink, appearing to read 'Md. Sultan Mahmud', is written over a horizontal line. The signature is somewhat stylized and includes a large loop at the end.

(Md. Sultan Mahmud)

*To*  
*My Beloved Daughter*  
*Faria Mahmud.*

# Table of Contents

Table of Contents	v
List of Figures	vii
Abstract	ix
Acknowledgements	x
<b>1 INTRODUCTION</b>	
1.1 Introduction	1
1.2 Organization of the Work	3
<b>2 PREPARATION OF NANOCRYSTALLINE AMORPHOUS SOFT MAGNETIC MATERIALS BY RAPID QUENCHING METHOD</b>	
2.1 An Overview of Nanocrystalline Materials	5
2.2 Properties of Nanocrystals as Determined by Preparation Techniques	8
2.3 Viscosity Condition for the Formation of Metallic Glass	9
2.4 Conditions Necessary for Preparing Nanocrystalline Materials	9
2.5 Preparation Technique of Amorphous Materials	10
2.5.1 The Atomic Deposition Method	10
2.5.2 The Fast Cooling of The Melt	11
2.5.3 Rapid Quenching Method:	12
2.6 Experimental Details of the Preparation of Amorphous Ribbons	14
2.7 Important Factors to Control the Thickness of Ribbons	14
2.8 Examining the Amorphousity of the Nanocrystalline Materials	15
<b>3 THEORETICAL ASPECTS</b>	
3.1 Stability of Amorphous Alloys	18
3.2 Transition-Metal Based Alloys	19
3.3 Theories of Permeability	21
3.3.1 Initial Permeability of Nanocrystalline Soft Magnetic Materials	22
3.4 Magnetization of the Amorphous Ribbons	25
3.4.1 Low Temperature Behaviour of $M_s$ of Amorphous Ribbons:	26

3.4.2	High Temperature Behaviour of $M_s$ of Amorphous Ribbons: . . . . .	27
-------	---	----

#### 4 EXPERIMENTAL DETAILS

4.1	The Differential Thermal Analysis . . . . .	29
4.1.1	Introduction . . . . .	30
4.1.2	The Principle of Differential Thermal Analysis . . . . .	30
4.1.3	Apparatus . . . . .	32
4.2	Experimental Determination of Complex Permeability . . . . .	36
4.2.1	Real and Imaginary Components of Complex Permeability . . . . .	36
4.2.2	Preparation of the Samples for Complex Permeability . . . . .	36
4.2.3	Frequency Characteristics of Nanocrystalline Materials . . . . .	37
4.3	Experimental Setup for Measurements of Magnetization . . . . .	38
4.3.1	The Principles of Vibrating Sample Magnetometer (V.S.M) . . . . .	38
4.3.2	Mechanical Design of the V.S.M. . . . .	39
4.3.3	Electronic Circuits of the V.S.M. . . . .	42
4.3.4	Calibration of the V.S.M. . . . .	45
4.3.5	High Temperature Magnetization Measurements . . . . .	48

#### 5 RESULTS AND DISCUSSIONS

5.1	Differential Thermal Analysis (DTA) Results . . . . .	50
5.1.1	Differential Thermal Analysis (DTA) of Nanocrystalline Samples . . . . .	51
5.2	Specific Magnetization Measurement of Nanocrystalline Amorphous Ribbons . . . . .	55
5.2.1	Field Dependence of specific magnetization at room temperature . . . . .	55
5.2.2	Temperature Dependence of Magnetization of Nanocrystalline Amorphous Ribbons . . . . .	56
5.3	Dynamic Magnetic Properties of Nanocrystalline Amorphous Magnetic Materials . . . . .	60
5.3.1	Frequency Dependence of the Real Part of Complex Permeability of composition of $(Fe_{0.9}Co_{0.1})_{73.5}Cu_1Nb_3Si_{13.5}B_9$ with Different Annealing Temperature and Annealing Time . . . . .	63
5.3.2	Frequency dependence of the Real Part of Complex Permeability of composition of $Fe_{74}Cu_{1.5}Nb_{2.5}Si_{12}B_{10}$ with Different Annealing Temperature and Annealing Time . . . . .	66
5.3.3	Frequency Dependence of Imaginary Part of the Complex Permeability of composition $(Fe_{0.9}Co_{0.1})_{73.5}Cu_1Nb_3Si_{13.5}B_9$ with Different Annealing Temperature and Annealing Time . . . . .	69
5.3.4	Frequency Dependence of Imaginary Part of the Complex Permeability of composition $Fe_{74}Cu_{1.5}Nb_{2.5}Si_{12}B_{10}$ . . . . .	75
5.4	Annealing Temperature Dependence of Initial Permeability at Constant Low Field for Sample 2 with Composition of $Fe_{74}Cu_{1.5}Nb_{2.5}Si_{12}B_{10}$ . . . . .	82

#### 6 CONCLUSION

#### Bibliography

87

90

# List of Figures

2.1	Thin layer of molten alloy in intimate contact with the outer surface of metallic rotor is quenched into an amorphous ribbon . . . . .	13
2.2	X-Ray diffraction Pattern of Sample 1 . . . . .	16
2.3	X-Ray diffraction Pattern of Sample 2 . . . . .	17
4.1	Heating Curve of Sample and Reference Substance . . . . .	31
4.2	DTA Curve . . . . .	31
4.3	DTA Thermocouple Assembly . . . . .	34
4.4	Block diagram of a differential thermal analysis equipment: (S) sample thermo-couple, (R) Reference thermo-couple (M) Monitor thermo-couple. . . . .	35
4.5	Mechanical construction of the vibrating sample magnetometer . . . . .	41
4.6	Schematic diagram of the electronic system of the V.S.M. . . . .	43
4.7	Calibration curve of magnetic field vs. decade transformer reading (V.S.M.) . . . . .	47
5.1	Differential Thermal Analysis for Sample 1 . . . . .	53
5.2	Differential Thermal Analysis for Sample 2 . . . . .	54
5.3	Magnetization Vs. Applied Magnetic Field for Samples 1 and 2 . . . . .	57
5.4	Magnetization Vs. Temperature for Sample 1 . . . . .	58
5.5	Magnetization Vs. Temperature for Sample 2 . . . . .	59
5.6	$\frac{dM}{dT}$ VS. Temperature for Sample 1 . . . . .	61
5.7	$\frac{dM}{dT}$ VS. Temperature for Sample 2 . . . . .	62
5.8	Real Part of Complex Permeability Vs. Frequency for Sample 1 . . . . .	64
5.9	Real Part of Complex Permeability Vs. Frequency for the as-cast sample and samples annealed at temperatures 200 <sup>o</sup> C, 350 <sup>o</sup> C, 550 <sup>o</sup> C for 5 minutes each . . . . .	67
5.10	Real Part of Complex Permeability Vs. Frequency for the as-cast sample and samples annealed at temperatures 200 <sup>o</sup> C, 350 <sup>o</sup> C, 550 <sup>o</sup> C for 1 hour each . . . . .	68

5.11	Imaginary Part of Complex Permeability Vs. Frequency for Sample 1 . . . . .	70
5.12	Relative Quality Factor Vs. Frequency for Sample 1 . . . . .	72
5.13	Torroidal Core Loss Factor Vs. Frequency for Sample 1 . . . . .	73
5.14	Imaginary Part Vs. Real Part of Complex Permeability for Sample 1 . . . . .	74
5.15	Imaginary Part of the Complex Permeability Vs.Frequency for for the as-cast sample and samples annealed at 200 <sup>o</sup> C, 350 <sup>o</sup> C and 550 <sup>o</sup> C for 5 minutes . . . . .	76
5.16	Imaginary Part of the Complex Permeability Vs. Frequency for different samples annealed at 200 <sup>o</sup> C, 350 <sup>o</sup> C, 550 <sup>o</sup> C and 615 <sup>o</sup> C for 1 hour . . . . .	77
5.17	Torroidal Loss Factor Vs. Frequency in the as-cast condition and for annealing at temperatures 200 <sup>o</sup> C, 350 <sup>o</sup> C and 550 <sup>o</sup> C for 5 minutes . . . . .	78
5.18	Torroidal Loss Factor Vs. Frequency in the as-cast condition and for annealing at temperatures 200 <sup>o</sup> C, 350 <sup>o</sup> C and 550 <sup>o</sup> C for 1 hour . . . . .	80
5.19	$\mu''$ VS. $\mu'$ of Sample 2 . . . . .	81
5.20	The Relative Quality Factor vs. Frequency of Sample 2 for Different Annealing Temperatures for 5 minutes . . . . .	83
5.21	The Relative Quality Factor vs. Frequency of Sample 2 For Different Annealing Temperatures for 1 hour . . . . .	84
5.22	Initial Permeability vs. Annealing Temperatures of Sample 2 . . . . .	85



# Abstract

Nanocrystalline soft magnetic materials constitute a new phase of condensed matter with highly interesting properties which are mostly structure dependent. The basic conditions of preparing nanocrystalline soft magnetic material has been studied by the dependence of the nucleation of nanocrystals on composition and the cooling process. This has been done by using the principle that nanocrystalline state can be attained by alloying which lead to two clearly separate stages of crystallization with onset temperatures,  $T_{x1}$  and  $T_{x2}$ . By annealing at temperature  $T_a$  such that  $T_{x1} < T_a < T_{x2}$  only the phase forming above  $T_{x1}$  is crystallized. The grain size dependence of magnetic properties has been explained as due to the counter play of local magneto crystalline anisotropy energy and ferromagnetic exchange interaction.

Two samples of nanocrystalline alloys of compositions  $(Fe_{0.9}Co_{0.1})_{73.5}Cu_1Nb_3Si_{13.5}B_9$  and  $Fe_{74}Cu_{1.5}Nb_{2.5}Si_{12}B_{10}$  have been studied. Cu has been used to help the crystallization process and Nb to stabilize the nanocrystals; Si and B are used as glass forming materials, Fe and Co have been used for use in high frequency and with high initial probabilities which have been tailored by changing composition and heat treatments. The materials have been characterized by Differential Thermal Analysis (DTA). Magnetization as a function of temperature up to  $700^\circ C$  starting from room temperature has been measured using Vibrating Sample Magnetometer (VSM). The Curie temperature of these specimens have been determined from  $\frac{dM}{dT}$  vs. temperature curve. The results are discussed in the model where microcrystalline structures are assumed to be embedded randomly in an amorphous matrix. The frequency dependence of permeability of these samples has been studied by using an impedance analyzer ranging from 100 Hz to 13 MHz. From the effect of heat treatment it has been found that maximum permeability and its frequency independence can not be attained simultaneously. The suitable annealing temperatures for maximum permeability, for frequency independence of permeability and for highest quality factor have been found out experimentally for these samples.

# Acknowledgements

I express my deep sense of gratitude to Dr. M. Ali Asgar, Professor of Physics, Bangladesh University of Engineering and Technology, Dhaka who was always with me to supervise this work and whose guidance, assistance and encouragement helped me a lot to perform this research work successfully.

I would like to thank Dr. Nazma Zaman, Professor and Head, Department of Physics, Bangladesh University of Engineering and Technology, Dhaka and also to Professor Gias Uddin Ahmad, Professor Mominul Huq, Professor Md. Abu Hashan Bhuiyan, Professor Jiban Podder, Dr. Md. Feroz Alam Khan, Associate Professor and Dr. A. K. M. Akther Hossain, Assistant professor of the same Department for their encouragement and interest in my work.

My special thanks and gratefulness are due to Dr. S. S. Sikder, Associate Professor, Khulna BIT for his sincere co-operation and help in my experimental work.

My thanks are also due to Mr. A K M. Mozibul Haque, Director, Soil Resource Development Institute (SRDI) Krishi Khannar Sarak, Dhaka-1215 and Mr. Iftekhar Uddin Ahmed, Senior Scientific officer, Central Laboratory, SRDI, Dhaka for their generous help in doing measurements of Differential Thermal Analysis.

I would like to extend my special thanks to the Vice-Chancellor and Registrar of the University of Asia Pacific (UAP) for having given me permission and granting me leave to pursue my research at Bangladesh University of Engineering and Technology.

My thanks are due to Mr. A.K.M. Zakaria, Senior Scientific Officer, Institute of Nuclear Science and Technology, Bangladesh Atomic Energy Commission, Dhaka for his cooperation and help in my work.

My thanks are due to my dearest colleague Mr. Md. Iqbal Bahar Chowdhury, Assistant Professor, Dept of CSE, UAP for his tireless cooperation in writing my thesis.

There are numerous people who could not be mentioned individually but their interesting discussions have prompted much thought on various aspects, whom I would also like to thank.

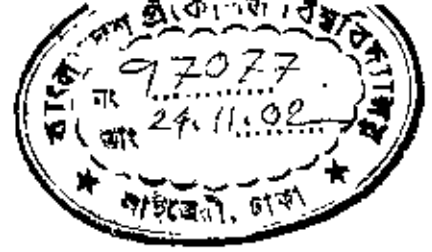
I would like to mention the name of my wife Shahnaj Parvin whose constant and volatile inspiration has inspired me a lot to undergo this work. I possess an everlasting soft corner for my loving daughter. Faria Mahmud, who has been deprived of my company during the research period.

Finally I record my sincerest gratitude to Bangladesh University of Engineering and Technology, Dhaka for providing me with the financial assistance during the period of the work.

# Chapter 1

## INTRODUCTION





## 1.1 Introduction

During the last few years nanostructured magnetic materials have become increasingly important for both theoretical understanding and technological applications. Nanostructured and amorphous magnetic materials are similar in many respects. In fact amorphous ribbons are the precursor state for the preparation of nanostructured materials in our method of preparation, although other methods like vapor deposition and sputtering have also been used by others for preparing nanocrystalline materials [1, 2, 3, 4].

The special advantage of nanocrystalline magnetic materials over amorphous ribbons lie in their higher stability and elevated curie temperature. Amorphous materials are meta stable thermodynamically and tend to crystalize when used at elevated temperature due to the development of nucleation centers or growth of the nucleation centers already embedded in the amorphous matrix during the preparation process. In fact this characteristics of amorphous ribbons are used in our process of preparing nanostructured magnetic alloys. This particular method has been stimulated by the recent advances in material synthesis and characterization techniques [5, 6]. Since the unique properties of nanostructured materials are dictated by the dimensions of the crystallites, it is very advantageous to control the size of the particles by controlling the annealing temperature of the specimens. The magnetic softness or hardness in respect of permeability is determined by the grain size of the nanocrystals which are embedded in the amorphous matrix in our nanostructured system. The single domain permanent magnets as theoretically proposed by Stoner and Wohlfarth [7], have no domain walls, because the domain wall energy increases as the square of the radius of the grains while the magnetic anisotropy energy increases as the cube of the radius. As a result with decreasing grain size a critical point is reached when the increase in the domain wall energy becomes greater compare to the anisotropy energy. The high coercivity of single domain permanent magnets is obtained by mechanically locking the magnetized single domain particles. However, by reducing the size of the magnetic particles much below this critical size, which is normally of micrometer order,

we can produce soft magnetic materials. This happens because the anisotropy of the randomly oriented particles of nanometer dimensions are averaged out algebraically, giving rise to very low magnetic anisotropy and associated magnetic softness. One further advantage of this new technique of preparing nanostructured magnetic system is that one can play with different compositions and annealing temperatures to control the grain size and their distribution and thereby tailor the magnetic properties of this new type of material. In choosing the composition one has to consider the magnetic components like Fe, Co, Ni etc, the crystalizing component such as Cu and the component Nb for stabilizing the nanocrystals by inhibiting their growth and glass forming materials like silicon, carbon, boron etc. Nanocrystalline materials are more complex compared to conventional materials because it contains nanocrystalline magnets embedded in an amorphous matrix and as such represents surface, interfacial and bulk magnetic properties. The nanosized magnetic particles are coupled by exchange force and is susceptible to inter granular distance, grain size and their distributions. Responds of nanostructured magnetic materials to the frequency of the external field can be controlled by varying the grain sizes and their distributions.

The great scope of technical applications of this material arises from this freedom of tailoring the magnetic properties [8, 9, 10, 11]. The present work is therefore mainly aimed at finding out empirically of the complex permeability of two nanostructured magnetic systems of compositions  $(Fe_{0.9}Co_{0.1})_{73.5}Cu_1Nb_3Si_{13.5}B_9$  and  $Fe_{74}Cu_{1.5}Nb_{2.5}Si_{12}B_{10}$ .

## 1.2 Organization of the Work

The preparation procedures are described in Chapter 2. The theoretical aspects of the stability of amorphous alloys, theories of permeability and magnetization are discussed in Chapter 3. Chapter 4 contains the experimental details including Differential Thermal Analysis (DTA), Vibrating Sample Magnetometer (VSM), X-Ray Diffractometer and Impedance Analyzer.

The details of the results regarding DTA, field dependence of magnetization and frequency

dependence of real and imaginary parts of permeability are discussed in Chapter 5. It also contains comments on the suitability of the specimens studied, in respect of relative quality factor, loss factor and the frequency range in which these materials can be used. Chapter 6 contains conclusion, achievement of works and future suggestion of this work.

## Chapter 2

# PREPARATION OF NANOCRYSTALLINE AMORPHOUS SOFT MAGNETIC MATERIALS BY RAPID QUENCHING METHOD



## 2.1 An Overview of Nanocrystalline Materials

Nanocrystalline material can be considered as an off-shoot of amorphous material. There are many aspects of nanocrystalline materials which are common with those of amorphous magnetic materials. In fact nanocrystalline material is a composite material where nanocrystals are embedded in an amorphous matrix. As a result the magnetic characteristics of nanocrystalline materials are controlled by both the nanocrystals and the amorphous medium in which these crystallites of nanometer dimensions are set. It is therefore important to analyze the properties of amorphous magnetic materials as a back ground for understanding the nanocrystalline magnetic systems. Moreover the preparation of nanocrystalline materials that has been followed in the present work is by the formation of amorphous ribbons by melt spinning technique and then by the crystallization of this amorphous ribbons by heat treatment at elevated temperature. To facilitate the nucleation of the crystallites and their stability, special composition has been chosen.

Since the discovery of metallic glass in 1960 by Dewez et. al. [12] in the same year Gobanov [13] predicted the possible existence of ferromagnetic ordering in noncrystalline solids on the basis of theoretical analysis. The interest in amorphous materials is increasing steadily for technological application and scientific understanding. A real technological interest developed after Pond and Maddin in 1969 [14] which is reported on the preparation of continuous ribbons of amorphous alloys. The theoretical expected retention of ferromagnetic behavior in amorphous was first demonstrated by Mader and Nowick in 1965 [15] in their work on vacuum deposited Co-Au alloy and soon thereafter by Tsuci and Duwez in 1966 [16] in their works on split cooled Pd-20 at % Si containing some ferromagnetic element partially substituted for Pd. Nanocrystalline materials represent one of the most active research item in recent times for the atomic tailoring of materials with specific properties and property combinations. However, it is still in its infancy since its emergence as a major materials science has just begun at this stage of development, there have been glimpses of exciting new properties like super plasticity, giant

magneto resistance (GMR), transparency in opaque ceramics, enhanced homogeneity, unusual soft ferromagnetism and giant caloric effects, possessed by materials which has been reduced to nanometer dimension. In addition to the understanding of the unusual properties possessed by nano phase materials, there are three other associated areas, which need serious attention

1. Identification and development of suitable preparation methods, especially those, which are scalable to providing large industrial quantities of nanometer scale materials.
2. Development of processing methods for manufacturing these materials into useful size and shapes without losing there desirable nanometer size feature and
3. Identification of proper characterization methods, where the nanometer-size range of these materials falls just below or at the resolution limit of the conventional tools.

Nanocrystalline soft magnetic alloy have received considerable attention due to their excellent soft magnetic properties [17]. Small addition of Cu and Nb into Fe-Si-B amorphous materials changes considerably their crystallization process, which is executed under appropriately controlled conditions.

1. The element Cu is used for helping the formation of nuclei of ultra fine grains.
2. The element Nb is used to impede the growth of the crystallites.

In this material, the nanocrystalline state is composed of a fine structure of  $\alpha$ -Fe(Si) nanocrystallites embedded in an amorphous matrix. The average size of  $\alpha$ -Fe (Si) is usually around 10 nm. For such an average grain size the exchange interaction dominates the magnetic behavior of randomly oriented crystallites guided by random anisotropy [18]. The relation between alloy components and the rotating speed is of importance in fabricating the high quality product. This new magnetic material of high quality is called finemet.

## 2.2 Properties of Nanocrystals as Determined by Preparation Techniques

The formation and structure of nanocrystalline grains are related to the chemical compositions and details of the heat treatment. There are diverse heating techniques of which nonconventional thermal treatment by joule heating in vacuum is quite convenient [19, 20, 21]. This method consists essentially in subjecting an amorphous ribbon to a current pulse of a few seconds duration which forces the crystallization to occur at higher temperatures in shorter time than conventional annealing. The nanocrystalline structure obtained by this method displays improved mechanical and magnetic properties in comparison with those obtained by conventional annealing. The thermal heating temperature and duration determines the size and grain boundary structure of the nanocrystalline system. The grain size and the boundary structure in their turn determine the soft magnetic properties of nanocrystalline alloys. The grain size dependence of coercivity is explained by random anisotropy model where the nanocrystalline materials are considered as single magnetic phase system by Herzer [1]. An improved model is suggested by Hernando et. al. [22]) where a two phase situation is introduced. This helps the explanation of temperature dependence of coercivity. The difference between the two models become important only at very low crystallized volume fraction or at temperatures close to the curie temperature of the amorphous phase. A nanocrystalline material can in fact show a variety of phenomena ranging from soft and hard ferromagnets as well as superparamagnets depending on the ratio of the exchange co-relation length  $L$  to the average crystallite size  $D$  and volume fraction  $x$ . The complex permeability is also dependent on these parameters.

## 2.3 Viscosity Condition for the Formation of Metallic Glass

In terms of viscosity and diffusion co-efficient we can find the condition for formation of glass.

1. The metals atomic bonding is metallic, the viscosity is lower than the diffusion co-efficient and mobility is high.
2. In the amorphous state viscosity becomes high and the mobility and the diffusion co-efficient decreases. Atomic bonds tend to be covalent as in the case of silicate ( $\text{SiO}_2$ ).

## 2.4 Conditions Necessary for Preparing Nanocrystalline Materials

The necessary conditions for preparing nanocrystalline materials are:

1. The magnetic properties are highly dependent on grain size; if the grain size is longer, the magnetic anisotropy would be very high, which in turn will have diverse effect on the soft magnetic properties specially the permeability.
2. There should be nucleation centers initiated for the crystallization process to be distributed throughout the bulk of the amorphous matrix.
3. There must be a nucleation for stabilizing the crystallites.
4. Nanocrystalline materials obtained from crystallization must be controlled so that the crystallites do not grow too big. The grain growth should be controlled so that the grain diameter is within 15-20 nm.
5. The size of the grains can be limited to nanometer scale by doping group-II metals

→  $Cu(Au, \dots, \dots)$

→  $Nb, W, Mo, Cr, Ta$  etc.

6. The stability must be lower and the crystallization temperature must be higher.

## 2.5 Preparation Technique of Amorphous Materials

There are various techniques in use to produce a metallic alloy in an amorphous state where the atomic arrangements have no long-range periodicity. The different experimental techniques developed to produce amorphous metallic glass can be classified into two groups:

1. The atomic deposition method.
2. The fast cooling of the melt.

### 2.5.1 The Atomic Deposition Method

Deposition can be described in terms of whether the added atom is prevented from diffusing more than an atomic distance before it is fixed in position due to cooling and associated increased viscosity. The atomic deposition methods include condensation of a vapor on a cooled substrate by

1. Vacuum deposition
2. Sputter deposition
3. Electro deposition
4. Chemical deposition

### 2.5.2 The Fast Cooling of The Melt

For producing an amorphous state by any of the liquid quenching devices, the alloy must be cooled through the temperature range from the melting temperature ( $T_m$ ) to the glass transition temperature ( $T_g$ ) very fast allowing no time for crystallization. The factors controlling ( $T_g$ ) and crystallization are both structural and kinetic. The structural factors are concerned with atomic arrangement, bonding and atomic size effects. The kinetic factors as discussed by Turnbull [23] are the nucleation, crystal growth rate and diffusion rate compared to the cooling rate. The interest in this method originates from the wide variety of alloys that can be made as well as from the potential low preparation cost. In the pioneering work of Duwez et al [24] a number of devices have been reported for obtaining the necessary high quenching rates and for producing continuous filaments. The methods using the principle of fast cooling of melt techniques are:

1. The gun techniques
2. Single roller rapid quenching techniques
3. Double roller rapid quenching techniques
4. Centrifuge and rotary splat quencher techniques
5. Torsion catapult techniques
6. Plasma -jet spray techniques
7. Filamentary casting techniques
8. Melt extraction techniques
9. Free jet spinning techniques
10. The melt spinning techniques

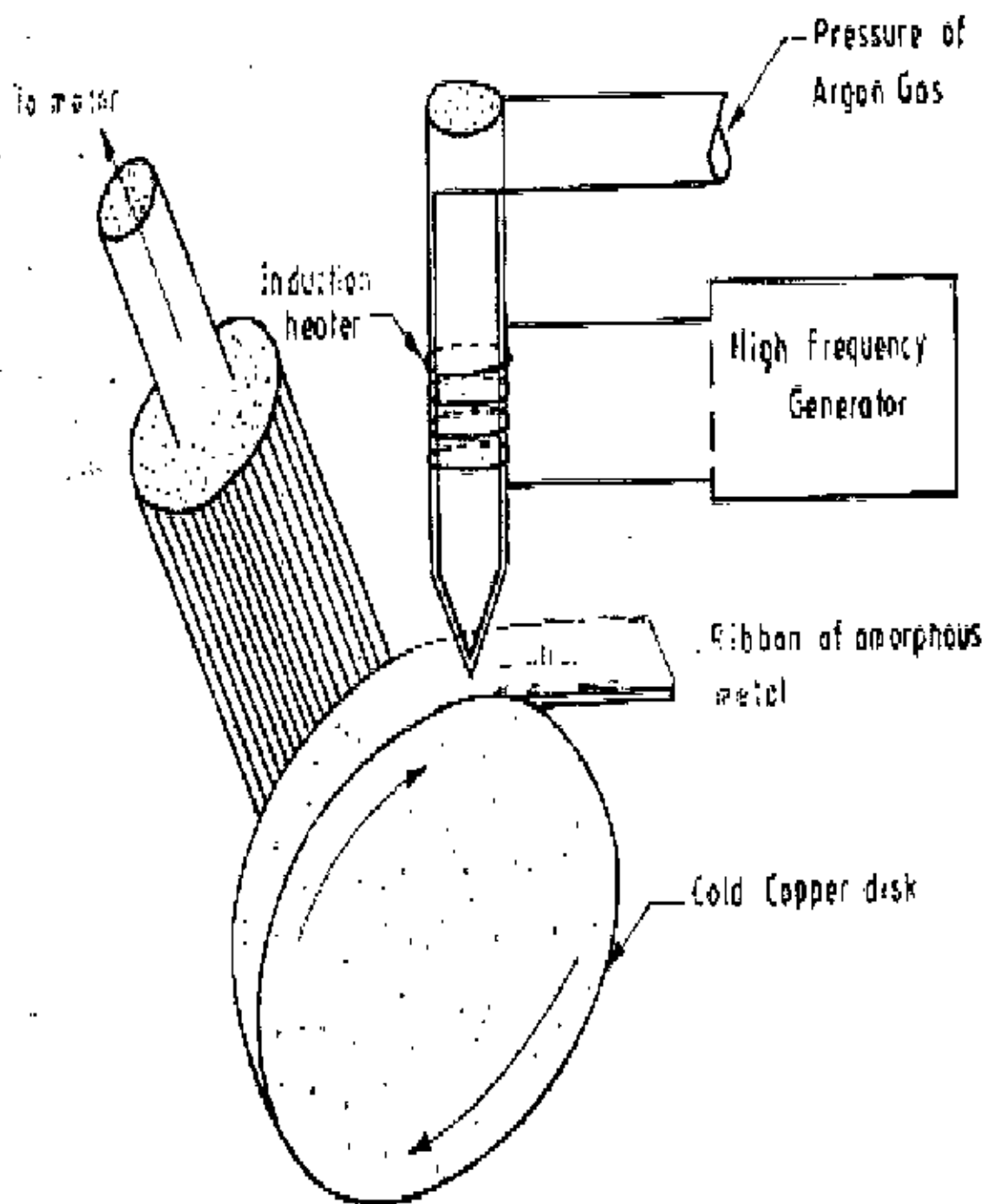
Although the differential methods used in preparation amorphous metallic ribbons are mentioned here only the single roller rapid quenching technique, which was used to prepare the specimens for the present work, will be discussed.

### 2.5.3 Rapid Quenching Method:

As shown in a schematic diagram in Fig 2.1 the rapid quenching technique apparatus consists mainly of a copper roller, an induction heater and a nozzle. A variable speed motor drove the roller via a tooth belt. The angular velocity was 2000 rev/min. Use of log wheel rotation enable us to vary the surface velocity in the range of 20 to 30 m/s. The diameter of the copper roller was 10 cm. The use of copper for the roller material was chosen for its good conductivity and mechanical softness, which allowed cleaning and polishing to be carried out easily. For room temperature work, it showed no contamination of the ribbon from the roller material and the careful preparation of the surface was more important than the material of the roller.

In this process the vibration of the roller should be well below the high frequency vibration of the melt puddle to avoid any influence of it on the geometry and uniformity of the ribbon. One has to be careful and see that the ribbon does not remain in contact with surface of the roller for a whole revolution and be hit, from the back. A bigger diameter is thus preferred for the roller. The induction heater coil is made of hollow copper tubing which is cooled simultaneously by circulating water through its inner whole. The shape and diameter of the induction heater as also its winding is to be adjusted to produce proper temperature gradient. This is to avoid sudden cooling of the melt in its way out of the crucible and blocking the nozzle. The quartz tubing having outer diameter 20 mm which is narrowed down conically to 1mm with a hole for the nozzle 0.1 to 0.2 mm.

The nozzle geometry is selected to minimize the contraction in the cross-sectional area of the molten jet as it leaves the nozzle orifice. Quartz tube is suitable for repeated use in several successful runs and should be transparent to make the melting process visible.



•Figure 2.1: Thin layer of molten alloy in intimate contact with the outer surface of metallic rotor is quenched into an amorphous ribbon



## 2.6 Experimental Details of the Preparation of Amorphous Ribbons

The amorphous ribbons are prepared in a furnace in an argon atmosphere (0.2 to 0.3 atms). The buttons prepared are about 50 grams each. Care is taken to ensure thorough mixing and homogeneity of the alloy composition, by turning over and remelting each button few times. The mother alloys which are formed in the form of buttons in a furnace by sudden cooling is then and is then cut in to small pieces and is introduced in the quartz tube. The quartz tube is connected from the top by rubber "o" rings and metal rings to the argon cylinder through a valve and a pressure gauge. After proper cleaning of the roller surface and adjusting its speed to the desired value, as measured by stroboscope the induction furnace is powered using high frequency generator. When the melting temperature is reduced as observed through a protective spectacle, the injection pressure is applied by opening the pressure valve. To avoid the turbulence of the wind, arising from the high speed of the roller in disturbing the melt puddle, cotton pad and metallic shield are usually just beneath the roller. To avoid oxidation of the ribbon during its formation an inert atmosphere can be created around the roller by a slow stream of helium gas. The speed of the roller, the volumetric flow rate, the orifice diameter, the substrate orifice distance, the injection angle etc. are adjusted by trial and error to get the best result in respect of the quality and the geometry of the ribbon.

## 2.7 Important Factors to Control the Thickness of Ribbons

### 1. Rotating speed

(a) Angular velocity  $\omega = 2000$  rev/min.

(b) Surface velocity  $v = 20$  m/s

Nanocrystalline Amorphous Material	Thickness
$(Fe_{0.9}Co_{0.1})_{73.5}Cu_1Nb_3Si_{13.5}B_9$	22 $\mu m$
$Fe_{74}Cu_{1.5}Nb_{2.5}Si_{12}B_{10}$	20 $\mu m$

2. Gap between nozzle and rotating copper drum  $h = 100$  to  $150 \mu m$ .
3. Oscillation of the rotating copper drum both static and dynamic have maximum displacement 1.5 to 5  $\mu m$ .
4. Pressure = 0.2 to 0.3 argon atmosphere.
5. Temperature of metals  $T_m \simeq 1500^{\circ} C$ . The temperature did not exceed  $1800^{\circ} C$ ; otherwise quartz tube would be melted.
6. Stability was ensured for the drop in the surface of drum.

## 2.8 Examining the Amorphousity of the Nanocrystalline Materials

To check the amorphousity of the nanocrystalline sample, X-ray diffraction for such samples with compositions of  $(Fe_{0.9}Co_{0.1})_{73.5}Cu_1Nb_3Si_{13.5}B_9$  and  $Fe_{74}Cu_{1.5}Nb_{2.5}Si_{12}B_{10}$  are taken with  $Cu - K_{\alpha}$  radiation by the x-ray diffractometer (JDX-8P GEOL, JAPAN) at BUET.

Figure 2.2 and Figure 2.3 show x-ray diffraction pattern of the samples. No peak is observed within the scanning range 300 to 1450 and hence the amorphousity of the samples are confirmed. Although there are few small humps in the diffraction pattern, there is no reason to believe that those humps are due to existing of crystalline pocket. These nanocrystalline ribbons were also ductile and those cases for which low angle scattering appear and the broad diffraction peak are subdued there is some presence of nanocrystalline phase. The average pattern of the x-ray diffraction shows the amorphous phase of the sample

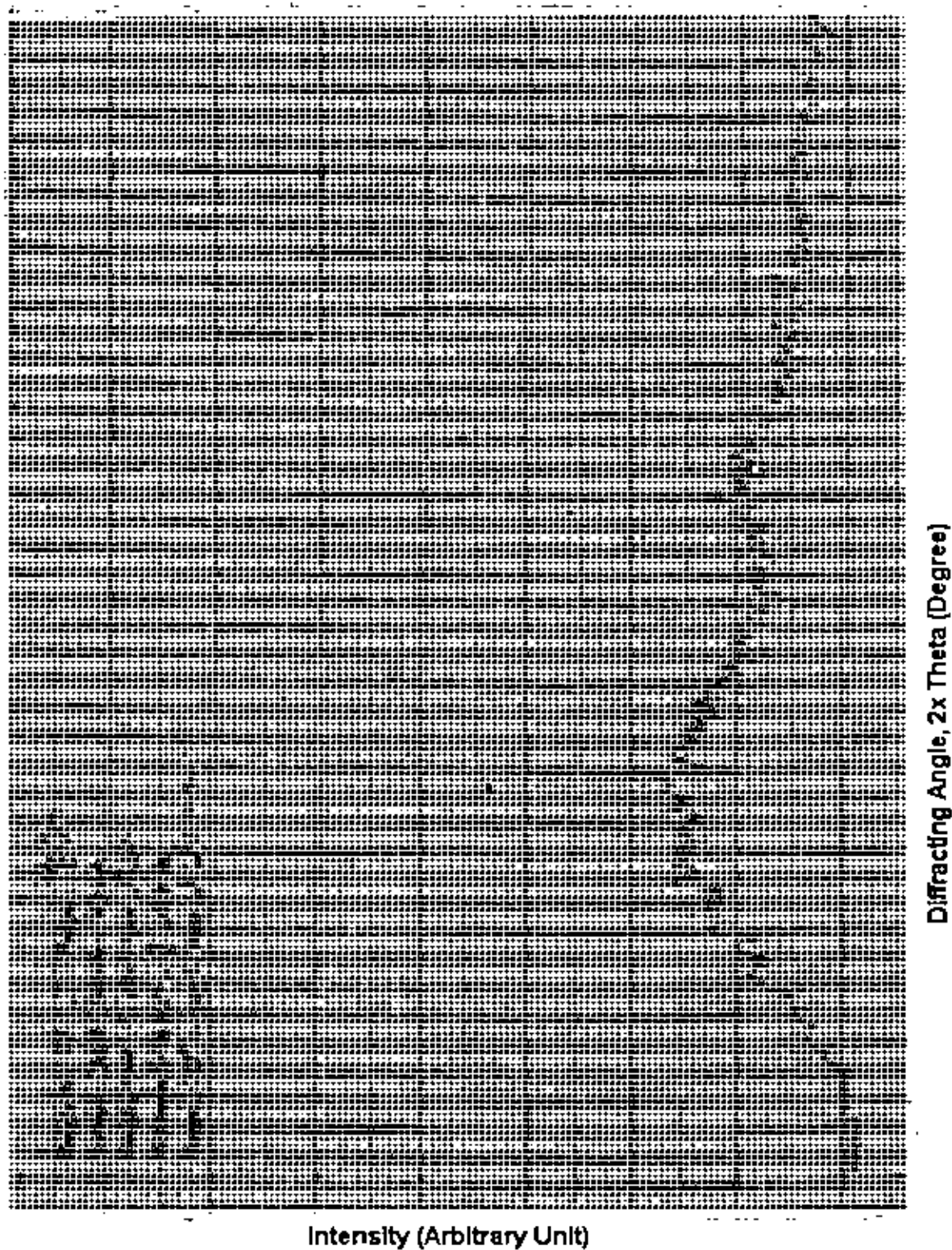


Figure 2.2: X-Ray diffraction Pattern of Sample 1



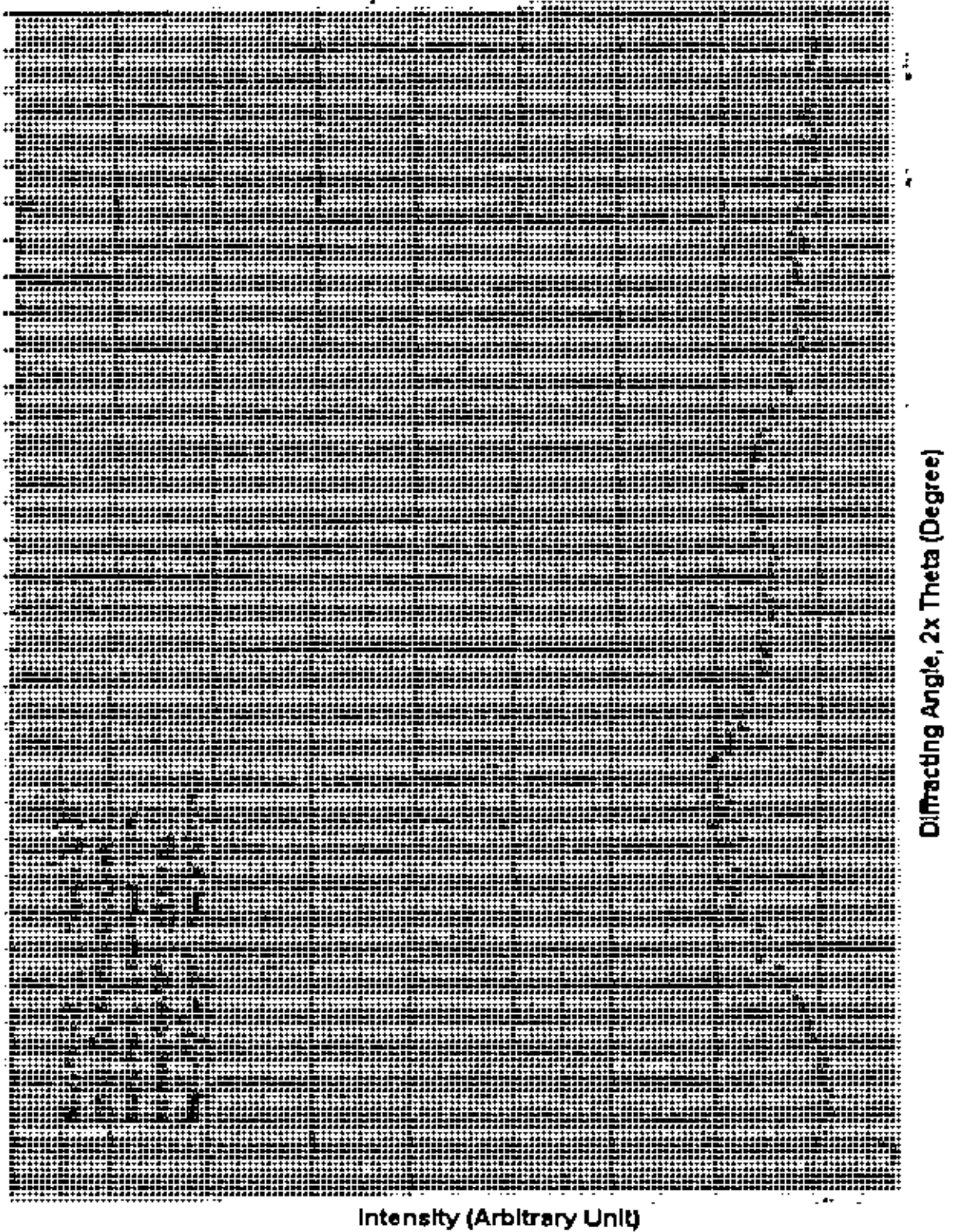


Figure 2.3: X-Ray diffraction Pattern of Sample 2

## Chapter 3

# THEORETICAL ASPECTS

### 3.1 Stability of Amorphous Alloys

Amorphous alloys represent metastable states and tend to transform into stable crystalline phase. At temperature below the crystallization temperature structural relaxation effect takes place and is caused by atomic rearrangements. The formation and stability of amorphous alloys are important topics both for theoretical understanding and technical application. There have been treated by Turnbull [25] and Takayama [26]) from thermodynamic view point. The ability of an alloy to be quenched in to glassy state is generally measured by the quantity,

$$\Delta T_g = T_m - T_g \quad (3.1)$$

Where  $T_m$  and  $T_g$  are the melting and glass transition temperatures respectively . In a similar manner the stability of the glass after formation is generally measured by the magnitude of the quantity,

$$\Delta T_x = T_x - T_g \quad (3.2)$$

Where  $T_x$  is the temperature for the onset of crystallization . As the temperature decreases from  $T_m$ , the rate of crystallization will increase rapidly but then fall as the temperature decreases below  $T_g$ . Thus by quenching a molten alloy rapidly enough to a temperature below  $T_g$ , a quasi-equilibrium amorphous phase can be obtained. There is no direct relation between the ease of formation and the resultant stability of an amorphous alloy. The amorphous alloy composition most favorable for glass formation is near the eutectic: the deeper the eutectic the better is the glass formation ability as noted by Cohen and Turnbull([27]). At eutectic point liquid is particularly stable against crystallization. The crystallization is associated with nucleation and growth process. Since the formation of an amorphous alloy depends on the absence of long-range order, change of composition is expected to affect  $T_g$  and  $T_x$ . This is because the long range ordering of atoms depends on the free energy difference between the crystalline state and the amorphous state. The change of composition affects the growth

kinetics in a complicated way, which can only be determined experimentally. The transition to the glassy state and the crystalline state is accompanied by an exothermic heat effect giving rise to a sharp peak in temperature dependence of the exothermic heat. Therefore, differential thermal analysis (DTA) is a widely used technique to study thermally induced transformation in amorphous alloys and to determine  $T_g$  and  $T_x$ . The magnitude of  $T_g$  and  $T_x$  are very different for amorphous materials and depend strongly on composition. The activation energy ranges typically between 2 eV and 6 eV [28]. The dependence of  $T_g$  on the heating rate  $S = \frac{dT}{dt}$  can be used to determine the activation energy of crystallization [29], considering the fraction  $x$  of amorphous material transformed in to the crystalline state in time  $t$  and at temperature  $T$ , one obtains for the first order rate process.

$$\left(\frac{\partial x}{\partial t}\right)_T = \kappa(1-x) \quad (3.3)$$

For thermally activated process, the rate constant  $\kappa$  obeys an Arrhenius type of equations.

$$\kappa = \kappa_0 e^{-\frac{\Delta E}{RT}} \quad (3.4)$$

Where  $\kappa_0$  is a constant and  $\Delta E$  is the activation energy. Combining Equation 3.3 and Equation 3.4 and using  $dx = \left(\frac{\partial x}{\partial t}\right)_T dt + \left(\frac{\partial x}{\partial T}\right)_t dT$  with  $\left(\frac{\partial x}{\partial T}\right)_t dt \cong 0$ , one obtains

$$\frac{dx}{dt} = \kappa_0(1-x)e^{-\frac{\Delta E}{RT}} \quad (3.5)$$

At the peak of the exothermic heat, the change of the reaction rate  $\frac{dx}{dt}$  is equal to zero, yielding, with  $T = T_x$

$$\kappa_0 e^{-\frac{\Delta E}{RT_x}} = \left(\frac{\Delta E}{RT_x^2}\right) S \quad (3.6)$$

The value of  $\delta T_x$  for the stability of amorphous alloys as given by Equation 3.2 is obtained from DTA. The values of  $E$  also appear to correlate well with the number of atomic species in the alloy. The more complex the alloy, the greater is  $E$ . Similar correlation between thermal stability as measured by  $T_x$  and  $\delta E$  appears to be small.

## 3.2 Transition-Metal Based Alloys

The temperature dependence and the Curie temperature reflect the strength of the exchange coupling. The structural disorder in amorphous alloys induces an exchange fluctuation that causes a pronounced flattening of the  $M_s(T)$  curves. The temperature curve for the amorphous alloy lies substantially below that for crystalline compound. This reduction of  $M_s$  was explained in terms of the mean field theory equation using an exchange fluctuation parameter

$$\Delta = \frac{\sqrt{\langle (\sum_{ij} \Delta J_{ij})^2 \rangle}}{\sum_{ij} J_{ij}} \quad (3.7)$$

Which is defined according to the  $\Delta_{ij}$  introduced in Equation 3.7 and adapts values in the range  $0.4 \leq \Delta \leq 0.6$ . The experimental data lies typically below the theoretical curve at low temperature and above it at high temperatures. The calculated curve representing an overall fit was explained by Kaul [30] and Pan et. al [31]. This inadequate description of the experimental data corresponds to the situation for crystalline alloys and has to be attributed to the mean-field approximations and the temperature independent treatment of  $\Delta$ . In general,  $\Delta$  is a function of temperature. Using the empirical relation

$$\Delta = \Delta_0 \left[ 1 - \left( \frac{T}{T_c} \right)^2 \right] \quad (3.8)$$

Deviation from the calculated line occur for  $T \geq 0.2 T_c$  to  $0.4 T_c$  due to the neglect of critical fluctuations or the temperature dependence of the spin-wave stiffness constant. In the corresponding crystalline compounds, deviations from the  $T^{\frac{1}{2}}$  law occur for  $T \geq 0.15 T_c$ . However not all amorphous Ferro magnets obey the  $T^{\frac{1}{2}}$  dependence. In the case of Ni-based alloys, the weak itinerant ferromagnetism leads to a temperature dependence of  $M_s$  as given by

$$M_s^2(T) = M_s^2(0) \left[ 1 - \left( \frac{T}{T_c} \right)^n \right] \quad (3.9)$$

Amorphous alloys containing Co exhibit significantly higher  $T_c$  values due to the stronger Fe-Co exchange as compared to the Fe-Fe exchange. Amorphous Fe-Ni alloys show sharper fall of  $m(T)$  around  $T_c$  indicating non-local exchange interaction and long range co-operative



phenomena. It should be noted that the pronounced sensitivity of the exchange interaction on the structural disorder gives rise to a dependence of  $T_r$  on preparation conditions.

### 3.3 Theories of Permeability

The primary requirement is the highest possible permeability, together with low losses in the frequency range of interest. The initial permeability  $\mu_i$  is defined as the derivative of induction  $\mathbf{B}$  with respect to the initial field  $\mathbf{H}$  in the demagnetization state.

$$\mu_i = \frac{d\mathbf{B}}{d\mathbf{H}}, \mathbf{H} \rightarrow 0, \mathbf{B} \rightarrow 0 \quad (3.10)$$

At microwave frequencies, and also in low an isotropic amorphous materials,  $d\mathbf{B}$  and  $d\mathbf{H}$  may be in different directions. the permeability then has a tensor character. In the case of amorphous materials containing a large number of randomly oriented magnetic atoms the permeability will be scalar. As we have

$$\mathbf{B} = \mu_0(\mathbf{H} + \mathbf{M}). \quad (3.11)$$

and susceptibility

$$\chi = \frac{d\mathbf{M}}{d\mathbf{H}} = \frac{d}{d\mathbf{H}} \frac{1}{\mu_0}(\mathbf{B} - \mathbf{H}) = \frac{1}{\mu_0}(\mu - 1) \quad (3.12)$$

The magnetic energy density

$$E = \frac{1}{\mu_0} \int \mathbf{H} \cdot d\mathbf{B} \quad (3.13)$$

For time harmonic fields  $\mathbf{H} = H \sin \omega t$ , the dissipation can be described by a phase difference  $\delta$  between  $\mathbf{H}$  and  $\mathbf{B}$ . In the case of permeability, defined as the proportional constant between the magnetic field induction  $\mathbf{B}$  and applied intensity  $\mathbf{H}$ :

$$\mathbf{B} = \mu \mathbf{H} \quad (3.14)$$

This naive definition needs further sophistication. If a magnetic material is subjected to an ac magnetic field as we get,

$$\mathbf{B} = B_0 e^{i\omega t} \quad (3.15)$$

Then it is observed that the magnetic flux density  $\mathbf{B}$  experiences a delay. This is caused due to the presence of various losses and is thus expressed as

$$\mathbf{B} = B_0 e^{i(\omega t - \delta)} \quad (3.16)$$

Where  $\delta$  is the phase angle and marks the delay of  $\mathbf{B}$  with respect to  $\mathbf{H}$ . The permeability is then given by

$$\begin{aligned} \mu &= \frac{\mathbf{B}}{\mathbf{H}} \\ &= \frac{B_0 e^{i(\omega t - \delta)}}{H_0 e^{i\omega t}} \\ &= \frac{B_0 e^{-i\delta}}{H_0} \\ &= \frac{B_0}{H_0} \cos\delta - \frac{B_0}{H_0} i \sin\delta \\ &= \mu' - i\mu'' \end{aligned} \quad (3.17)$$

Where

$$\mu' = \frac{B_0}{H_0} \cos\delta \quad (3.18)$$

and

$$\mu'' = \frac{B_0}{H_0} \sin\delta \quad (3.19)$$

The real part  $\mu'$  of complex permeability  $\mu$  as expressed in equation 3.17 represents the component of  $\mathbf{B}$  which is in phase with  $\mathbf{H}$ , so it corresponds to the normal permeability. If there are no losses, we should have  $\mu = \mu'$ . The imaginary part  $\mu''$  corresponds to that part of  $\mathbf{B}$  which is delayed by phase angle from  $\mathbf{H}$ . The presence of such a component requires a supply of energy to maintain the alternating magnetization, regardless of the origin of delay. It is useful

to introduce the loss factor or loss tangent ( $\tan\delta$ ). The ratio of  $\mu''$  to  $\mu'$ , as is evident from equation gives.

$$\frac{\mu''}{\mu'} = \frac{\frac{B_0}{H_0} \sin\delta}{\frac{B_0}{H_0} \cos\delta} = \tan\delta \quad (3.20)$$

This  $\tan\delta$  is called the loss factor. The Q-factor or quality factor is defined as the reciprocal of this loss factor i.e.

$$Q = \frac{1}{\tan\delta} \quad (3.21)$$

And the relative quality factor =  $\frac{\mu_1}{\tan\delta}$ . The behavior of  $\mu'$  and  $\mu''$  versus frequency is called the permeability spectrum. The initial permeability of a ferromagnetic substance is the combined effect of the wall permeability and rotational permeability mechanisms.

### 3.3.1 Initial Permeability of Nanocrystalline Soft Magnetic Materials

For application in electronic devices, the nanocrystalline amorphous ribbon have better performance than the amorphous ribbons in other respects. Where the design optimization requires lower cost of the nanocrystalline alloys, their lower losses compare to the amorphous ribbons at higher frequencies, the use of the core materials will be favored. The complex magnetic properties of initial permeability  $\mu_i$  may be strongly affected by the presence of an electric current particularly in a c condition. The measurement of magnetic properties as a function of frequency and its analysis by means of the complex permeability formalizing has recently lead to the resolution of several aspects of the magnetization process [32, 33, 34]). The measurement of complex permeability gives us valuable information about the nature of the domain wall and their movements. In dynamic measurements the eddy current loss is very important which occurs due to irreversible domain wall movements that are frequency dependent. A large number of possible mechanisms can contribute to the magnetic loss such as local variation of exchange energy, surface defects, compositional inhomogeneities, anisotropy and magnetostriction [35, 36] whose relative values are determined by grain size, grain orientation and thickness of the sample. The present goal of most of the recent amorphous ribbons researches is to fulfill this

requirement. Before going into the complexity of initial permeability measurement, we discuss in short the theories and mechanism involved in frequency spectrum of initial permeability

### 3.4 Magnetization of the Amorphous Ribbons

The saturation magnetization of material at a temperature of  $0^{\circ}$  K is one of its basic properties. Measurements are usually expressed as average moment per magnetic atom in units of Bohr magneton,  $\mu_B$  or as specific saturation magnetization for the amorphous alloy,  $\sigma_s$ , in units of  $Am^2/Kg$ . The moments of most amorphous alloys are lower than those of the crystalline transition metals, which they contain. However the direct effect of the structural disorder on the moments is very small. This points out the importance of chemical instead of structural disorder. The reduction is least in B-based glass and highest in P-based glass. The observed moments on TM-M glasses can approximately fitted to a formula

$$\mu = \frac{\mu_{TM}C_{TM} - C_B - 2C_{Si} - 3C_P}{C_{TM}} \quad (3.22)$$

Where  $\mu_{TM}$  is the magnetic moment of TM-M atoms, taken as 2.6, 1.6 and 0.6 respectively in Bohr magneton for Fe, Co and Ni, C's are respective concentrations. This clearly demonstrates the charge transfer from metalloid to d-band of transition metal and seems to suggest that 1, 2 or 3 electrons are transferred from each of B, Si (C, Ge) or P atom. The relative number of electrons donated can be listed as  $-P_{13}C_7) - S_{15}B_{10}) - P_{16}B_6Al_3) - P_{14}B_6) - Si_9B_{13}) - B_{20}$  based on the relative magnitudes of  $M_s$ . Amorphous alloys are rather poor conductors but their 3d-electrons are just as "itinerant" as in the crystalline transition metal alloys. Only itinerant exchange between 3d moments is of importance in the metal-metalloid alloys. Itinerant exchange arises because single site exchange taken together with the inter site electron hopping terms produce a correlation between moments on different sites. This mechanism depends on the band structure and can lead to ferromagnetism, antiferromagnetism or complex spin arrangements. The theoretical treatment of spin ordering in amorphous solids is a much more difficult problem than the regular crystalline lattices and has not been satisfactorily

solved. If the molecular field approximation (MFA) is used, even though its use is doubtful, the paramagnetic Curie temperature can be expressed as

$$T = \frac{2S(S+1)}{3K} \times \sum_{ij} J_{ij} \quad (3.23)$$

Where S is the spin number,  $k$  is the Boltzmann's constant and  $J_{ij}$  is the exchange interaction between atoms at the position  $r_i$  and  $r_j$ , and can be expressed in terms of the radial distribution function.

In first case, a unique constant exchange interaction between the magnetic atoms is assumed and the amorphous nature of the alloy is taken into account by calculating a random distribution of the local anisotropy field [37]. In the second approach to treating this problem a distribution of exchange integrals is assumed in order to reflect the structural fluctuation in the amorphous alloy [38]. Both approaches predict that the M vs. T curve will flat below that for the crystalline counter part. The first model however predicts that amorphous alloys should exhibit a structure less Mossbauer spectrum, contrary to the observed spectra. Thus the second approach is preferred of the various theories the molecular field approach (MFA) and mean field theories.

### 3.4.1 Low Temperature Behaviour of $M_s$ of Amorphous Ribbons:

The mean field theories do not account for local magnetic excitations and thus can not provide an accurate description of the low temperature behavior of the magnetic properties. In the quasicrystalline approximation and the long wavelength limit, the spin-wave energy can be expressed by Keffler [39].

$$E_K = E_0 + DK^2 + FK^4 + \dots \quad (3.24)$$

Where K is the wave vector of the spin-wave and D and F are the spin stiffness constants. The presence of spin waves gives rise to a reduction of the average magnetization, leading to a temperature dependence of the form

$$M_s(T) = M_s(0)[1 - BT^{3/2} - CT^{3/2} + \dots] \quad (3.25)$$

Where  $M_s(0)$  is the saturation moment. The coefficients B and C are related to the spin-wave stiffness constant D by

$$B = \xi \left( \frac{3}{2} \right) \left( \frac{g\mu_B}{M_s(0)} \right) \left( \frac{K_B}{4\pi D} \right)^{3/2} \text{ and} \quad (3.26)$$

$$C = \frac{3}{4}\pi \langle r^2 \rangle \xi \left( \frac{5}{2} \right) \left( \frac{g\mu_B}{M_s(0)} \right) \left( \frac{K_B}{4\pi D} \right)^{5/2} \quad (3.27)$$

Where g is the g-factor ( $\sim 2.1$ )  $\mu$  is the Bohr magneton,  $\xi \left( \frac{3}{2} \right) = 2.612$  and  $\xi \left( \frac{5}{2} \right) = 1.341$  are the zeta functions and  $\langle r^2 \rangle$  represents the average mean-square range of the exchange interaction. D is directly proportional to the exchange constants. The  $T^{3/2}$  terms comes from quadratic dependence of spin-wave on wave vector. With increasing exchange strength, the slope of  $M_s(T)$  versus  $T^{3/2}$  decreases are expected from experimental results of alloys with increasing  $T_c$ .

### 3.4.2 High Temperature Behaviour of $M_s$ of Amorphous Ribbons:

The overall temperature behavior of reduced magnetization  $m = \frac{M_s(T)}{M_s(0)}$  in TM-M glass goes to zero quite sharply at critical temperature  $T_c$  and in many glasses the phase transition is as sharp as in crystalline system. Near  $T_c$ ,

$$M_s(T) = (T_c - T)^\beta \quad (3.28)$$

Where the  $\beta$  is a critical exponent. At intermediate temperature there is flattening, which is found in almost all TM-M glasses studied. The effect of high temperature has been treated in two different approaches. The first approach is given by Harris et.al. ([40]) considers a constant exchange interaction between magnetic atoms and a random distribution of the local anisotropy field is considered which changes with temperature. The other approach is to consider a distribution of exchange integral is assumed in order to take into account the fluctuation in the amorphous alloys as taken by Handrich [38]). Both the approaches are unrealistic and infact no rigorous theory of the high temperature behavior for amorphous materials has been

developed. We have determined the experimental power law from the temperature variation of magnetization in the high temperature range.

## Chapter 4

# EXPERIMENTAL DETAILS



## 4.1 The Differential Thermal Analysis

### 4.1.1 Introduction

The technique of differential thermal analysis is an important tool to study the structural change occurring both in solid and liquid materials under heat treatment. This changes may be due to dehydration transition from one crystalline variety to another, destruction of crystalline lattice, oxidation, decomposition etc. The principle of differential thermal analysis (DTA) consists in measuring the heat changes associated with the physical or chemical changes occurring when a standard substance is gradually heated. This technique has been used in determining the glass transition temperature and crystallization temperature of our nanocrystalline soft magnetic material. The glass transition temperature  $T_g$  is defined as the temperature at which the alloy passes from the solid to the liquid state. For our purposes it is sufficient to describe  $T_g$  as the temperature at which atomic mobility is great enough to allow diffusive atomic rearrangement to occur in a matter of minutes. The crystallization temperature  $T_x$  defined as the temperature at which crystallization occurs with long range ordering and is usually determined by DTA technique by a heating rate of  $\approx 20^\circ \text{C}/\text{min}$ . The DTA technique has been used in determining  $T_g$  and  $T_x$  of our nanocrystalline amorphous soft magnetic material with compositions  $(\text{Fe}_{0.9} \text{Co}_{0.1})_{73.5} \text{Cu}_1 \text{Nb}_3 \text{Si}_{13.5} \text{B}_9$  and  $\text{Fe}_{74} \text{Cu}_{15} \text{Nb}_{25} \text{Si}_{12} \text{B}_{10}$ .

### 4.1.2 The Principle of Differential Thermal Analysis

The DTA technique was first suggested by Le Chatelier [41] in 1887 and was applied to the study of clays and ceramics. DTA is the process of accurately measuring the difference between a thermocouple embedded in a sample and a thermo-couple in a standard inert material such as aluminum oxide while both are being heated at uniform rate.

These differences of temperature arise due to the phase transitions or chemical reactions in the sample involving the evolution of heat or absorption of heat. The exothermic and endothermic reactions are generally shown in the DTA trace as positive and negative deviations

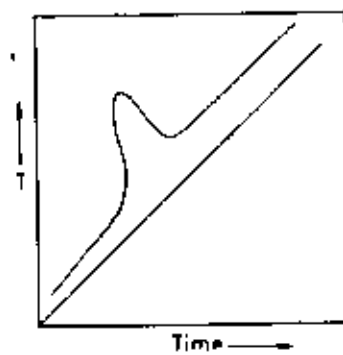


Figure 4.1: Heating Curve of Sample and Reference Substance

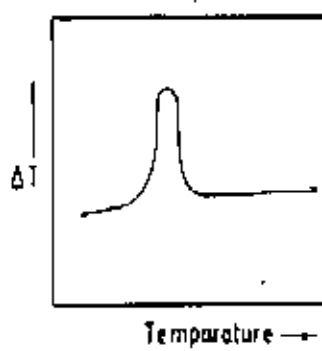


Figure 4.2: DTA Curve

respectively from a base line. So DTA gives a continuous thermal record of reactions accruing in a sample. When a sample and reference substance are heated or cooled at a constant rate under identical environment, their temperature differences are measured as a function of time or temperature (as shown by the curve in Figure 4.1- 4.2). The temperature of the reference substance, which is thermally inactive rises uniformly when heated, while the temperature of a sample changes anomalously when there is a physical and chemical change of the active specimen at a particular temperature. When there is an exothermic reaction there is a peak in the temperature vs time curve, heat supplied from outside is consumed by the reaction. And when the reaction is over, the sample temperature is different from the ambient, and it rises rapidly to catch it up, and then it begins to change uniformly. The temperature difference  $\Delta T$  is detected, amplified and recorded by a peak as shown in Fig 4.1. The temperature in the sample holder is measured by a thermo-couple the signal of which is compensated for the ambient temperature and fed to the temperature controller. This signal is compared with the program signal and the voltage impressed to the furnace is adjusted. Thus the sample and reference substance are heated or cooled at a desired rate. The temperature in the sample holder is digitally displayed on the DTA-50 (Differential Thermal Analyzer, Shimadzu Corporation, Kyoto, Japan) and is also recorded on the recorder

### 4.1.3 Apparatus

The apparatus of the differential thermal analysis consists of a of a thin walled refractory specimen holder made of sintered aluminum with two adjacent cubical compartments of exactly the same size, 1 cm in length (Figure 4.3) of which one is for the reference (inert) material and the other for the test material. The compartments are separated by a 1 mm wall. The specimen holder is placed in the cavity of the heating blocks, which is operated in the center of the cylindrical refractory tube of an electrical furnace, which supplies a uniform heating rate. The furnace (9" x 6" x 9" deep) is peaked with calcined china clay. The input of current into the furnace is secured through the secondary of a variable transformer, which controls the current.

Fine chromelalumel wires (28 gauge) are used for thermocouples. A cold junction is used for thermocouples leads and the e.m.f is recorded almost continuously, while the temperature of the inert material is measured at 3 minutes interval.

It is essential to use perfectly dry materials as otherwise errors will be introduced in the analysis. Approximately 0.1 g anhydrous alumina is used in the reference cup and the sample weights varies over a range 0.05 to 0.125 g; depending on their packed density. An average heating rate of  $10^{\circ}\text{C}$  per minute of the furnace is maintained which gave satisfactory results in most cases. A block diagram of DTA is shown in Fig. 4.4. The thermal analysis runs generally for 1 to 1.5 hrs. Thermal analysis curves are obtained by plotting heating temperature and the difference between the temperatures of the test and the reference substances. From these plots the reaction temperature could be determined. Under standard conditions of the experiment, characteristics curves for different composition iron-Boron amorphous ribbon were obtained. A sharp exothermic peak indicates Glass transition and crystallization temperature points, usually. Exothermic peaks similarly give the temperatures of decomposition of phases and in cases typical endothermic curves afford useful information about the structural changes taking place in the compound.

All experiments are run at atmospheric pressure in a continuous flow of a purified inert gas usually argon, Nitrogen or helium. Gases are normally purged into the furnace chamber at the lower and through a purification train in which oxygen and water are removed by heated copper wool and exhausted from the top into a condensed trap for collecting the condensable volatile products.

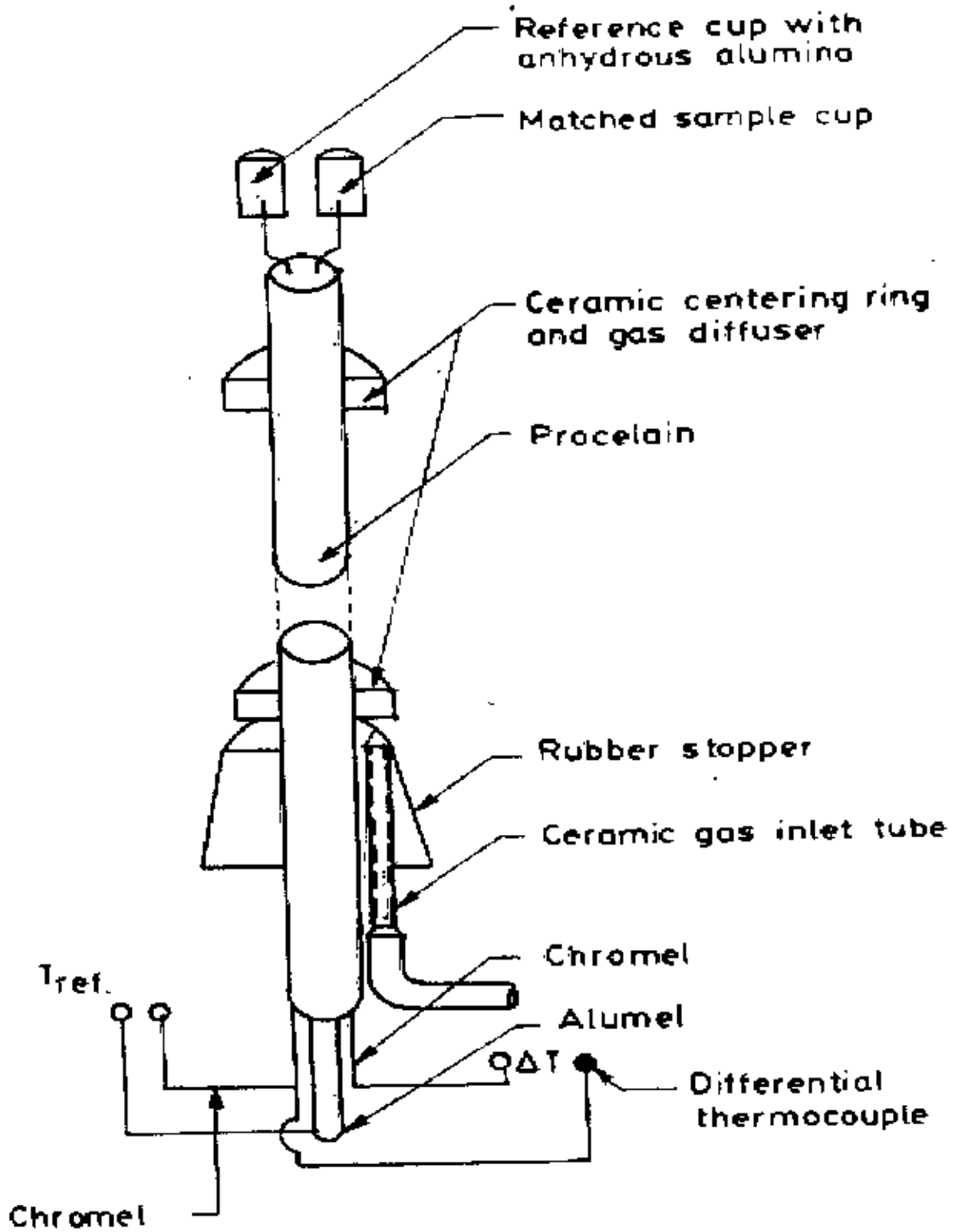


Figure 4.3. DTA Thermocouple Assembly

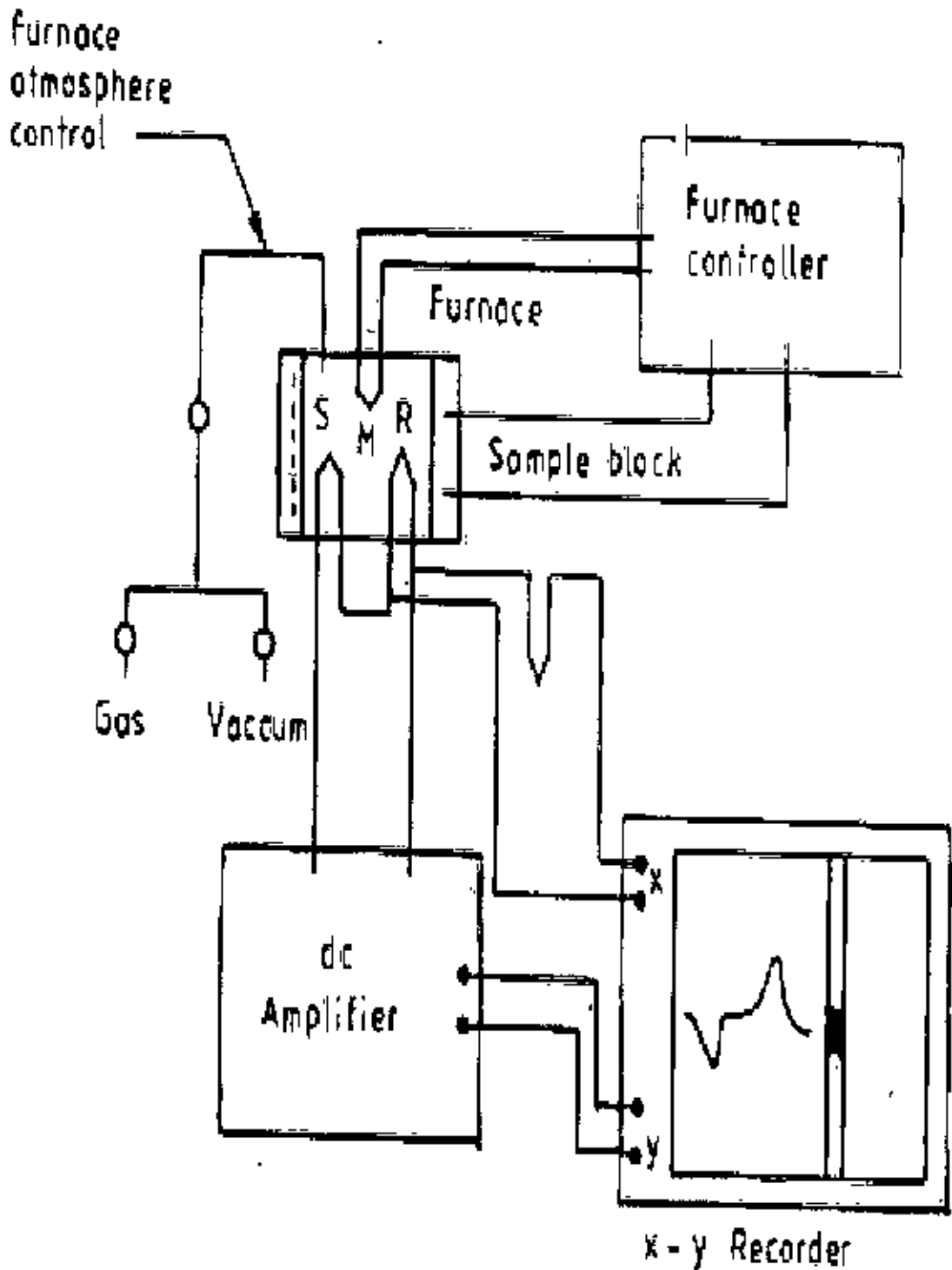


Figure 4.4: Block diagram of a differential thermal analysis equipment: (S) sample thermocouple, (R) Reference thermocouple (M) Monitor thermocouple.

## 4.2 Experimental Determination of Complex Permeability

### 4.2.1 Real and Imaginary Components of Complex Permeability

Determinations of permeability normally involve the measurements of the change in self inductance of a coil in the presence of magnetic core. The behavior of a self inductance can now be described as follows. If we have an ideal lossless air coil of inductance  $L_0$ , on insertion of magnetic core with permeability  $\mu$ , the inductance will become  $\mu L_0$ . The complex impedance  $Z$  of this coil can then be expressed as

$$Z = R + iX = i\omega L_0\mu = i\omega L_0(\mu' - i\mu''), \quad (4.1)$$

where the resistive part is

$$R = \omega L_0\mu'' \quad (4.2)$$

and the reactive part is

$$X = \omega L_0\mu'. \quad (4.3)$$

The r.f permeability can be derived from the complex impedance of a coil in Equation 4.1. The core is taken in the toroidal form to avoid demagnetizing effects. The quantity  $L_0$  is described geometrically as shown in section 4.2.1.

### 4.2.2 Preparation of the Samples for Complex Permeability

The amorphous ribbons were wound in to toroidal cores having outer and inner diameters 13 to 15 mm and with the ratio of outer and inner diameters always kept less than 1.2 in order to improve the homogeneity of the applied field, as also to reduce the possibility of an inhomogeneous inductance response. A low capacitance with 8 to 10 turns was wound around the toroids to allow the application of magnetic fields over a wide range of amplitudes. While measuring the permeability of the amorphous ribbon cores at high frequency, the high electric resistance of these materials generally precludes the troublesome skin effect found in

ribbons. However, the cross-section of the amorphous ribbon core to be measured may have to be kept small in order to avoid dimensional resonance phenomena. To avoid an increase in resistance owing to skin effect, braided copper wire is used at frequencies higher than 100 KHz. The thickness of the separate wire stands being adapted in the measuring frequency of up to about 13 MHz. The thumb rule is that the wire thickness in microns must be smaller than the wavelength in meters. At higher frequencies the capacitance arising from winding gives inaccurate values of R &  $L_s$ . It is, therefore, necessary to keep the capacitance of the winding as low as possible. Frequency response characteristics were then investigated on these ring shaped specimens as a function of frequency.

### 4.2.3 Frequency Characteristics of Nanocrystalline Materials

The frequency characteristics of the amorphous ribbons samples ie the permeability spectra, were investigated using an impedance analyzer(LCR bridge).LF 4192A,Agilent technologies Lt.,Japan at BUET. The measurement of inductances were taken in the frequency range 0.5 Hz to 13 MHz. The values of measured parameters obtained as a function of frequency and the real and imaginary parts of permeability and the loss factor,  $\mu'$  is calculated by using the following formula.

$$L_s = L_0 \mu' \quad (4.4)$$

$$\mu' = \frac{L_s}{L_0} \quad (4.5)$$

and

$$\tan \delta = \frac{\mu''}{\mu'} \quad (4.6)$$

$$\mu'' = \mu' \tan \delta \quad (4.7)$$

Here  $L_s$  is the self- inductance of the sample core and

$$L_0 = \frac{\mu_0 N^2 S}{d} \quad (4.8)$$



where  $L_0$  is the inductance of the winding coil without the sample core,  $N$  is the number of turns of coil and  $S$  is the area of cross section as given below

$$S = dh, \quad (4.9)$$

where

$$d = \frac{d_2 - d_1}{2} \quad (4.10)$$

and  $h$  is the height. And  $\bar{d}$  is the mean diameter of the sample given as follows:

$$\bar{d} = \frac{d_2 + d_1}{2} \quad (4.11)$$

The relative quality factor is determined for the ratio  $\mu_i/\tan\delta$ .

## 4.3 Experimental Setup for Measurements of Magnetization

### 4.3.1 The Principles of Vibrating Sample Magnetometer (V.S.M)

All magnetization measurements have been made on EG and G Princeton applied research Co. make vibrating sample magnetometer (VSM) [42, 43]. The principle of VSM is as follows: when the sample of a magnetic material is placed in a uniform magnetic field, a dipole moment proportional to the product of the sample susceptibility times the applied field is induced in the sample. If the sample is made to undergo a sinusoidal motion, an electrical signal is induced in suitably located stationary pick-up coils. This signal which is at the vibrating frequency is proportional to the magnetic moment, vibration amplitude and vibration frequency. In order to obtain the reading of the moment only, a capacitor is made to generate another signal for comparison, which varies in its moment, vibration amplitudes and vibration frequency in the same manner as does the signal from the pick-up coil. These two signals are applied to the two inputs of a differential amplifier. And because the differential amplifier passes only difference between the two signals, the effect of vibration amplitude and frequency changes are

cancelled. Thus only the moment determines the amplitude of the signal at the output of the differential amplifier. This signal is in turn applied to a lock-in amplifier, where it is compared with the reference signal which is at its internal oscillator frequency and is also applied to the transducer which oscillates the sample rod.

Thus the out put of the Lock- in amplifier is proportional to the magnetic moment of the sample only avoiding any noise of frequency other that of the signal. The Lock-in action yields an accuracy of 0.05 % of full scale. The absolute accuracy of this system is better than 2% and reproducibility is better than 1%. Least measurable moment is  $5 \times 10^{-4}$  emu. Variable magnetic field is achieved with a Newport Electromagnet Typen 177 with 17.7 cm diameter pole pieces. The magnet is mounted on graduated rotating base. The standard model is modified to provided an adjustable pole gap in order that the highest possible field strength is available. The field can be varied from 0 to 9 Kg. The field is measured directly by using Hall probe.

### 4.3.2 Mechanical Design of the V.S.M.

The various mechanical parts of the magnetometer are shown in the Figure 4.5. The base B of the V.S.M is a circular brass plate of 8mm thickness and 250 mm diameter. A brass tube T of 25 mm outer diameter and 0.5 mm thickness runs normally through the base such that the axis of the tube and the center of the plate coincide. The base and the tube are joined together by soft solder. The tube extends 60 mm upward and 24 mm downward from the base. There is a vacuum port on the lower part of the tube 120 mm below.

Electrical connections from the audio amplifier to the speaker and from the reference coil system to the phase-shifter are taken via the Perspex feed-through. By connecting the vacuum port of the tube T to a vacuum pump the sample environment can be changed. The speaker SP is fitted 25 mm above the tube T with the help of our brass stands. The lower ends of the stands are screwed to the base plate while the rim of the speaker is screwed on the tops of the stands. The speaker has a circular hole of 10 mm diameter along the axis of it. An aluminium disc having female threads in it is fitted to the paper cone with araldite. The aluminium connector

having male threads on it and attached to the drive rod assembly fits in the aluminium disc and thus the drive rod assembly is coupled to the speaker. The drive rod assembly consists of two detachable parts which are joined together by means of aluminium threaded connectors. Each part is a thin Pyrex glass tubing of 4 mm diameter. The upper part has a small permanent magnet P situated 100 mm below the aluminium connectors attached to it. At the lower end of the drive rod assembly a Perspex sample holder having quite thin wall can be fitted tightly with the sample in it. A few Perspex spacers are also attached to the driver rod throughout its length. The spacers guide the vibration of the sample only in the vertical direction and stops sidewise vibration or motion. The total length of the drive rod assembly is 920 mm up to the base. The lower end of the tube T is joined to a brass extension tube L by a threaded coupling and an o'ring seal. Another thin tube K made of German silver and of 8 mm inner diameter runs through the extension tube L from the coupling point C to about 50 mm below the sample position. Above the base there is hollow brass cylinder M of 180 mm length and 130 mm inner diameter, having 40 mm wide collars at its both ends. The lower collar seats on an o'ring seal which is situated in a circular groove in the base plate. On the upper collar, there rests an aluminium top N with an o'ring seal. The brass cylinder M has a side port VP. This is again a brass tube of 41 mm diameter and 43 mm length. The port has a collar at the end away from the cylinder. A Perspex vacuum feed-through is fitted at its end with o'ring seal. This port is connected to the cylinder by soft solder.

The base plate of the V.S.M rests on three levelling screws above a brass frame, which in turn rests on an iron angle bridge. The bridge is rigidly fitted to the sidewall of the room. The brass frame is provided with arrangements with the help of which it can be moved in two perpendicular directions in the horizontal plane.

The levelling screws are used to make the drive rod vertical and to put the sample at the center of the pole-gap between the sample coils. The travelling screws can also move up and down the sample.

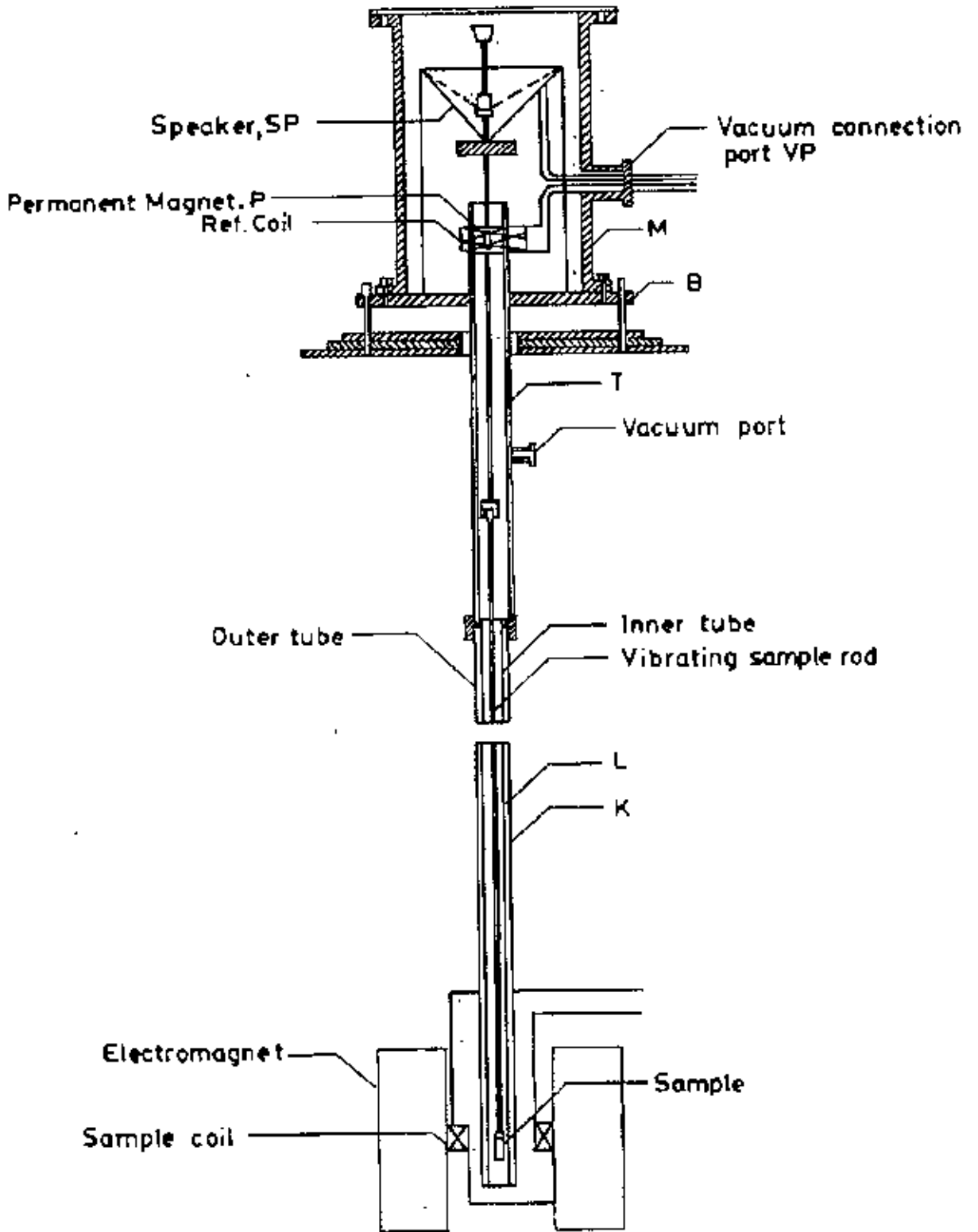


Figure 4.5: Mechanical construction of the vibrating sample magnetometer

### 4.3.3 Electronic Circuits of the V.S.M.

The function of the associated electronic circuits are:

1. To permit accurate calibration of the signal output obtained from the detection coils.
2. To produce a convenient AC output signal which is directly related to the input and which can be recorded.
3. To produce sufficient amplification for high sensitivity operation.

The block diagram of the electronic circuit used for the V.S.M consists of a mechanical vibrator, a sine wave generator, an audio amplifier, a ratio transformer, a phase-shifter, a lock-in amplifier, a pick-up coil system, a reference coil system and an electromagnet as shown in Figure 4.6. The sample magnetized by the electromagnet generates an e.m.f in the pick-up coils PC. The strength of this signal is proportional to the magnetization of the sample. The vibrating permanent magnet also generates an e.m.f of fixed amplitude in the surrounding reference coils. This signal is stepped down with the help of a ratio transformer so that its amplitude is equal to that of the sample signal. The two signals are then brought in phase and put to the Lock-in amplifier. The Lock-in amplifier works as a null detector. The ratio transformer reading is to be calibrated using spherical shape sample S of 99.99% pure nickel.

#### Sensitivity Limits

Limits of sensitivity are determined by signal to noise at the input circuit, where noise is defined as any signal not arising from the magnetic moment of the sample. The major sources of noise are the Johnson noise of the wire used for the pick-up coils, and the magnetic responses of the sample holder, which superimposes undersigned signals in phase with the wanted signal. Use of a minimum mass of weakly diamagnetic material for a sample holder, carefully checked to contain no ferromagnetic impurities, is essential to minimize this coherent noise contribution. Corrections for the small magnetic contribution of the sample holder can then be made by

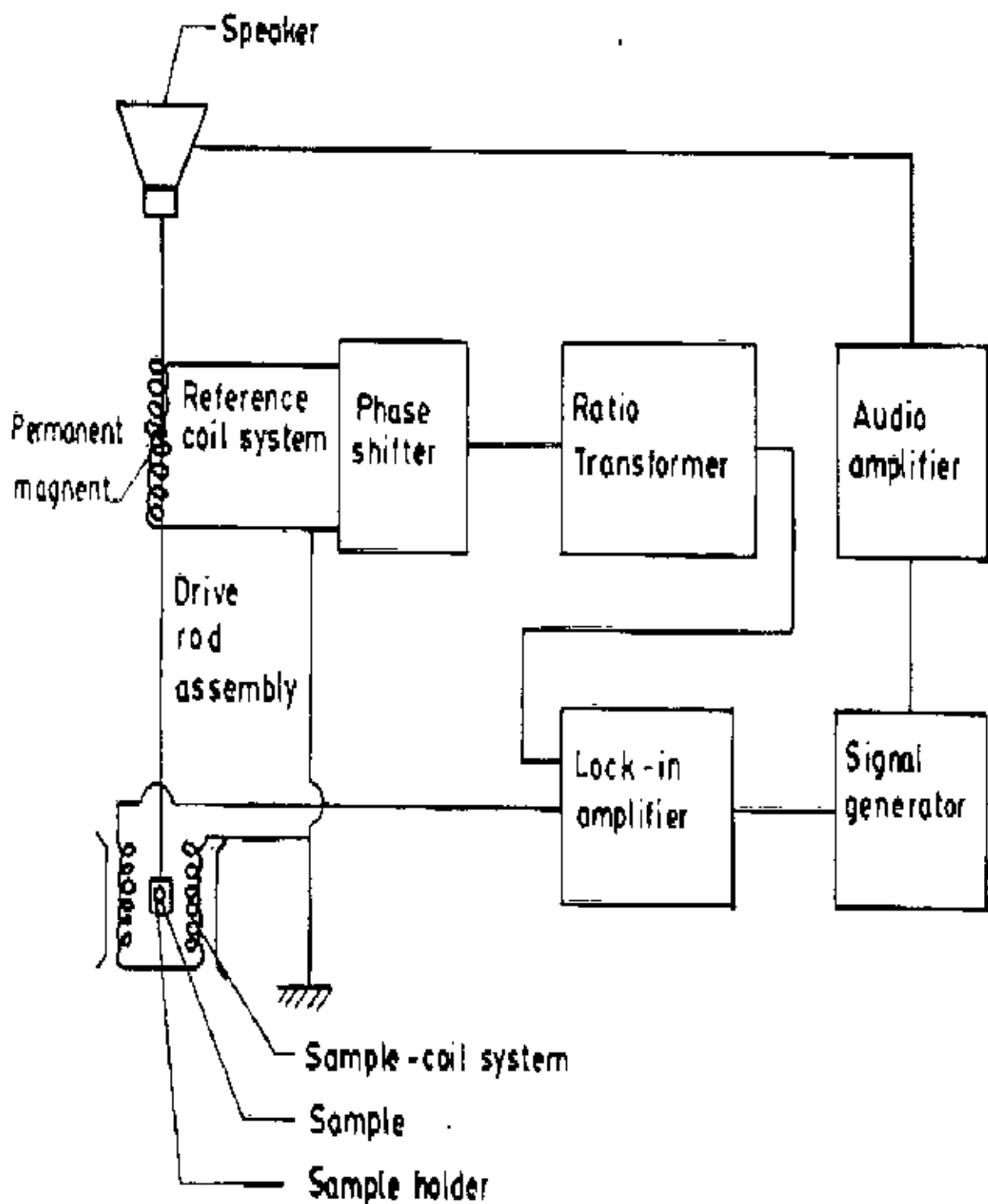


Figure 4.6: Schematic diagram of the electronic system of the V.S.M.

measurements with the sample removed. This correction is much less than the equivalent case with a moving coil system. Our standard sample used for calibration was spherical shaped specimens of mass 0.0584 gm. The different field susceptibility  $\Delta x \cong 5 \times 10^{-10}$  could be observed after synchronous phase detection with bandwidth  $\cong 2 \times 10^{-2}$  cps. The other tests used was small current at 81 Hz or an alternating current 81 Hz passed through the coil which remained stationary.

### Stability Tests Differential Measurements

With only the Lock-in amplifier and the oscilloscope as a null detector, it was found that the 0.0584 gm Ni-sample signal could be balanced reproducibly. Such reproducibility indicated that the long time drifts caused by the combined effects of vibration, amplitude changes, and frequency changes a bridge sample position and other effects were negligible. Chosen synchronous phase detector added differential changes about one-tenth the size that could be recorded reproducibly.

### Vibratiou Amplitnde

The pick-to-pick vibration amplitude has been varied from less than 0.1 mm up to 1.0 mm in order to examine errors caused by amplitude changes. Such tests show that the measured magnetic moment varied less than 0.5% over these range of amplitude, although at higher variation of amplitude, because of the larger signals involved.

### Image Effects

Image effects were also examined with a small vibrating coil carrying a dc current. The image effect was no greater than 1% for fields up to 5 Kg produced in an air gap of 3.6 cm. Undoubtedly, there is an image induced in the magnet poles. It appears, however, that when the sample is vibrated, eddy current shielding reduces the effective image vibration.

## Vibration Frequency

The vibration frequency is not critical. High frequency operation is limited by the driving mechanism and capacitive shunting in the detection coils. Frequencies of 100 Hz or less permit the use of inexpensive components and minimize eddy current shielding by the vacuum chamber. The measurements are completely independent of eddy currents in the surrounding parts, if measurements and calibration are made at the same temperature. The thickness of conducting parts has been minimized, so that the temperature dependence of penetration depth is less than 1%.

## Vibration Problems

Mechanical coupling between the vibrating system and the fixed detection coils must be avoided. Although the coils are arranged for minimum sensitivity to external vibration, a noticeable background signal is obtained when the vacuum chamber contacts the detection coils. Such mechanical effects are difficult to eliminate electronically, because the spurious background signal has the same frequency as the sample signal and maintains a constant phase difference with respect to the sample signal. Usually the magnetometer and detection coils are both supported by the magnetic coupling, so that some mechanical coupling may be noticed at highest sensitivity.

### 4.3.4 Calibration of the V.S.M.

There are usually two methods of calibration of a vibrating sample magnetometer (V.S.M)

1. by using a standard sample and
2. by using a coil of small size whose moment can be calculated from the magnitude of the d.c. current through it.

We have calibrated our V.S.M using a 0.0584 gm spherical sample of 99.99% pure nickel. The sample was made spherical with the help of a sample-shaping device. The saturation magnetic



moment of the sample has been calculated using the available data. The ratio transformer reading is obtained by actual measurement from the relation

$$M = K K' \quad (4.12)$$

Where  $M$  is magnetic moment,  $K'$  is saturation ratio transformer reading and  $K$  is V.S.M. calibration constant. But

$$M = m\sigma \quad (4.13)$$

Where  $s$  is the specific magnetization and  $m$  is the mass of the sample. From Equation 4.12 and Equation 4.13 calibration constant is given by

$$K = \frac{m\sigma}{K'} \quad (4.14)$$

The accuracy of this calibration, however, depends on the reliability of the standard nickel sample; the accuracy of the ratio transformer and the gain of amplifier. The equipment has been operated repeatedly with the same standard sample and stability has been found to be within 1 part in 100.

The absolute accuracy of the instrument depends on the knowledge of the magnetic properties of the calibration standard and reproducibility of the sample position. When the substitution method of calibration is used, the major error 1% is introduced by the estimation of standard nickel sample. The relative accuracy of this instrument depends on accurate calibration of the precision resistor divider network. The total error here can be kept less than 0.5%. A typical calibration curve of magnetic field Vs ratio transformer reading is shown in Figure 4.7

### Calibration Data

1. Reference signal with phase shifter and decade transformer in connection:

$$V_{ref_1} = \frac{1}{0.01} \times \frac{10\mu V}{20} \times 19 = 9.5\mu V \times 100 = 0.95 mV \quad (4.15)$$

2. Reference signal with decade transformer in connection:

$$V_{ref_2} = \frac{1}{0.01} \times 11\mu V = 1.1 mV \quad (4.16)$$

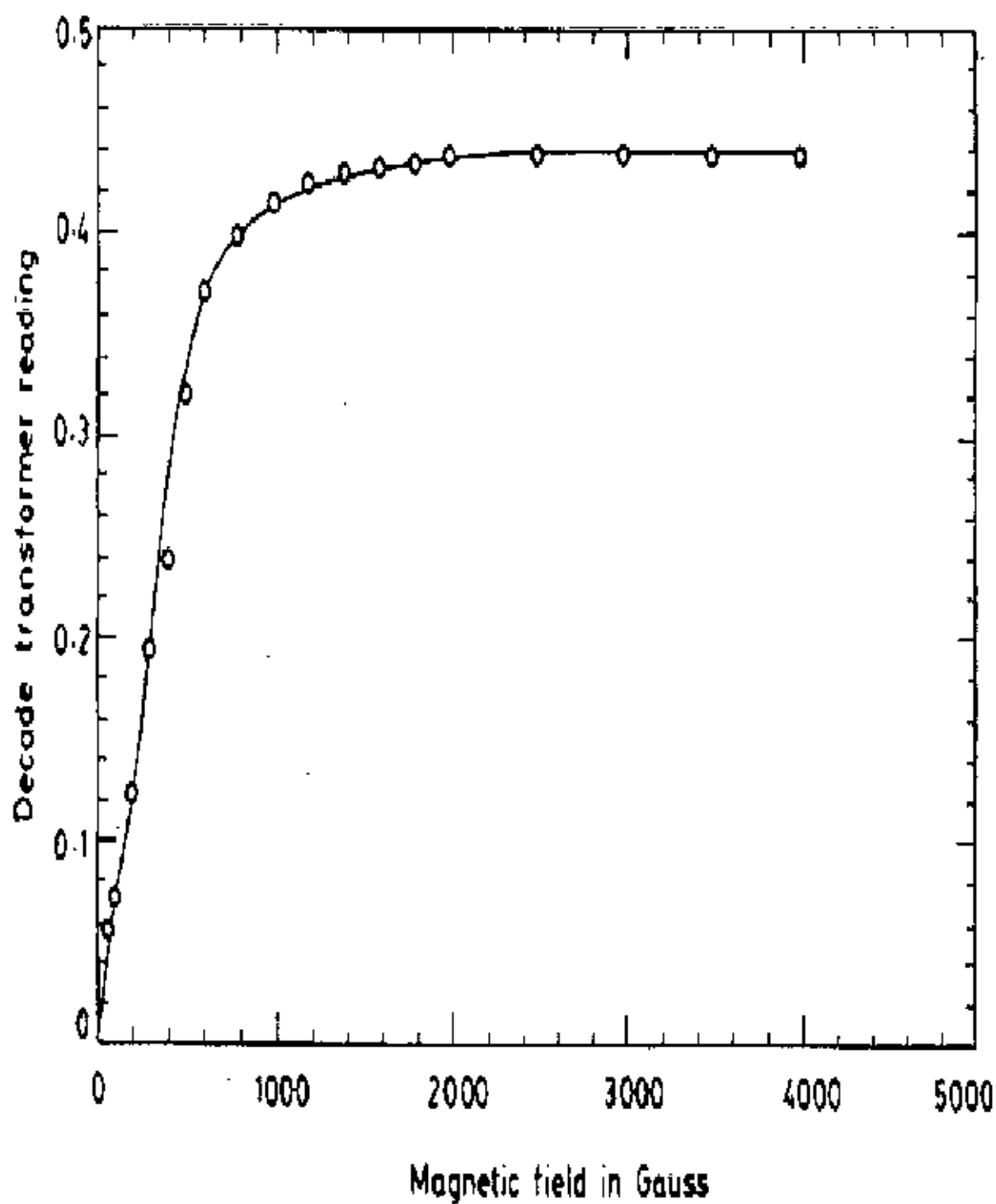


Figure 4.7: Calibration curve of magnetic field vs. decade transformer reading (V.S.M.)

3. Reference signal with direct connection:

$$V_{ref3} = 13 \times 0.1 \text{ mV} = 1.3 \text{ mV} \quad (4.17)$$

- Saturation decade transformer reading for pure Ni at  $200^{\circ}\text{C}$  is given as  $K' = 0.4386$ .
- Specific magnetization for pure Ni at  $200^{\circ}\text{C}$  is given by  $\sigma_s = 54.75 \text{ Am}^2/\text{Kg}$ .
- Mass of the pure Ni-sample  $m = 0.0584 \times 10^{-3} \text{ Kg}$ .
- Magnetic moment  $M = m\sigma = 3.1975 \times 10^{-3} \text{ Am}^2$
- And hence V.S.M. calibration constant is found as

$$K = \frac{m\sigma}{K'} = 7.29 \times 10^{-3} \text{ Am}^2 \quad (4.18)$$

#### 4.3.5 High Temperature Magnetization Measurements

Magnetization measurements at temperature above room temperature were done using a high temperature oven assembly (EG and G, Princeton Applied Research Co.). The oven consists of an electrically heated outer tube assembly with vacuum and reflective thermal insulation. The heater consists of an integral bifilar winding heating coil with a resistance of 80 ohms. The winding is therefore non inducting. The sample holder consists of a quartz tube extension attached to a sample cup. During operation of the high temperature assembly evacuation is accompanied by continuous flow of nitrogen gas to eliminate reaction of the sample with oxygen. A chromel- alumel thermocouple is used as a temperature sensor and the highest temperature that can be achieved is  $500^{\circ}\text{C}$ .

All the measurements of temperature dependence of magnetization were plotted using LI-SEIS make X-Y Recorder model LY18100. The magnetic moment from V.S.M and temperature from the potential differences in volts taken from panel meter are plotted on X-Y recorder. Magnetic moment can also be plotted as a function of time. A graph paper remains struck on

an electrically charged plate during the plotting in X and Y scales are calibrated and can be reduced or enlarged as per need.

## Chapter 5

# RESULTS AND DISCUSSIONS

## 5.1 Differential Thermal Analysis (DTA) Results

Nanocrystalline amorphous ribbons prepared by rapid quenching method have been subjected to differential thermal analysis using a Shimadzu thermal analyzer. The DTA of as-cast samples with a heating rate of  $20^{\circ} C/min$  are presented in fig 5.1 and 5.2. There appears two exothermic peaks, which corresponds to the crystallization of  $\alpha - Fe(Si)$  and  $Fe_3B(Nb)$  phases respectively. DTA is a direct and effective technique for analyzing kinetics of the nanocrystalline materials in respect of phase transitions. The change of composition affects atomic ordering through nucleation and growth of crystallites. The first crystallization phase, with the short range ordering of atoms, is associated with change in the free energy of the system. The long range ordering of atoms depends on the free energy difference between the crystalline state and nanocrystalline amorphous state. The change of composition affects the growth kinetics in a complicated way, which can only be determined experimentally. The composition of the alloy affects both the primary and secondary crystallization phases  $T_{L1}$  and  $T_{T2}$ , because the time needed for the constituent atom to have long range order depends on their bond energies C. L. Chen et. al. [44] and K. Moorjani et. al. [45]. Crystallization phase are affected by the heating rate as well as by composition, the formation of nucleation centers and their growth need to be inhibited to avoid crystallization. Only the effect of composition on the stability of the crystalline amorphous state is thus studied by keeping the heating rate constant.

### 5.1.1 Differential Thermal Analysis (DTA) of Nanocrystalline Samples

The two specimens, sample 1 and 2, with compositions of  $(Fe_{0.9}Co_{0.1})_{73.5}Cu_1Nb_3Si_{13.5}B_9$  and  $Fe_{74}Cu_{1.5}Nb_{2.5}Si_{12}B_{10}$ , respectively have been examined for their stability and crystallization process by Differential Thermal Analysis.

For the sample 1 (Figure 5.1) the crystallization temperature for primary and secondary crystallization occur at temperatures  $635^{\circ} C$  and  $715^{\circ} C$ . Normally Cu and Nb are hardly soluble to the  $\alpha - Fe(Si)$  phase at  $635^{\circ} C$ . Rapid quenching technique forces the Cu and

Nb elements in to the atomic matrix. At high concentration in  $\alpha - Fe$ , which leads to a segregation of Fe and Cu atoms and results in forming Fe-rich and Cu-rich regions. In the Fe-rich region the crystallization temperature is low, so that the nuclei of crystallization can easily be created when the ribbons are thermally annealed. The presence of Nb however creates around the  $\alpha - Fe(Si)$  grains of Nb-rich region with higher crystallization temperature. This may occur at  $715^{\circ} C$ , suppressing the growth of the grains. The secondary crystallization temperature  $T_{x2}$  corresponds to the formation of  $Fe_3B(Nb)$  phase. As a result of doping of Cu and Nb, ultra fine grains are formed which are homogeneously distributed in the body of the nanocrystalline material. This model is in keeping with the finding of M.A. Willard et.al [46]. The primary crystallization temperature  $T_{x1}$  is quite prominent and the secondary crystallization temperature  $T_{x2}$  is not so. This is because, the exothermic reactions corresponding to  $T_{x1}$  is relatively much more vigorous compare to that in  $T_{x2}$ . At higher temperatures there are some endothermic peaks, which can be related to transitions to BCC to FCC structures and complex rearrangement of crystallites in the amorphous matrix. For our magnetization measurements, however, these structural changes are not considered to be important, because magnetic ordering is mainly controlled by sort range order.

For sample 2 (Figure 5.2), two exothermic reactions corresponding to the temperatures  $553^{\circ} C$  and  $683^{\circ} C$  are related to crystallization of  $\alpha - Fe(Si)$  phase and  $Fe_3B$  phase respectively. These peaks are quite broad and prominent. Structural phase change in  $Fe_{74}Cu_{1.5}Nb_{2.5}Si_{12}H_x$  alloys enables us to explain changes in the boundary energy brought about by heat treatment. Both the peaks, which correspond to release of heat at these temperatures, correspond to ordering of atoms. By repeating the DTA of the samples after crystallization it was observed that the results are not reproducible. This is quite expected because the specimens were subjected to irreversible transformations. No magnetic measurements have been done on these samples, as their chemical compositions are undetermined [46].

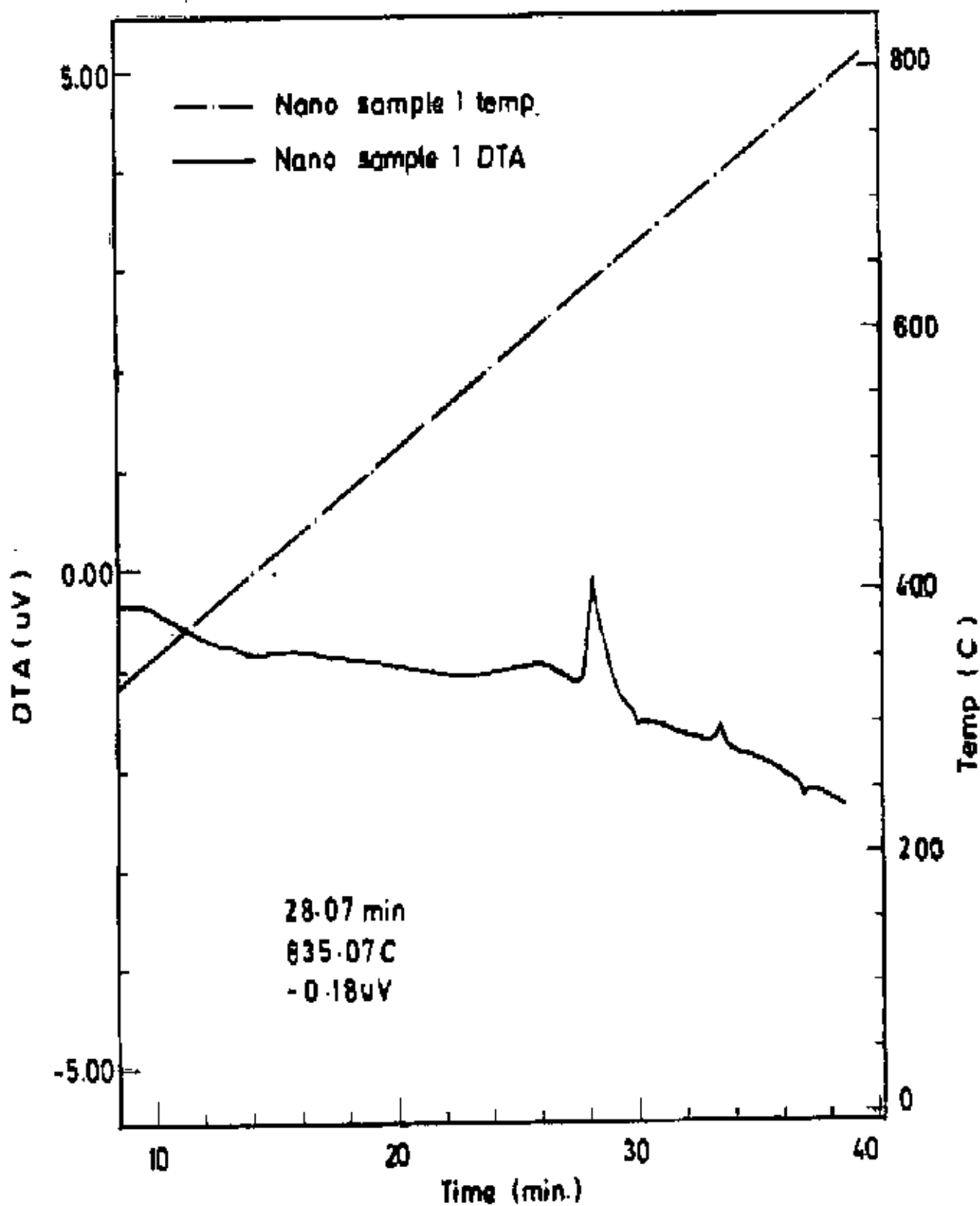


Figure 5 1: Differential Thermal Analysis for Sample 1



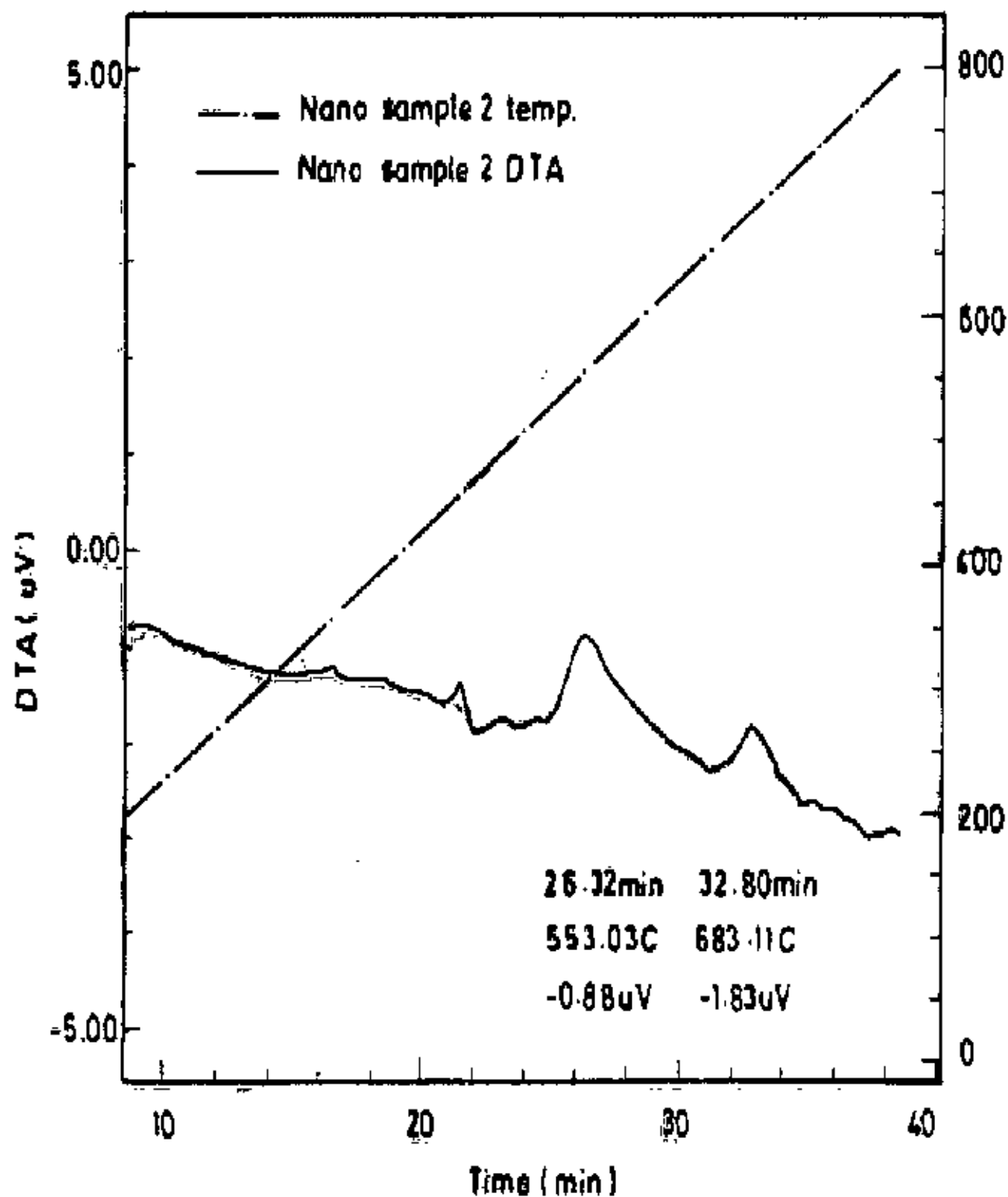


Figure 5.2: Differential Thermal Analysis for Sample 2

## 5.2 Specific Magnetization Measurement of Nanocrystalline Amorphous Ribbons

The magnetization of thin nanocrystalline materials of sample 1 and 2 with compositions of  $(Fe_{0.9}Co_{0.1})_{73.5}Cu_1Nb_3Si_{13.5}B_9$  and  $Fe_{74}Cu_{1.5}Nb_{2.5}Si_{12}B_{10}$ , respectively are measured as a function of magnetic field using a vibrating sample magnetometer (V.S.M) [42]. The ribbon samples were cut into circular shapes, weighed and glued to a standard sample mount. The magnetometer was used as field measuring device, which was not affected by the presence of sample for its low susceptibility. The lock in action of V.S.M yields an accuracy of 0.05% of the full scale. The absolute accuracy of this system is better than 2% and the reproducibility is better than 1%. Least measurable moment is  $5 \times 10^{-4}$  emu. The proportionality constant accounting for the particular coil geometry and susceptibility is obtained by calibration with a high purity circular disk shaped nickel sample. The sample has a saturation moment of about  $54.75 \text{ Am}^2/\text{kg}$  with a saturation flux of about 4 Kg. A relative accuracy of about 1% is obtained with the double coils; the absolute accuracy depends on the calibration method

### 5.2.1 Field Dependence of specific magnetization at room temperature

As prepared nanocrystalline materials with composition of  $(Fe_{0.9}Co_{0.1})_{73.5}Cu_1Nb_3Si_{13.5}B_9$  and  $Fe_{74}Cu_{1.5}Nb_{2.5}Si_{12}B_{10}$  have been studied for their specific magnetization as a function of field at room temperature and is shown in Figure 5.3. Magnetization is also evaluated as a function of field to find the field dependence of magnetization on the domain structure. Specific magnetization is observed to be  $113 \text{ Am}^2/\text{Kg}$  for nanocrystalline ribbon with composition  $(Fe_{0.9}Co_{0.1})_{73.5}Cu_1Nb_3Si_{13.5}B_9$  and  $138 \text{ Am}^2/\text{Kg}$  for nanocrystalline ribbon with composition  $Fe_{74}Cu_{1.5}Nb_{2.5}Si_{12}B_{10}$  at room temperature. The saturation magnetization for these ribbons has higher values for higher percentage of iron. This is quite understandable from the consideration of higher contribution of magnetic moments in iron-rich ribbons, while it is quite consistent with the results of crystalline Co-Fe alloys and is explained as due to higher magnetic moment

of Fe-atoms. The saturation field for both the samples is around 500 Gauss. The experimental data shows that these materials are quite soft magnetically and their magnetizations are almost field independent above 1000 Gauss. The saturation field decreases monotonously with increasing Nb content but the soft magnetic properties are greatly improved with increasing Nb content. This result indicates that the soft magnetic properties are not improved remarkably by the single Nb or Cu addition but are substantially improved by the simultaneous addition of Cu and Nb. It is observed that addition of cobalt by a small fraction i.e. replacing iron by 10% of cobalt decreases the magnetic moment significantly. The increase in specific magnetization of  $Fe_{74}Cu_{1.5}Nb_{2.5}Si_{12}B_{10}$  is quite in keeping with Slater Pauling curve [47].

### 5.2.2 Temperature Dependence of Magnetization of Nanocrystalline Amorphous Ribbons

Temperature dependence of magnetization of the nanocrystalline magnetic specimens is measured by using a V.S.M from room temperature to  $800^{\circ}C$  is shown in Figure 5.4 and Figure 5.5. It is observed that with increasing values of Fe in the nanocrystalline alloy the magnetization increases. The sample temperature was swept with rate of the  $30^{\circ}C/min$  or left steadily at elevated temperatures with fluctuation of the less than  $0.5^{\circ}C$ .

From the results of magnetization as different temperatures  $\frac{dM}{dT}$  has been calculated for the two samples as a function of temperature. These are shown in Figure 5.6 and Figure 5.7 for samples 1 and 2, respectively. From the maximum value of the slopes of the  $\frac{dM}{dT}$  VS. temperature, the Curie temperatures have been calculated. The Curie temperatures for the samples 1 and 2 are found to be  $595^{\circ}C$  and  $655^{\circ}C$  respectively from the magnetization VS. temperature slopes. However, the determination of the Curie temperatures is a bit uncertain because these materials are not single-phase materials. At high temperatures there is segregation of iron and cobalt and Fe-Co alloy crystallites, which have different Curie temperatures. Moreover each of two systems 1 and 2 are composites because the nanocrystals are embedded in amorphous matrix. The experimental curves however show smooth variation of slopes with asymptotic

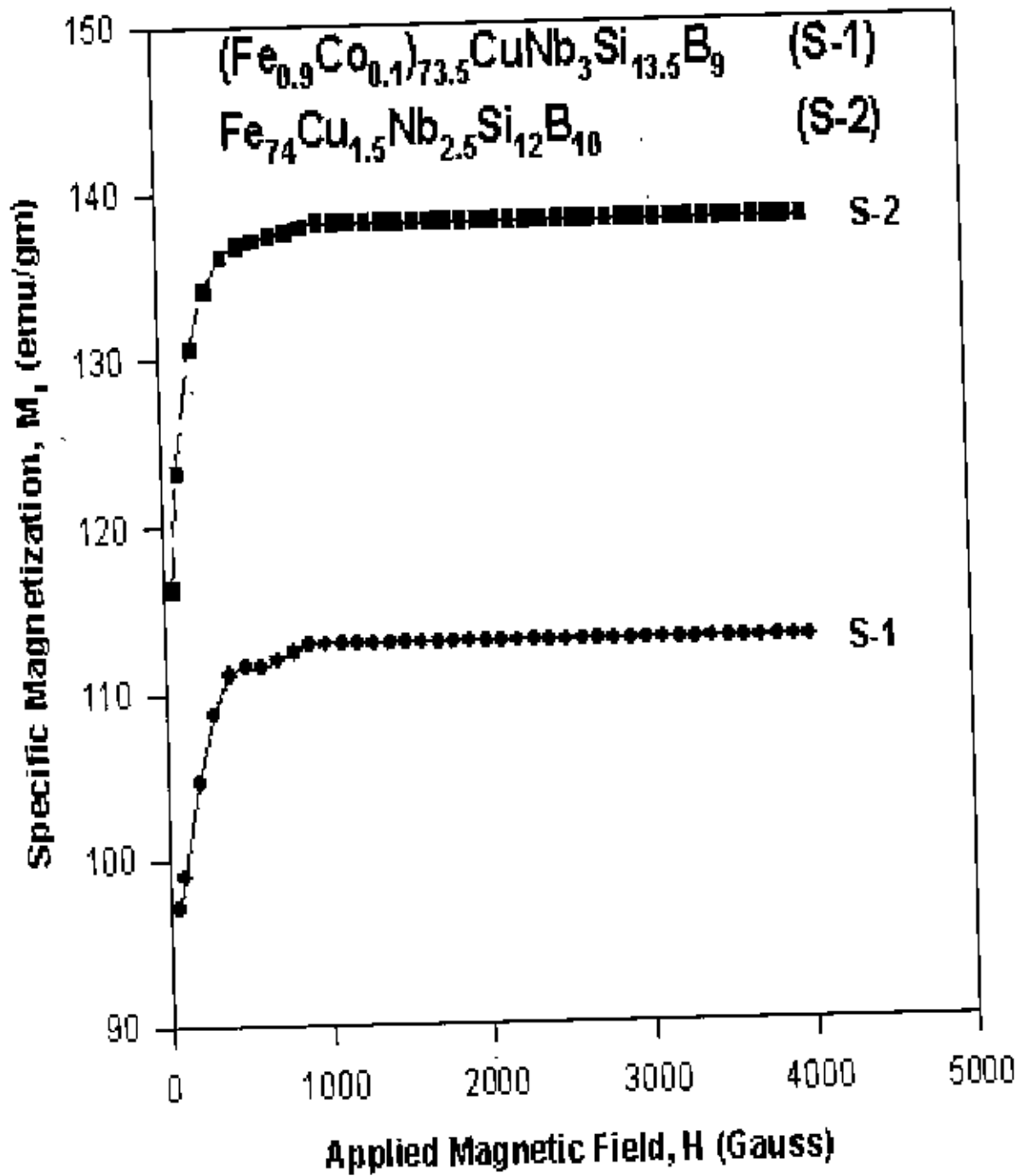


Figure 5.3: Magnetization Vs. Applied Magnetic Field for Samples 1 and 2

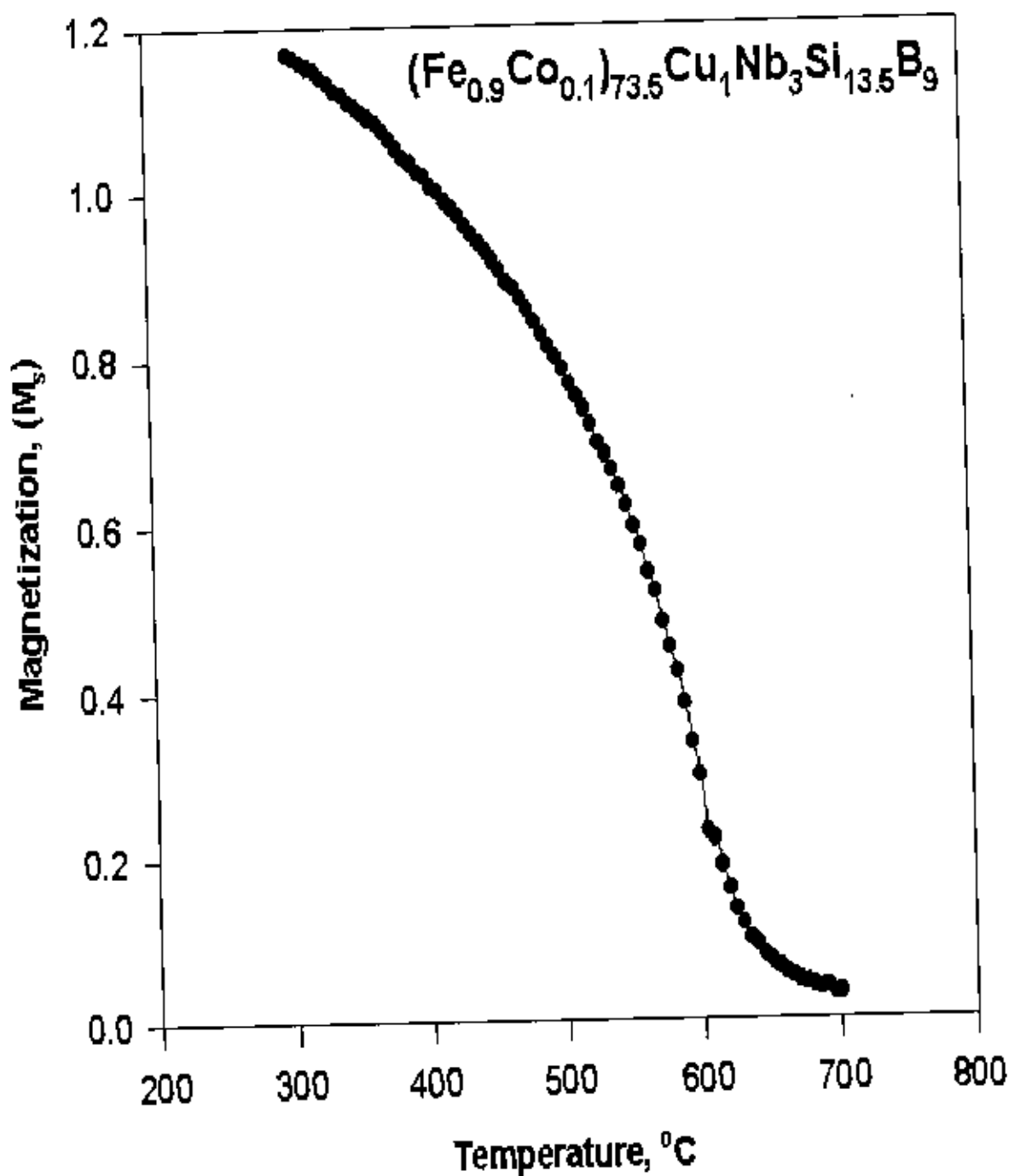


Figure 5.4: Magnetization Vs. Temperature for Sample 1

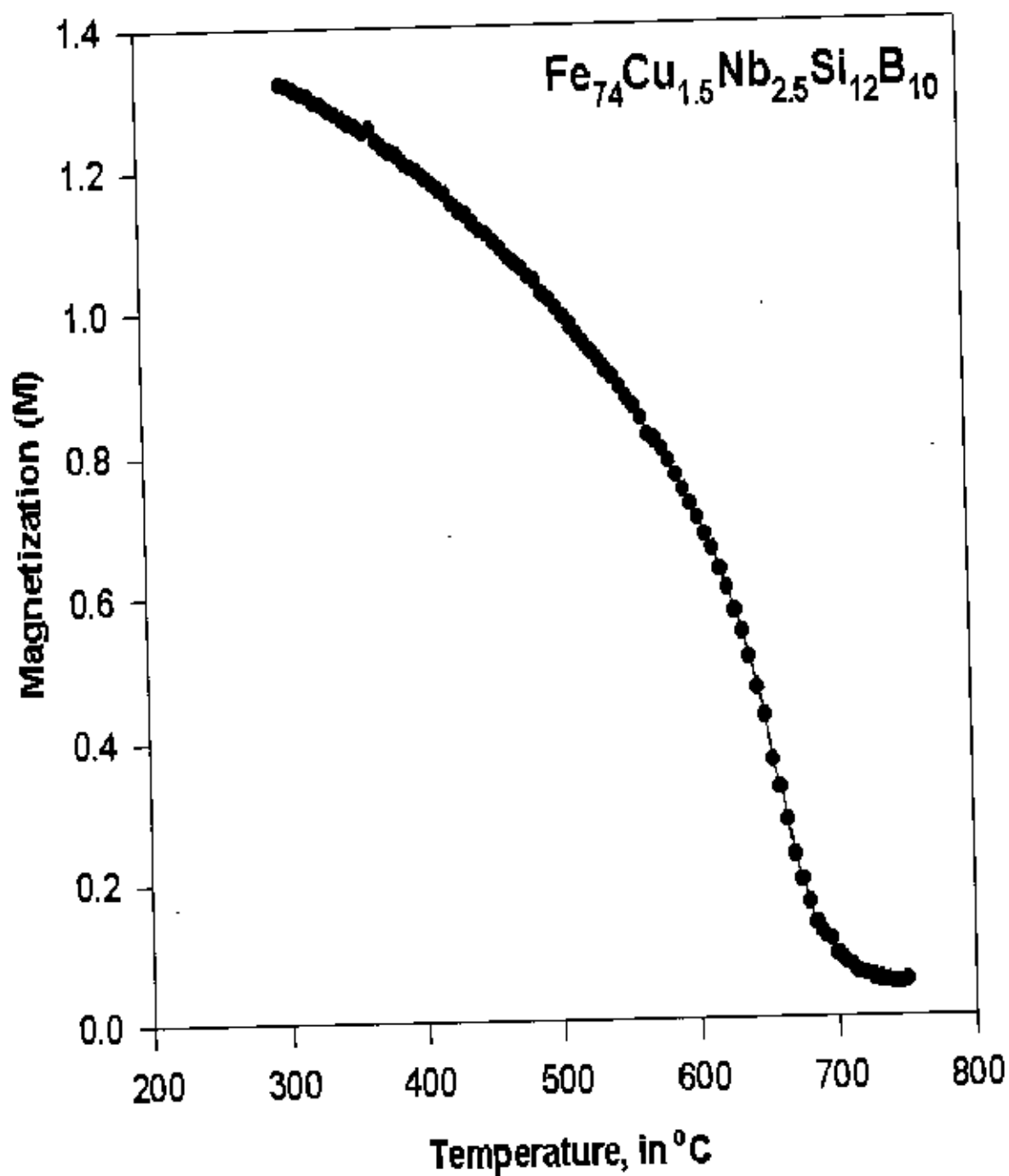


Figure 5.5: Magnetization Vs. Temperature for Sample 2

nature around  $700^{\circ}C$ . Although the  $T_c$  of Co ( $1057^{\circ}C$ ) is higher than that of Fe ( $770^{\circ}C$ ) in the amorphous state, exchange interaction between the magnetic ions is increased by the replacement of Co by  $Fe_3$  quite contrary to the crystalline state. Since the exchange interaction in the nanocrystalline magnetic material is of the RKKY type, which occurs via the conduction electron, the distance from magnetic atoms is very important. It is thus likely that Fe-based metallic glass can be gained by adding to the traditional alloy composition small amounts of Cu and Nb. Temperature dependence of Finemet amorphous ribbons leads to a ferromagnetic transition temperature up to certain range. There is a good correlation between crystallization phase transformations as obtained from Figure 5.1 and Figure 5.2 and  $T_c$  obtained from Figure 5.4 and Figure 5.5 for two samples. The former ferromagnetic transition temperature is ascribed to the Curie temperature of amorphous matrix and the latter to the one  $\alpha - Fe(Si)$  nanocrystalline particles.

### 5.3 Dynamic Magnetic Properties of Nanocrystalline Amorphous Magnetic Materials

Dynamic magnetic properties of as-quenched nanocrystalline samples 1 and 2 with compositions  $(Fe_{0.9}Co_{0.1})_{73.5}Cu_1Nb_3Si_{13.5}B_9$  and  $Fe_{74}Cu_{1.5}Nb_{2.5}Si_{12}B_{10}$ , respectively have been determined using LF impedance analyzer (LF impedance analyzer, 4192A, Range 5 Hz -13MHz, Agilent Technologies Japan limited, Japan). Frequency spectrum of complex magnetic characteristics, like real and imaginary parts of initial permeability, loss factor and relative quality factor are analyzed. Frequency measurements were performed with an impedance analyzer, in the range 0.1 KHz to 13 MHz at room temperature with very low field ( $H = 0.1 A/m$ ). All the starting as-quenched samples were nanocrystalline and their magnetic properties vary little with Nb concentration, while the complex permeability of the samples changed largely due to annealing. Nanocrystalline sample with low percentage of Nb loosed the soft magnetic property, so that its complex permeability spectrum changes the corresponding values of the as-quenched state. On the contrary our sample with 2.5 to 3%Nb, the thermal treatment improved very much

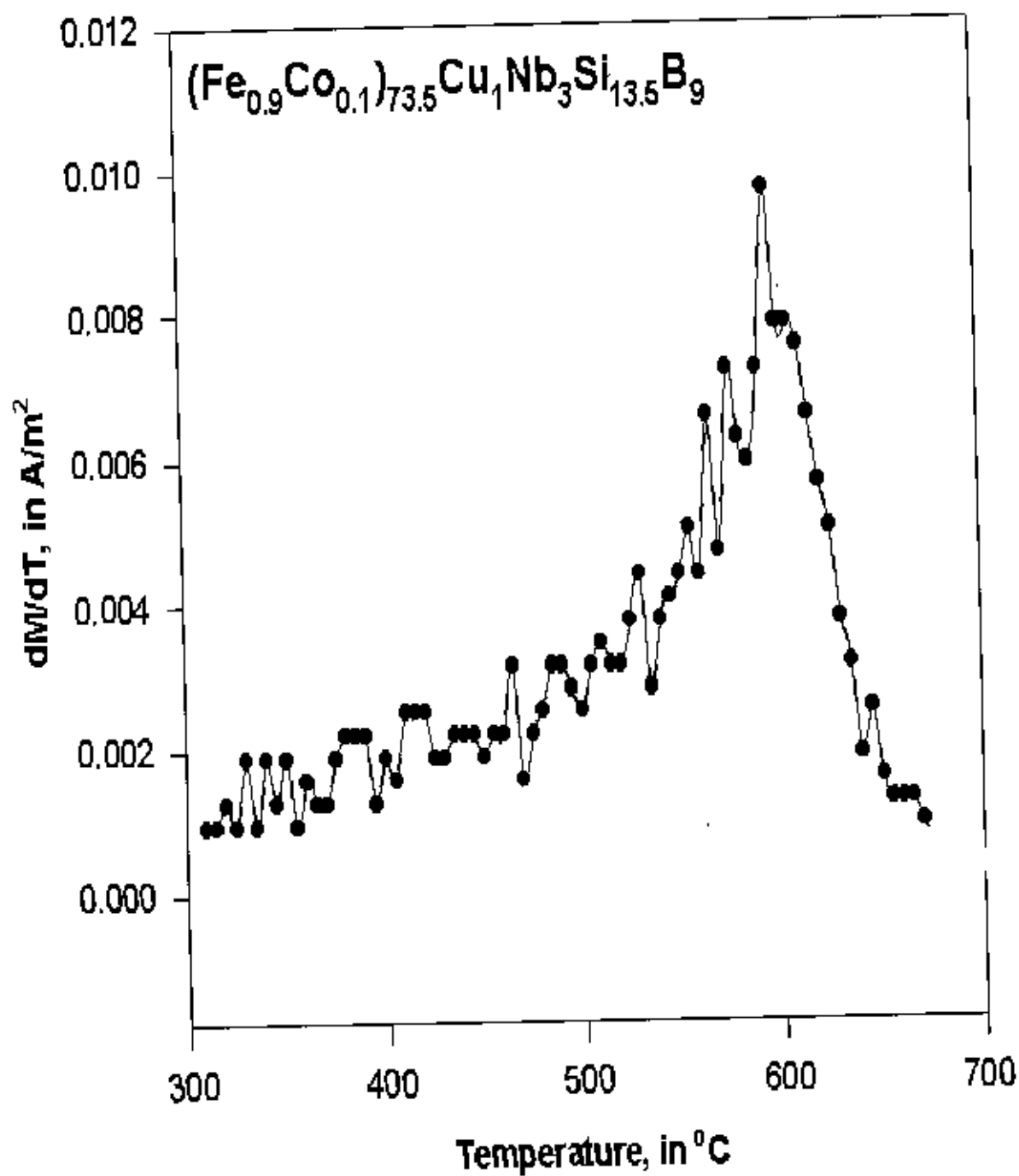


Figure 5.6:  $\frac{dM}{dT}$  VS. Temperature for Sample 1



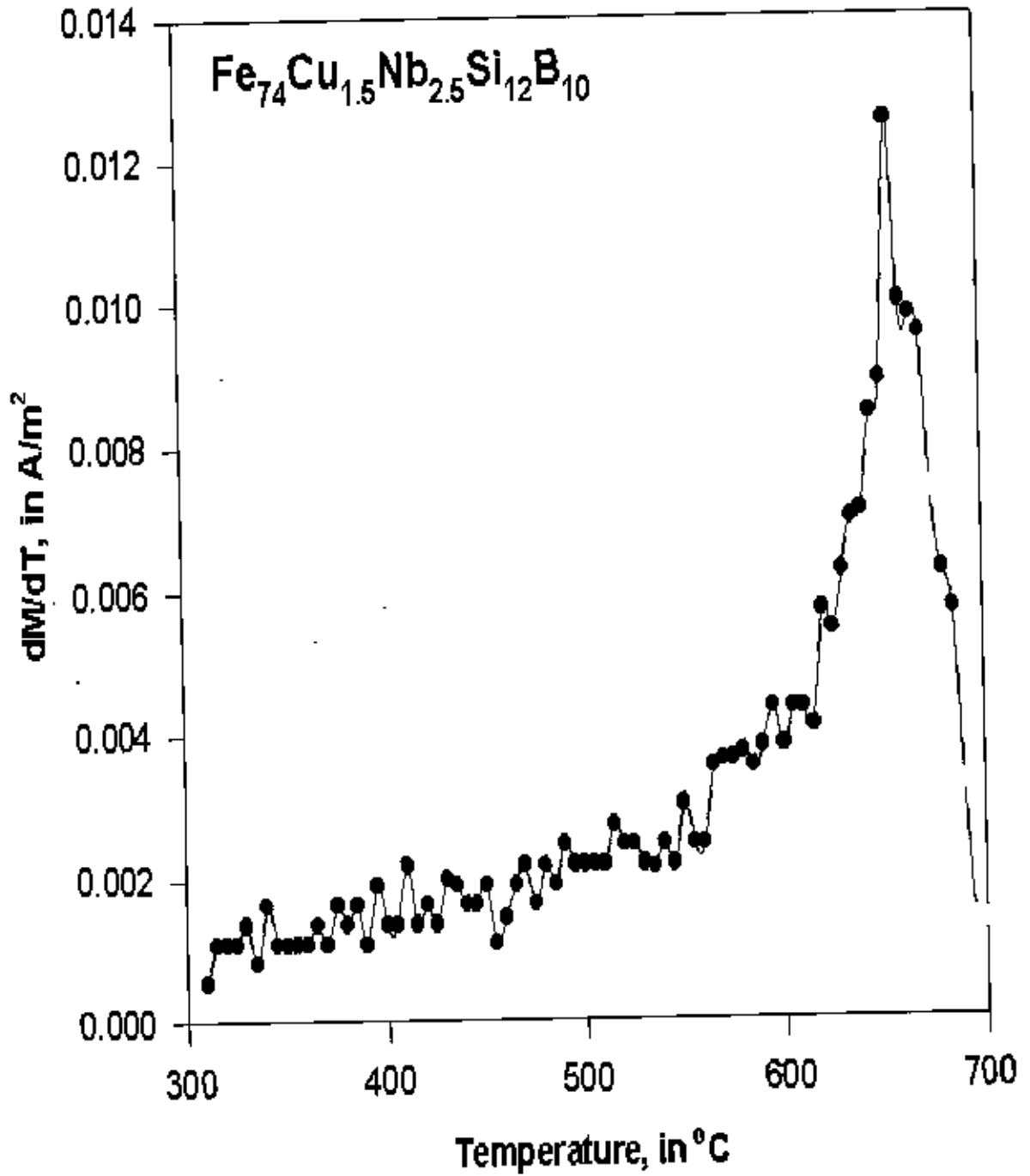


Figure 5.7:  $\frac{dM}{dT}$  VS. Temperature for Sample 2

the basic soft magnetic properties. Our idea is that the ultra fine grains might be produced if the composition is fluctuated in the alloy, because the fluctuation can create many nuclei sites, which become the nuclei of the crystals in the alloys. Cu is preferable additive to form these nuclei sites, but it is hardly solid soluble in Fe at room temperature. However, some amount of Cu can be forcedly dissolved by means of a rapid quenching technique, and nanocrystalline grain structure can be achieved. As nanocrystalline amorphous ribbon can be obtained from thin ribbons as in the case of amorphous ribbons, it is inferred from its low eddy current loss that the high initial permeability and low core loss in the high frequency range are achieved. The core loss of nanocrystalline sample is smaller than those of the Fe-based alloys and ferrites. The annealing temperature and annealing time are both important parameters in controlling the frequency spectrum response of permeability of the nanocrystalline sample as observed from the results of Figure 5.8 and Figure 5.9. The effect of annealing on complex permeability arises because two factors of apparently opposite nature influence the permeability. One is the removal of local defects in homogenously and stresses that hinder the movement of domains by pinning effect and the other is the growth of the nucleation centers of crystallites that also hinders the movement of domain walls. Since effect of annealing is to remove the pinning centers of the first kind and to enhance the growth of the pinning centers of the second kind, the result of annealing depends on the composition of the nanocrystalline amorphous ribbons and the conditions of preparation of the as-quenched samples.

### 5.3.1 Frequency Dependence of the Real Part of Complex Permeability of composition of $(Fe_{0.9}Co_{0.1})_{73.5}Cu_1Nb_3Si_{13.5}B_9$ with Different Annealing Temperature and Annealing Time

The real part of complex permeability of nanocrystalline soft magnetic sample with composition of  $(Fe_{0.9}Co_{0.1})_{73.5}Cu_1Nb_3Si_{13.5}B_9$  has been measured as a function of frequency from 100 Hz to 13 MHz using impedance analyzer. The measurement has been done on as-cast specimen and also on samples annealed at  $200^{\circ}C$  for one hour, at  $450^{\circ}C$  for one hour and at  $450^{\circ}C$

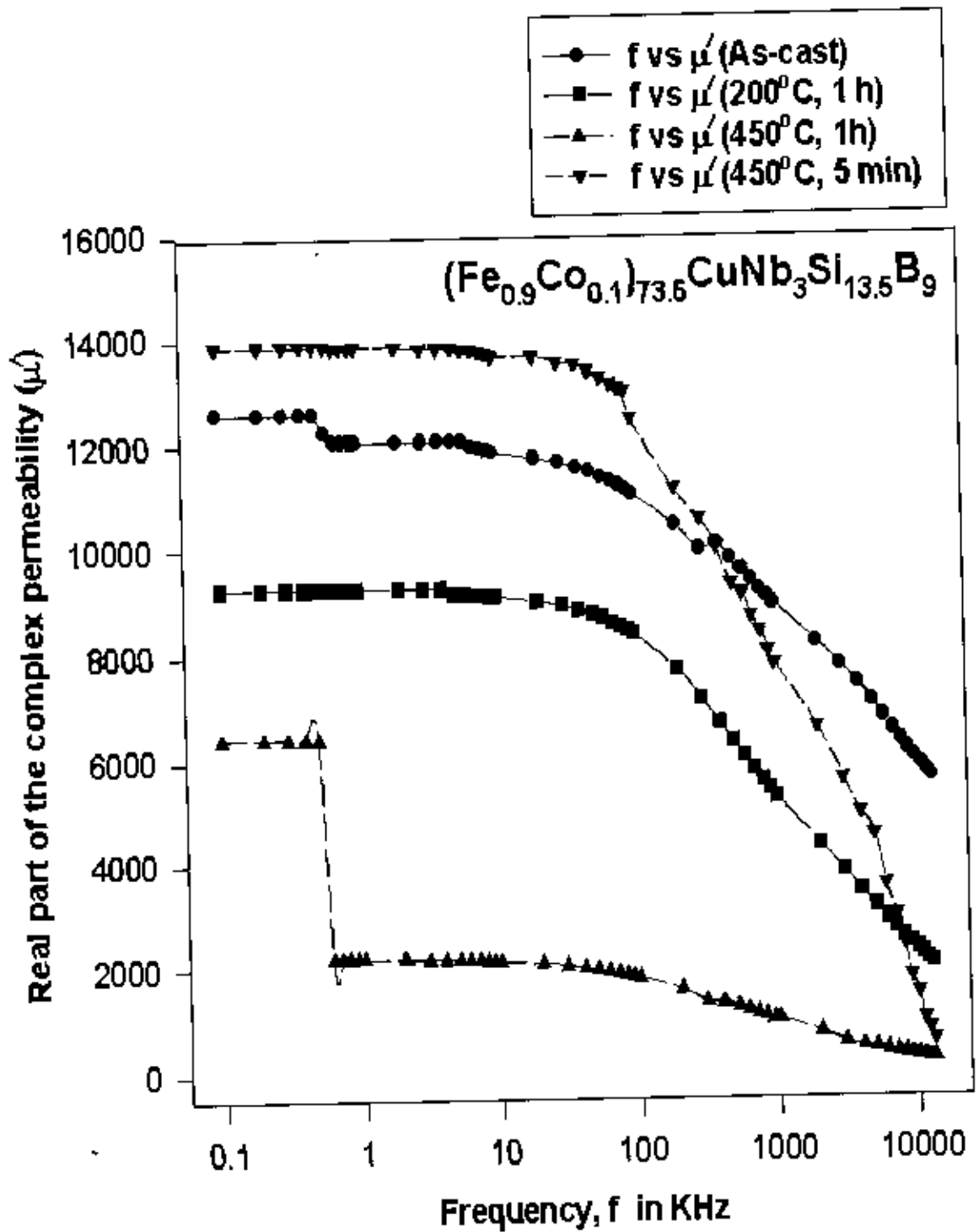


Figure 5.8: Real Part of Complex Permeability Vs. Frequency for Sample 1

for 5 minutes. The annealing process leads to the increase of the grain size. However, with concentration of Nb = 3%, the grain size increases slowly with annealing temperature  $450^{\circ} C$  and annealing time 5 minutes, whereas with the increase of the annealing time there is an increase of the grain size of nanocrystalline samples. These confirm the role of Nb in the delay growth of the  $\sigma - Fe(Si)$  phase. The purpose of this experiment was to determine empirically the optimum annealing temperature, annealing time corresponding to maximum permeability, constancy of the permeability and maximum frequency range over which the sample can be used as soft magnetic material. Figure 5.8 representing the results show that as-cast specimen has high relative permeability of 12500 at 100 Hz. At 1 KHz there is a slight drop in permeability but the value remains above 11500 up to 100 KHz, decreasing rather slowly and smoothly. At 13 MHz frequency, permeability goes down to 6000. The specimen annealed at  $200^{\circ} C$  for 1 hour reduces the permeability to 9500. However, the frequency dependence becomes more smooth remaining almost constant up to 100 KHz and then falling at a constant rate to a value of 2200 at 13 MHz. The sample annealed at  $450^{\circ} C$  for 1 hour brings a sudden drop from 6200 to 2000 in permeability around 900 Hz and the overall permeability has a low value in the range of 1 KHz to 13 MHz. The best response of the sample is obtained when the annealing temperature  $450^{\circ} C$  and annealing time is only 5 minutes. The maximum permeability realized is 14000, which remains almost uniform up to 100 KHz. Beyond this frequency permeability falls more sharply than the as-cast specimen and the value becomes only 2000 at 13 MHz. Interestingly this value of the permeability at 13 MHz is the same for both the specimens annealed at  $450^{\circ} C$  but with different annealing time, the interval being 1 hour and 5 minutes respectively. The frequency response of the samples annealed at different temperatures can in general be explained in terms of the growth of crystallites and their size distributions. The increase in permeability due to annealing at  $450^{\circ} C$  for 5 minutes indicates that this high temperature annealing removes the local defects as created during the preparation of the sample, which facilitates the domain wall movement. This explains the permeability response of (Fe-Co)CuNbSiB-alloy with Nb content of 3%, annealed at  $450^{\circ} C$ . The initial permeability is a maximum and the soft magnetic

properties are good. However, the size of the crystals are related to their response to frequency, since each crystallite is coupled to the matrix with a stiffness constant giving rise to its own natural frequency. The nature of the frequency dependence of permeability of a specimen at different temperature may be explained in terms of grain growths as controlled in a complex way by annealing temperature and annealing time. The best performance of the sample annealing at  $450^{\circ}C$  but with annealing time of only 5 minutes indicates that annealing temperature and annealing time are both very critical and can be obtained only empirically by trial and error method

### 5.3.2 Frequency dependence of the Real Part of Complex Permeability of composition of $Fe_{74}Cu_{1.5}Nb_{2.5}Si_{12}B_{10}$ with Different Annealing Temperature and Annealing Time

Magnetic permeability for its real part has been measured in a nanocrystalline sample of composition  $Fe_{74}Cu_{1.5}Nb_{2.5}Si_{12}B_{10}$  for different frequencies in the range 100 Hz to 13 MHz. The results of the as-cast sample and samples annealed at temperatures  $200^{\circ}C$ ,  $350^{\circ}C$ ,  $550^{\circ}C$  for 5 minutes each, are shown in Figure 5.9. The results for annealing time 1 hour are shown in Figure 5.10. When the annealing time was 5 minutes, the results show that there is consistent increase in the permeability value with increasing annealing temperature. From the constancy and high value of permeability over a long range of frequency the best annealing temperature is found to be  $550^{\circ}C$ . The permeability remains as high as 12000 up to the frequency 1000 KHz for this sample. The values of the initial permeability were determined for frequencies up to 1000 KHz for this sample, which was annealed in the optimum regime. This alloy is suitable for making magnetic core in the pulse transformer, which works well at frequencies around 40-60 KHz. The permeability then falls sharply with increasing frequency. For other annealing temperatures the samples show decreasing permeability with increasing frequency. These results can be explained as due to different distributions of nanocrystals in respect of their volumes. When the grain sizes are such that they respond to different frequencies differently because of

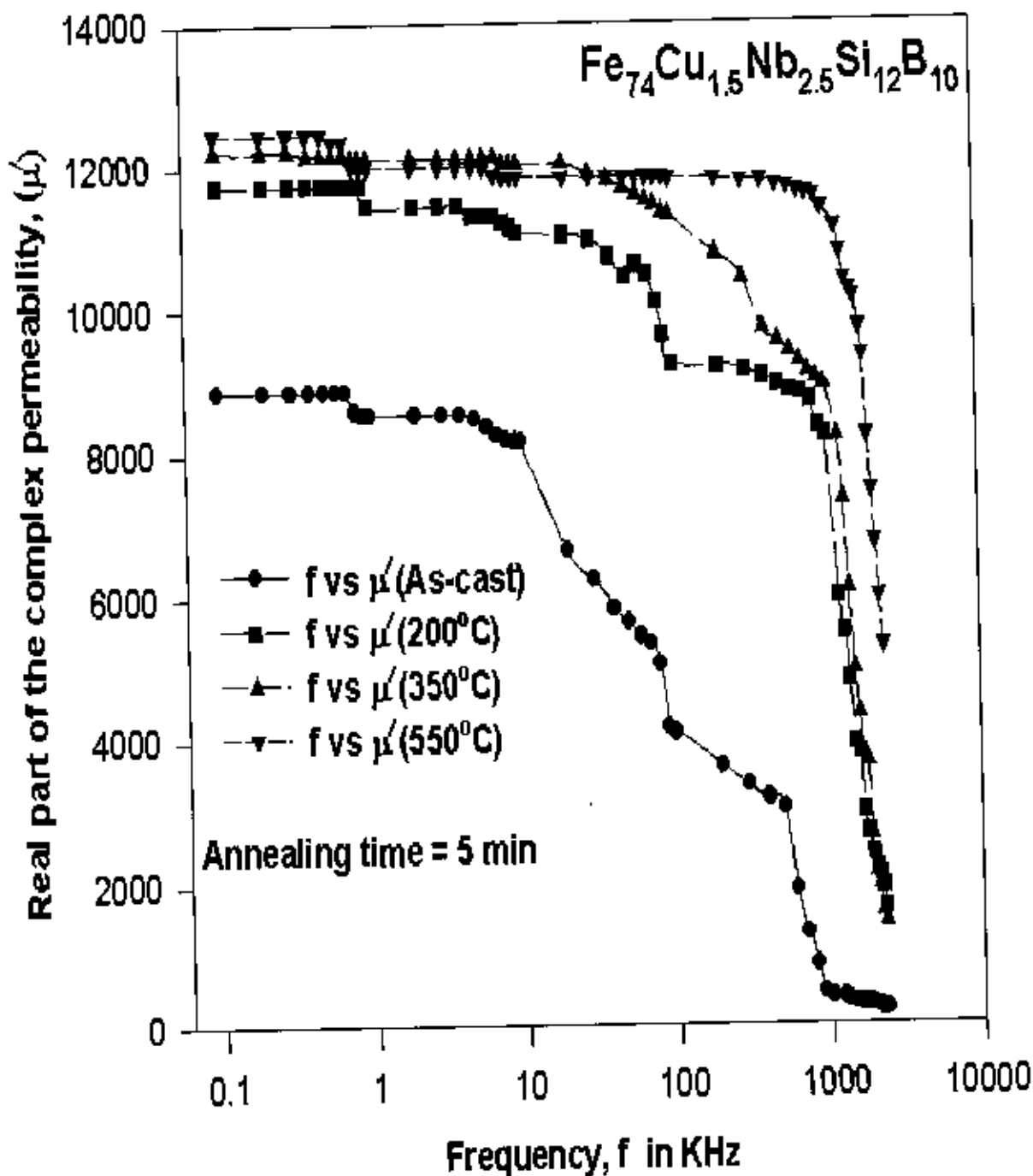


Figure 5.9: Real Part of Complex Permeability Vs. Frequency for the as-cast sample and samples annealed at temperatures  $200^\circ\text{C}$ ,  $350^\circ\text{C}$ ,  $550^\circ\text{C}$  for 5 minutes each

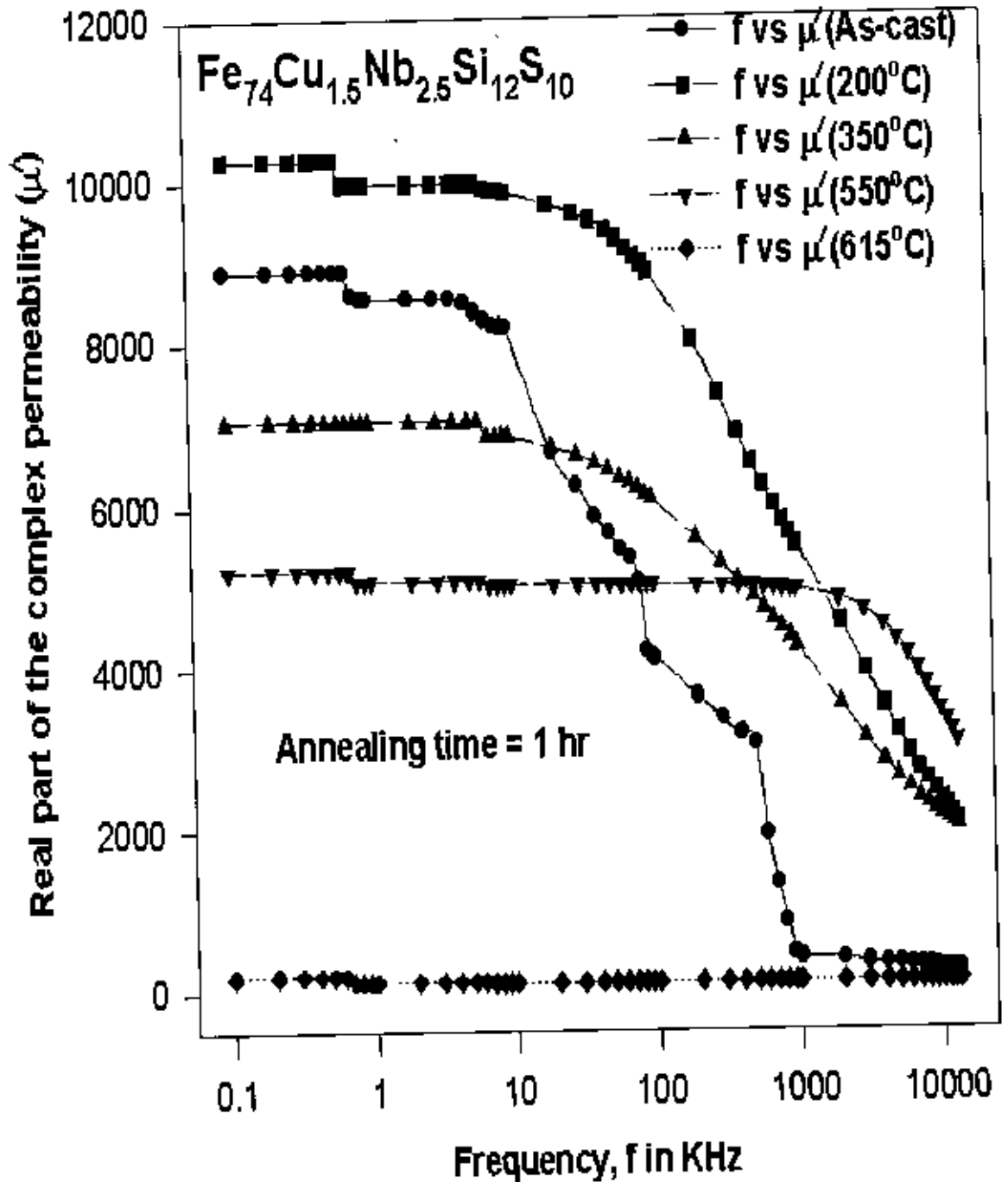


Figure 5.10: Real Part of Complex Permeability Vs. Frequency for the as-cast sample and samples annealed at temperatures 200°C, 350°C, 550°C for 1 hour each

their different natural frequencies, we can get frequency dependence of permeability. With the annealing time of 1 hour the annealing temperatures were taken as  $200^{\circ}C$ ,  $350^{\circ}C$ ,  $550^{\circ}C$ , and  $615^{\circ}C$ . We observed maximum permeability for the sample annealed at  $200^{\circ}C$ . The initial permeability was measured for the alloys annealed for 1 hour with annealing temperature up to  $615^{\circ}C$ , with boron content the magnetic hardening occurs. It can be expected that Nb concentration increases the size as well as the magnetocrystalline anisotropy as a result the permeability decreases, the value being 10200 in the low frequency range. The performance of this annealed sample is better than as-cast sample and with increasing annealing temperature the permeability is observed to decrease. There is a drastic fall in permeability, when the annealing temperature is  $615^{\circ}C$ . However, in respect of uniformity of permeability with frequency independent value, the sample annealed at  $550^{\circ}C$  is the best in its performance. Although the permeability is 5200 for this sample, this value remains constant over the frequency range 100 Hz to 1000 KHz.

From the results of Figure 5.8 and Figure 5.9 it is evident that annealing temperature and annealing time are both important parameter in controlling the frequency response of permeability of the sample. The best choice of these two parameters depends on the desired characteristics of the material in respect of permeability value and its frequency dependence.

### 5.3.3 Frequency Dependence of Imaginary Part of the Complex Permeability of composition $(Fe_{0.9}Co_{0.1})_{73.5}Cu_1Nb_3Si_{13.5}B_9$ with Different Annealing Temperature and Annealing Time

The effect of heat treatment on the complex permeability and its frequency dependence for the sample of composition of  $(Fe_{0.9}Co_{0.1})_{73.5}Cu_1Nb_3Si_{13.5}B_9$  is shown in Figure 5.11. These results are quite complimentary to the results for the real part of the complex permeability of the sample. The usefulness of the results of complex permeabilities lie in the determination of the quality factor of the sample. The complex permeability for all the samples at low frequencies has relatively high value and corresponds to high loss factor and lower quality factor as shown



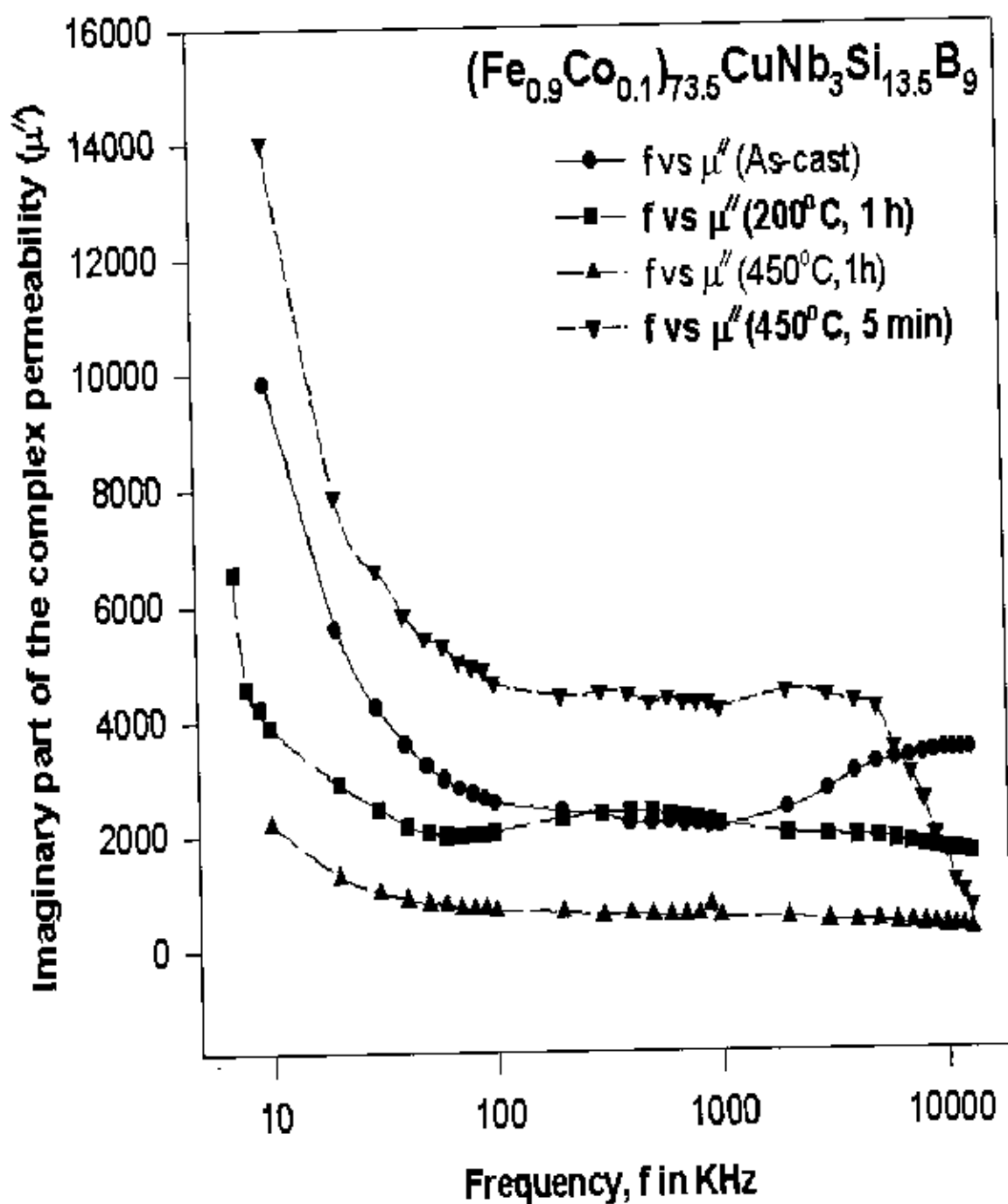


Figure 5.11: Imaginary Part of Complex Permeability Vs. Frequency for Sample 1

in Figure 5.12 and Figure 5.13.

### Relative Quality Factor

The frequency dependence of relative quality factor of the different annealed samples are shown in Figure 5.12. The relative quality factors as controlled by the real part of the initial complex permeability have quite high value in the range 75 KHz to 3 MHz for as-cast sample and 50KHz to 500KHz for the sample annealed at  $400^{\circ}C$  with 5 minutes as annealing time. The quality factor of the as-cast sample appears to be the highest in the range 50 KHz to the highest frequency. However, from the consideration of the uniformity of the quality factor with respect to the frequency, the sample annealed at  $450^{\circ}C$  for 5 minutes is quite satisfactory.

### Loss Factor

The results of the loss factor of the samples annealed at different temperatures are shown in Figure 5.13. The frequency range within which the loss factor has a reasonable low value is from 50 Hz to 1000 KHz. Loss factor has high value both in the low frequency range and high frequency range. The origin of the loss factors can be attributed to various domain defects, which include non-uniform and non-repetitive domain wall motion, domain wall bowing, localized variation of the flux density and nucleation and annihilation of domain walls. At low frequencies the loss is controlled by hysteresis losses and at high frequency the flux penetration becomes low and loss is controlled mainly by interaction between the grains. This can be explained as due to the increase in phase lag between the applied field and the induced magnetic flux. The natural frequencies of the domains in respect of the response to external field differ from the frequency of the applied field in this frequency range.

### Real Part vs. Imaginary part of the complex permeability with composition ( $Fe_{0.9}Co_{0.1}$ )<sub>73.5</sub>Cu<sub>1</sub>Nb<sub>3</sub>Si<sub>13.5</sub>B<sub>0</sub>

The ratio of  $\mu'$  and  $\mu''$  is shown in Figure 5.14. For the value of  $\mu'$  from 5000 to 11000 the complex permeability  $\mu''$  lies between 2000 to 4000 and as such remain quite steady. For low

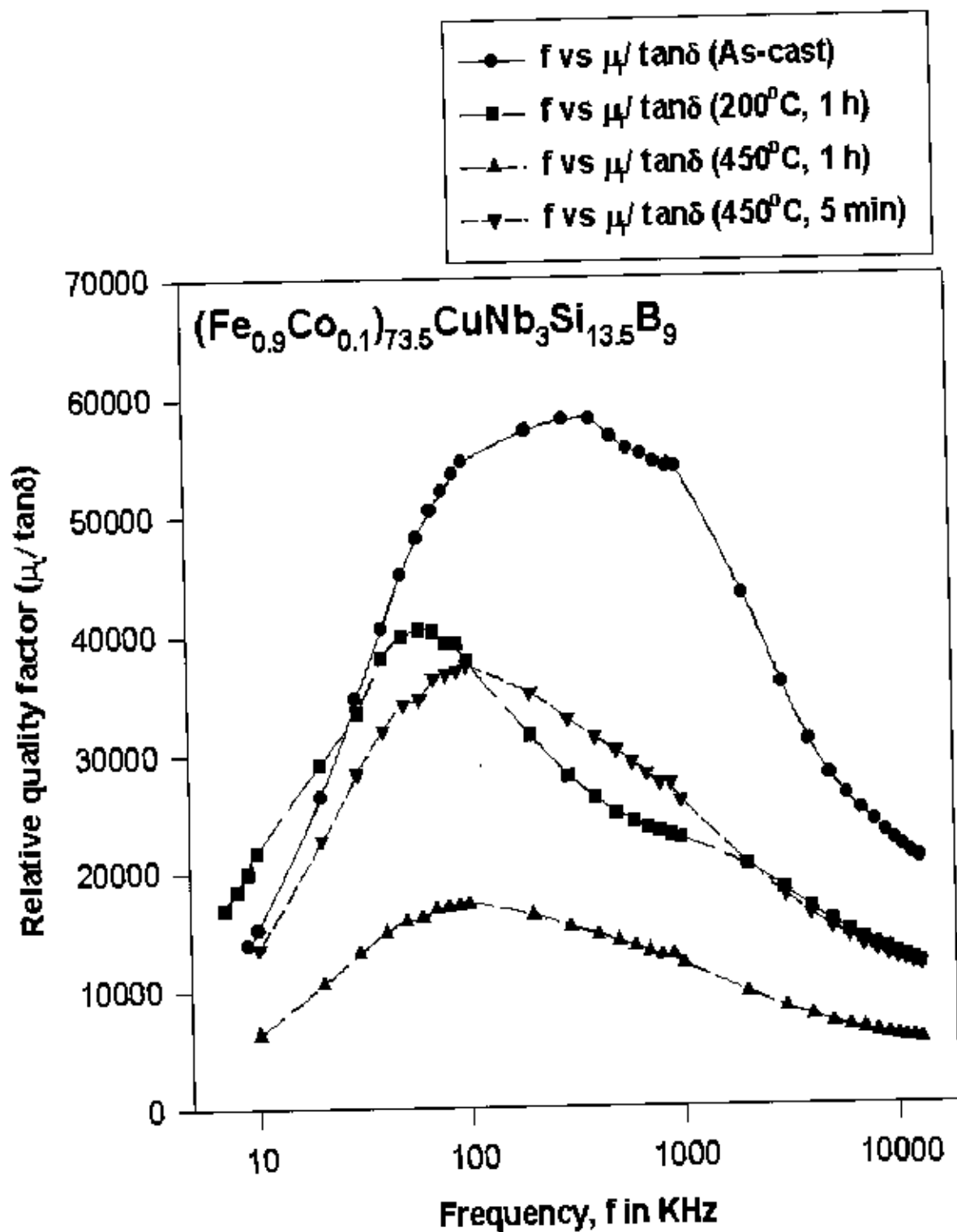


Figure 5.12: Relative Quality Factor Vs. Frequency for Sample 1

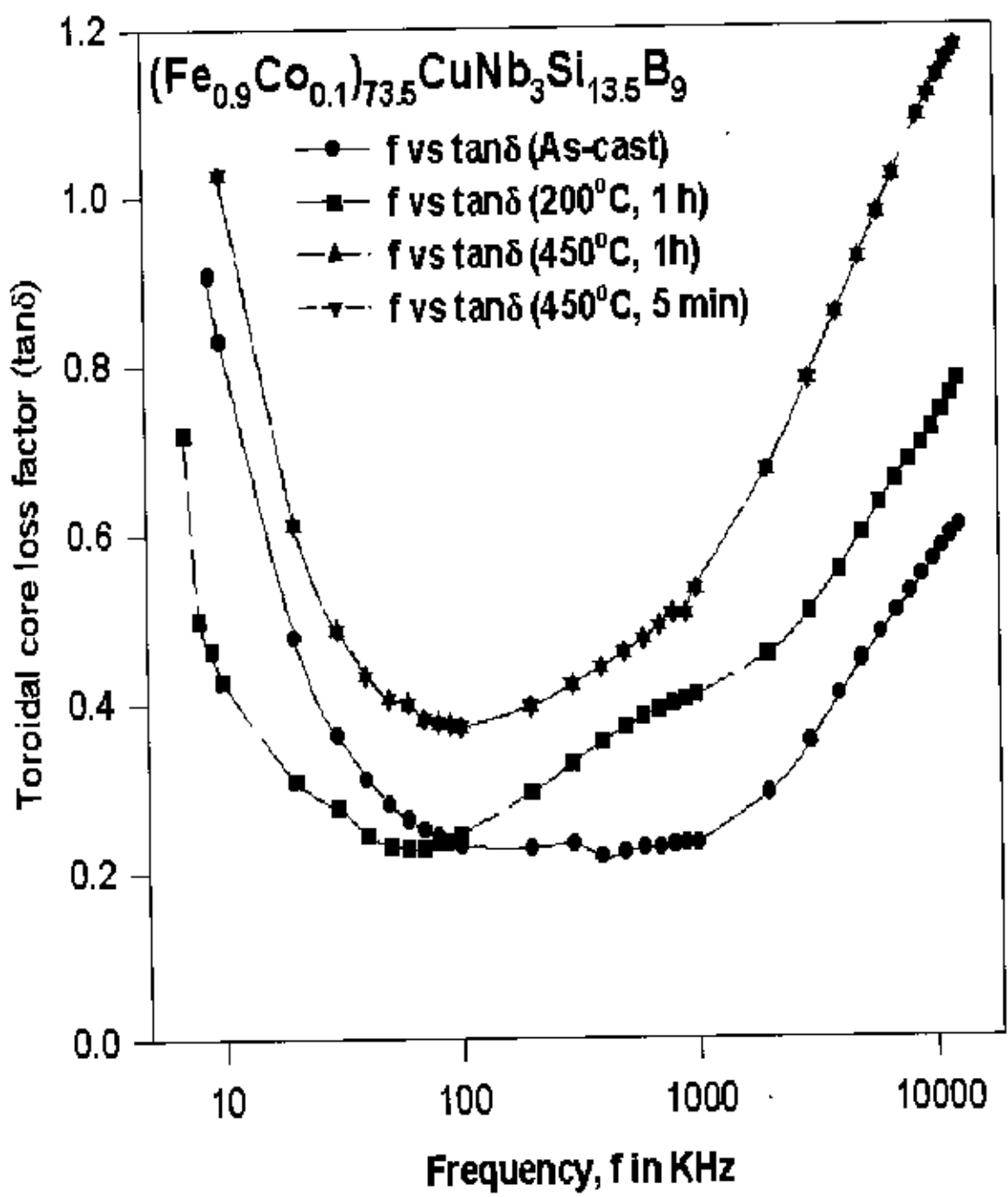


Figure 5.13: Toroidal Core Loss Factor Vs. Frequency for Sample 1

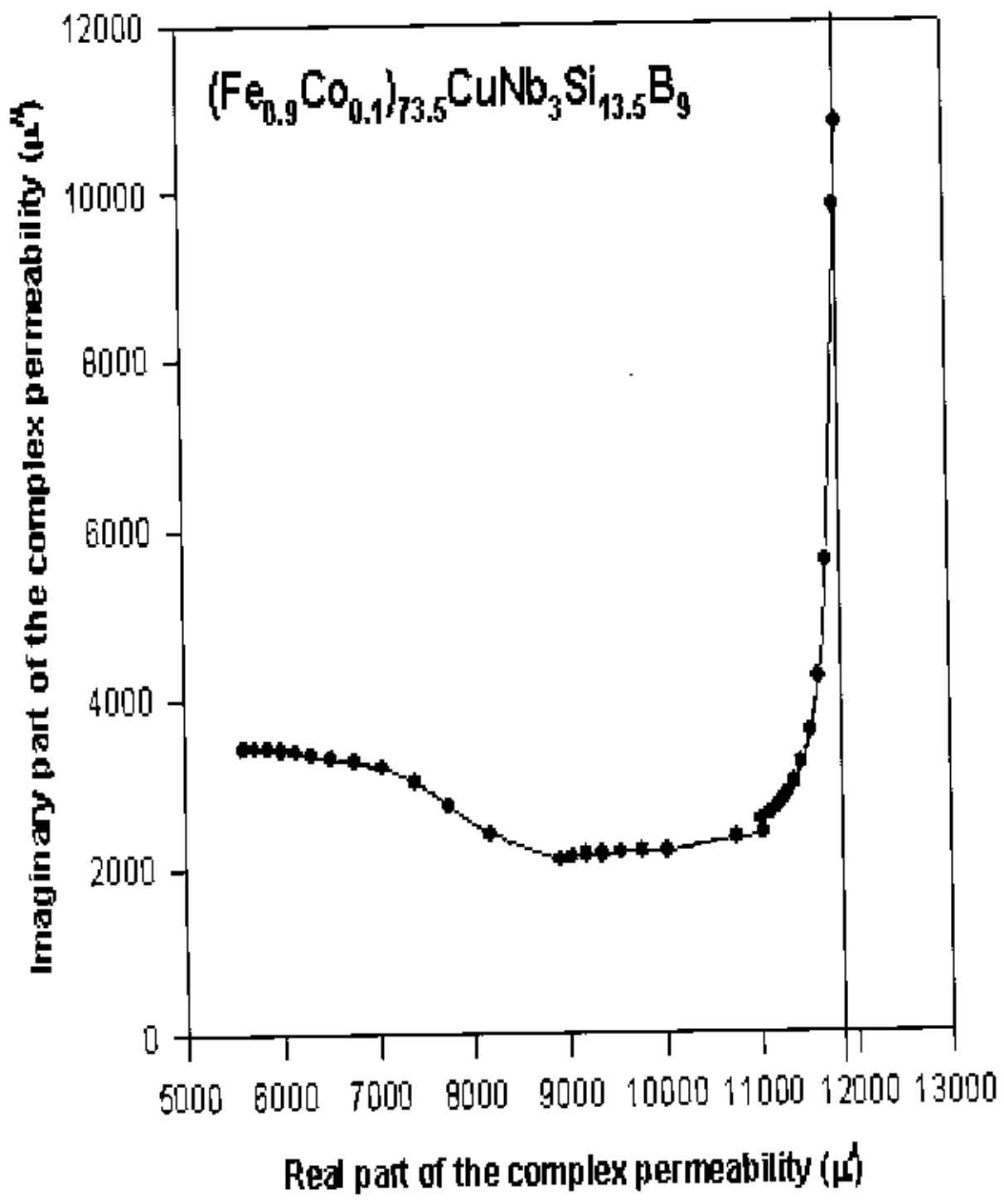


Figure 5.14: Imaginary Part Vs. Real Part of Complex Permeability for Sample 1



frequencies, if the applied field is lower than or equal to propagation field, a short vertical line is observed. The initial permeability is determined as 12595. The complex permeability increases sharply beyond 11000, from its relatively steady value of 3000. While the real permeability changes from 11000 to 12000 the complex permeability increases from 3000 to 11000 in the transition region. This curve provides complementary information in respect of loss factor and the range of the real part of the complex permeability. One can therefore find out the range of permeability, which can be obtained without having excessive loss.

### 5.3.4 Frequency Dependence of Imaginary Part of the Complex Permeability of composition $Fe_{74}Cu_{1.5}Nb_{2.5}Si_{12}B_{10}$

Figure 5.15 shows the frequency dependence of  $\mu''$  for the as-cast sample and samples annealed at  $200^{\circ}C$ ,  $350^{\circ}C$  and  $550^{\circ}C$  with annealing time of 5 minutes each. Annealing for 5 minutes increases the value of  $\mu''$  for all the annealed samples compare to the as-cast sample. The frequency dependence of  $\mu''$  of the samples annealed at different temperatures can be attributed to the growth and distribution of the crystallites.

Figure 5.16 shows the variation of  $\mu''$  with frequency for different samples annealed at  $200^{\circ}C$ ,  $350^{\circ}C$ ,  $550^{\circ}C$  and  $615^{\circ}C$  for 1 hour. The increase in annealing time brings about smoothness in the variation of  $\mu''$  with frequency. This is explained as due to the stabilization of the crystallites. Although there has been an increase in the value of  $\mu''$  for all the annealed samples, the sample annealed at  $615^{\circ}C$  shows an improvement in the reduction of  $\mu''$  and also in its frequency dependence.

### Frequency Dependence of Loss Factor of $Fe_{74}Cu_{1.5}Nb_{2.5}Si_{12}B_{10}$ for the as-cast State and for the Specimen Annealed at Different Temperatures for 5 Minutes

The sample with composition of  $Fe_{74}Cu_{1.5}Nb_{2.5}Si_{12}B_{10}$  in the as-cast condition and for annealing at temperatures  $200^{\circ}C$ ,  $350^{\circ}C$  and  $550^{\circ}C$  for 5 minutes have been studied for the dependence of loss factor on frequency (Figure 5.17). The loss factor in general is found to be high for all the samples at low frequency as well as for high frequency. The loss factor arises

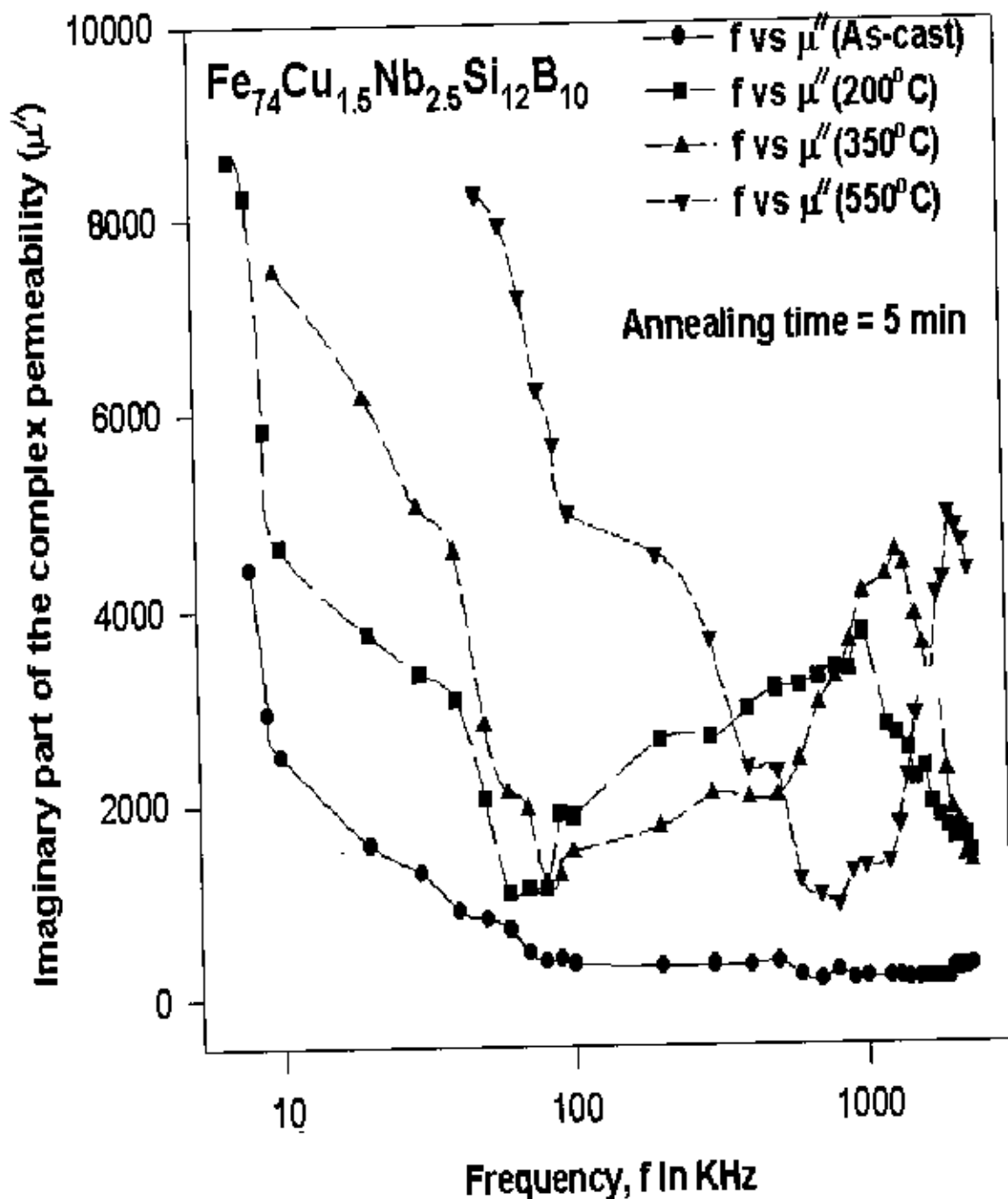


Figure 5.15: Imaginary Part of the Complex Permeability Vs. Frequency for the as-cast sample and samples annealed at 200°C, 350°C and 550°C for 5 minutes

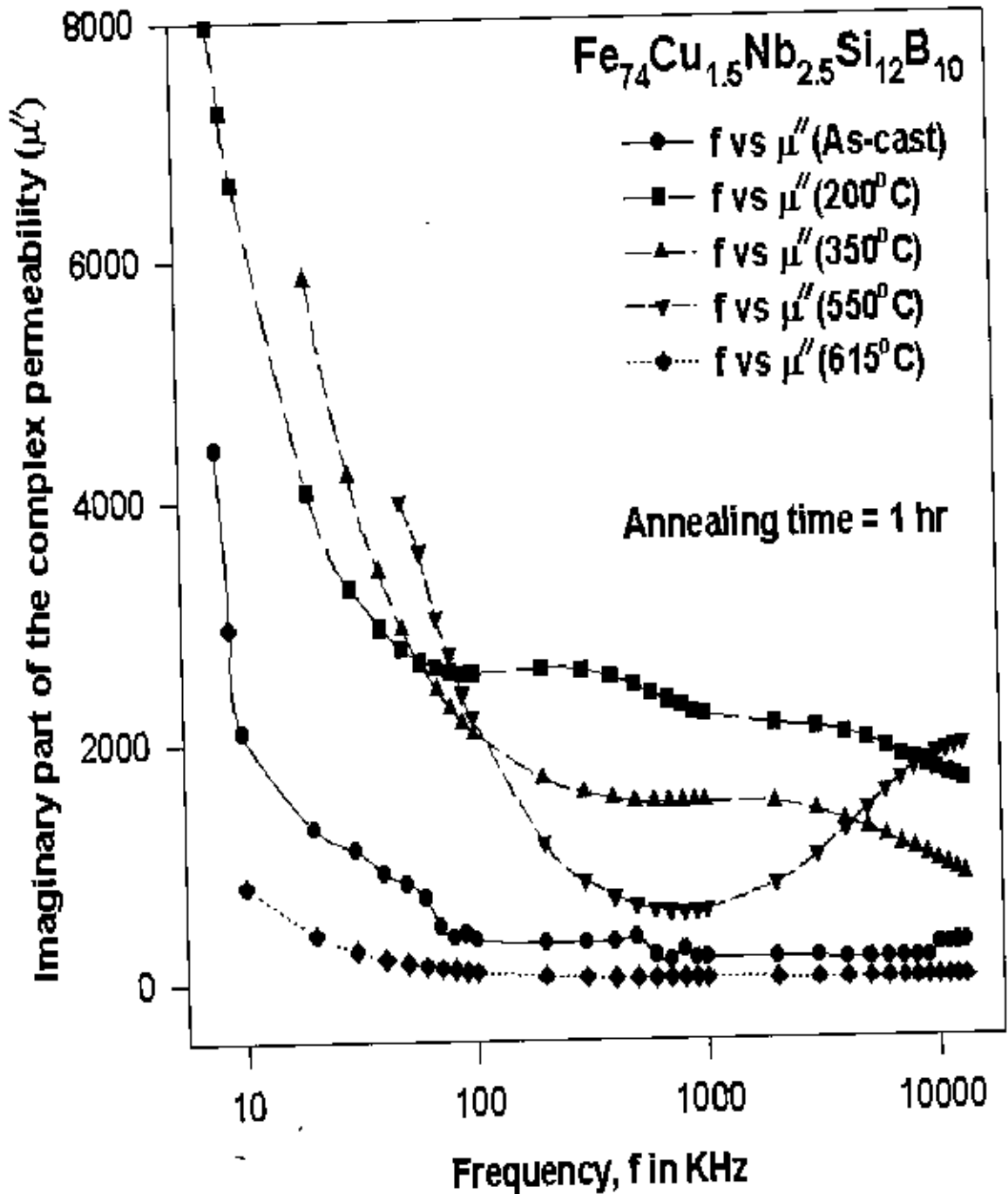


Figure 5.16: Imaginary Part of the Complex Permeability Vs Frequency for different samples annealed at  $200^\circ\text{C}$ ,  $350^\circ\text{C}$ ,  $550^\circ\text{C}$  and  $615^\circ\text{C}$  for 1 hour



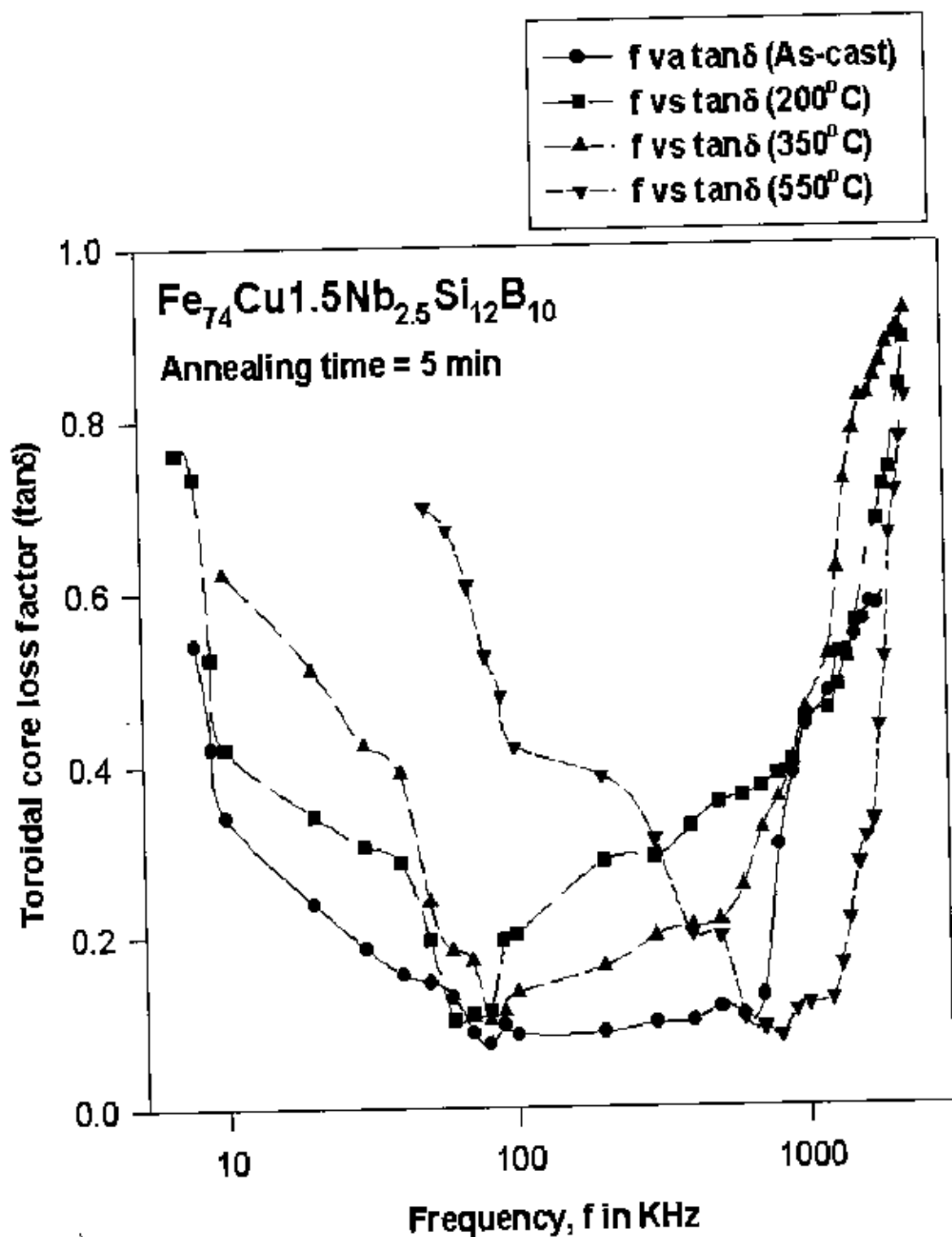


Figure 5.17: Torroidal Loss Factor Vs. Frequency in the as-cast condition and for annealing at temperatures 200<sup>o</sup> C, 350<sup>o</sup> C and 550<sup>o</sup> C for 5 minutes

due to eddy current loss as well as for the phase lag of the spin orientation with respect to the external field. Since these nanocrystalline materials are conducting the net loss factor given by  $\tan\delta$  is quite complex. It is difficult to separate out the contribution from the eddy current loss and the phase lag of the spins with respect to the field. For all the specimens the minimum loss occurs around 100 KHz. For the as-cast specimen the range of frequency for which the loss factor is minimum and remains almost is constant in the range 50 KHz to 900 KHz. The increase in the loss factor and its dependence on frequency for the different samples can be attributed to the distribution of grain sizes as affected by annealing.

### Frequency Dependence of Loss Factor of $Fe_{74}Cu_{1.5}Nb_{2.5}Si_{12}B_{10}$ Annealed at Different Temperatures for 1 Hour

The loss factor of the sample 2 with composition of  $Fe_{74}Cu_{1.5}Nb_{2.5}Si_{12}B_{10}$  annealed at  $200^{\circ}C$ ,  $350^{\circ}C$ ,  $550^{\circ}C$  and  $615^{\circ}C$  for 1 hour has been studied for its frequency dependence (Figure 5.18). It is observed that the increase in the annealing time brings about more uniformity in the loss factor. The loss factor however increases for the annealed samples indicating that longer annealing time causes further growth of crystallites and their stability. As a result, loss is controlled mainly by interaction between grains, the size of grains and grain orientation and as such the specimen thickness becomes important. The precipitation of very small percent of particles improve the high frequency losses and permeability. The phase lag between the induced flux and the applied field increases but with more consistency with the increase of frequency.

### Real Part vs. Imaginary Part of the Complex Permeability with Composition $Fe_{74}Cu_{1.5}Nb_{2.5}Si_{12}B_{10}$

$\mu''$  vs  $\mu'$  for sample 2 with composition of  $Fe_{74}Cu_{1.5}Nb_{2.5}Si_{12}B_{10}$  is shown in Figure 5.19. It is observed that the ratio of  $\mu''$  vs.  $\mu'$  remains almost steady up to the value of  $\mu'$  equal to 6000. As we go for higher values of  $\mu'$  beyond 6000,  $\mu''$  increases quite sharply from 300 to above 4000, while  $\mu'$  changes from 6000 to 8000. For low frequencies, if the applied field is lower

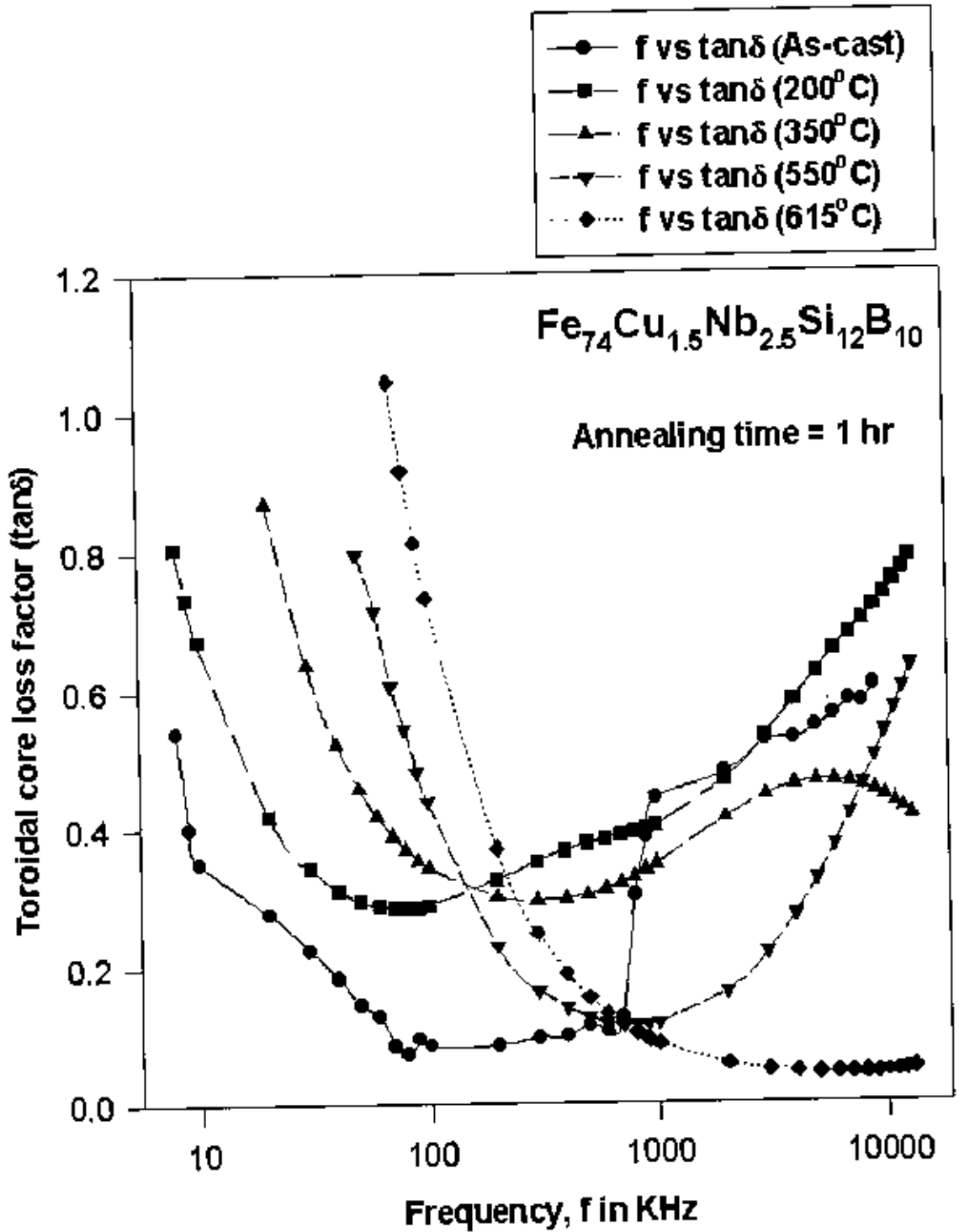


Figure 5.18: Toroidal Loss Factor Vs. Frequency in the as-cast condition and for annealing at temperatures 200°C, 350°C and 550°C for 1 hour

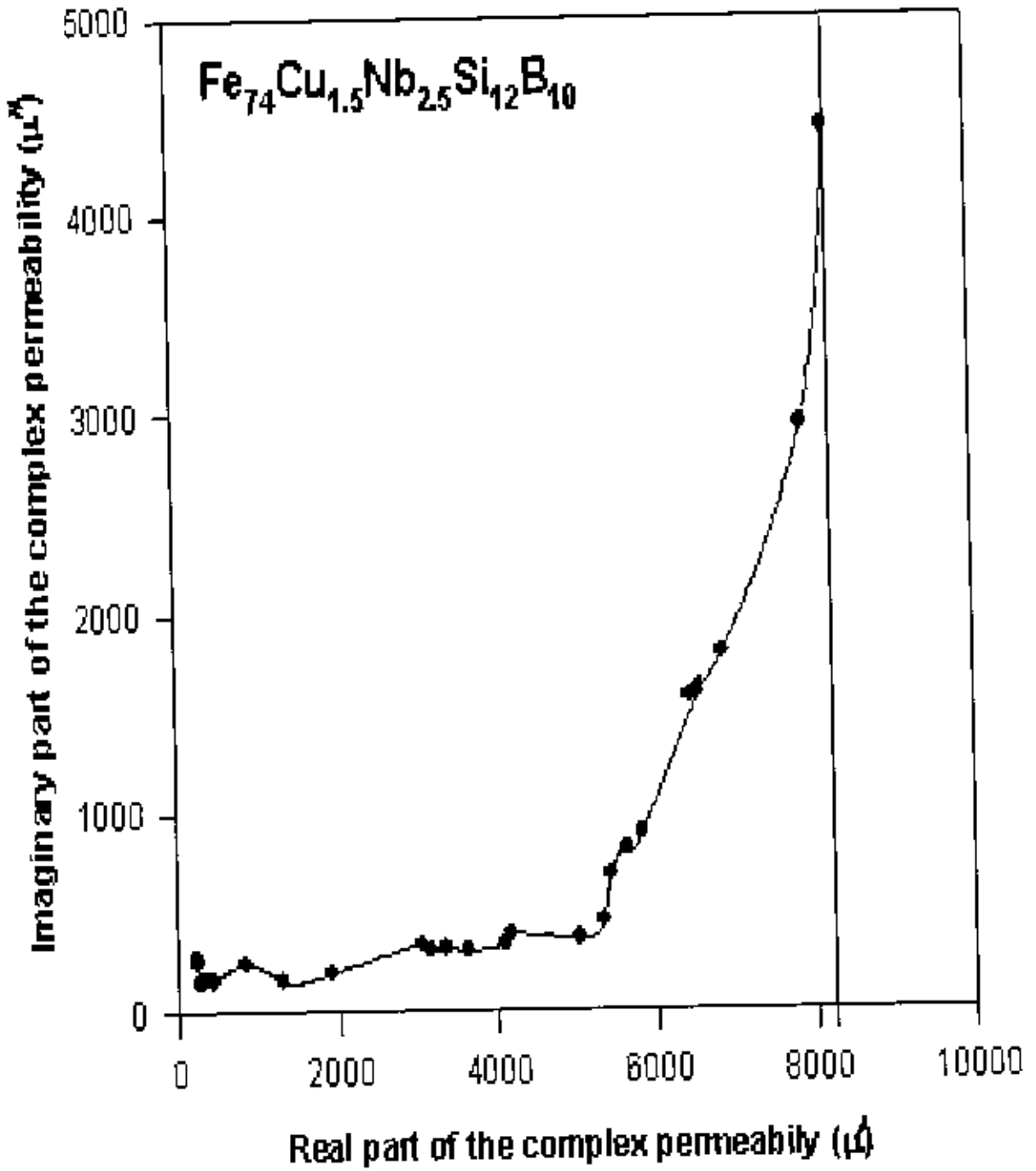


Figure 5.19:  $\mu''$  VS.  $\mu'$  of Sample 2

than or equal to the propagation field, a short vertical line is observed. The initial permeability determined from the intersection of  $\mu'$ -axis is 8870

#### Frequency Dependence of the Relative Quality Factor for sample 2 with Composition of $Fe_{74}Cu_{1.5}Nb_{2.5}Si_{12}B_{10}$

The frequency dependence of the relative quality factor of the different annealed samples are shown in Figure 5.20. Except for the sample annealed at  $550^{\circ}C$  all the samples show maximum quality factor around 100 KHz. The sample annealed at  $550^{\circ}C$  shows maximum quality factor around 1000 KHz. This gives a choice of annealing temperature depending on the operating frequency of the specimen having composition of  $Fe_{74}Cu_{1.5}Nb_{2.5}Si_{12}B_{10}$ . The relative quality factor vs. frequency for the sample annealed at 1 hour is shown in Figure 5.21. Annealing for longer time reduces the quality factor in general. The maximum reduction occurs when the sample is annealed at  $615^{\circ}C$ . The relative quality factors as controlled by initial permeability have quite high values in the range 70 KHz to 400 KHz for as-cast sample and 500 KHz to 5 MHz for the sample annealed at  $550^{\circ}C$  for 1 hour annealing time. However it is observed that when the quality factor is lower, it is more independent of frequency.

#### 5.4 Annealing Temperature Dependence of Initial Permeability at Constant Low Field for Sample 2 with Composition of $Fe_{74}Cu_{1.5}Nb_{2.5}Si_{12}B_{10}$

Figure 5.22 shows the effect of annealing on the initial permeability of nanocrystalline sample with composition of  $Fe_{74}Cu_{1.5}Nb_{2.5}Si_{12}B_{10}$ . The initial permeability of the samples affected by annealing at different temperatures with annealing time of 1 hour is measured at low frequency 100 Hz and in an applied field 0.11 A/m. Figure 5.22 observed that the initial permeability increases from 8600 to 10000 when the specimen annealed at  $200^{\circ}C$ . The significant increase in the initial permeability of the annealed samples as observed with respect to the as-cast samples is explained as due to the removal of local strain and energy barriers in the sample. This

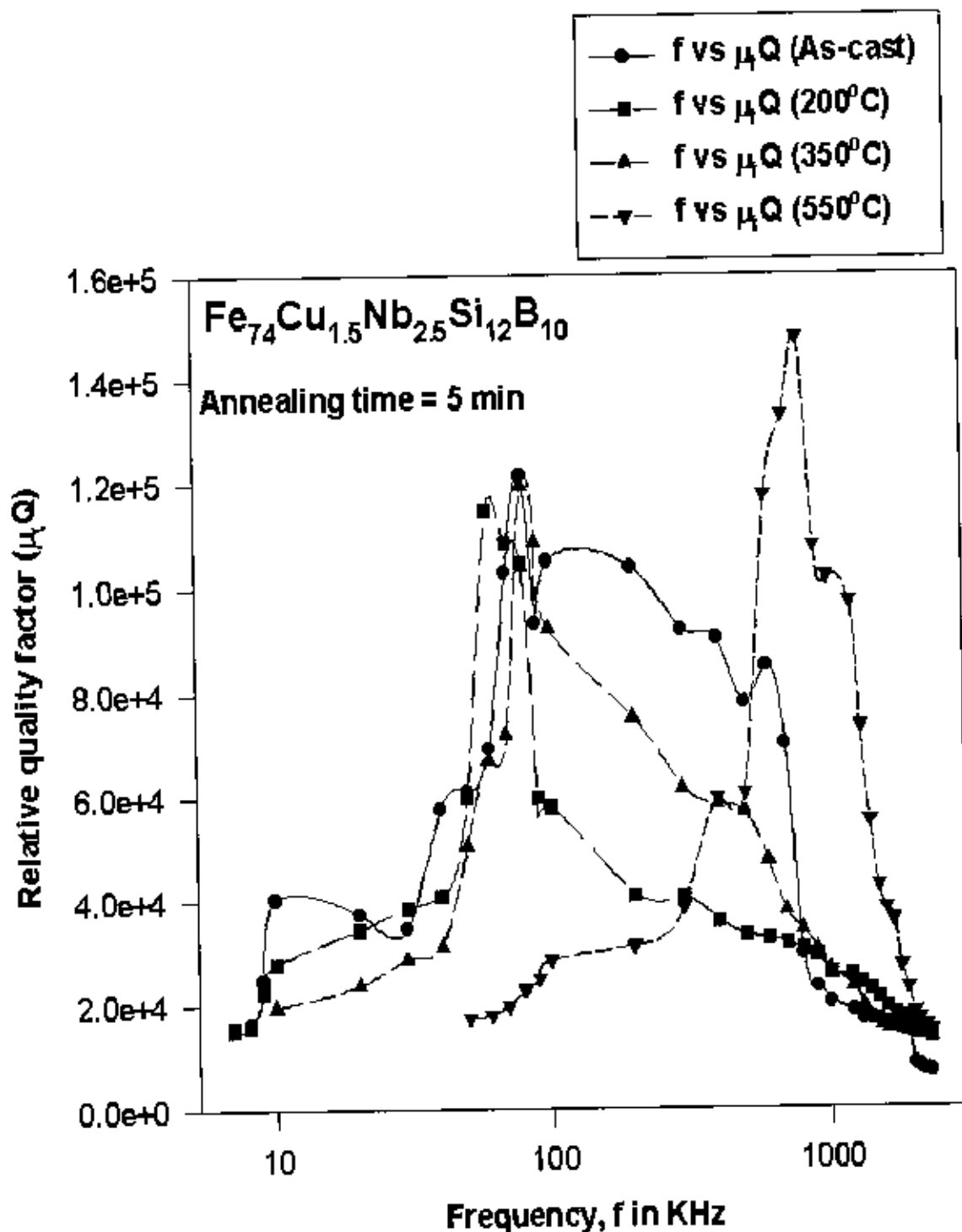


Figure 5 20: The Relative Quality Factor vs. Frequency of Sample 2 for Different Annealing Temperatures for 5 minutes

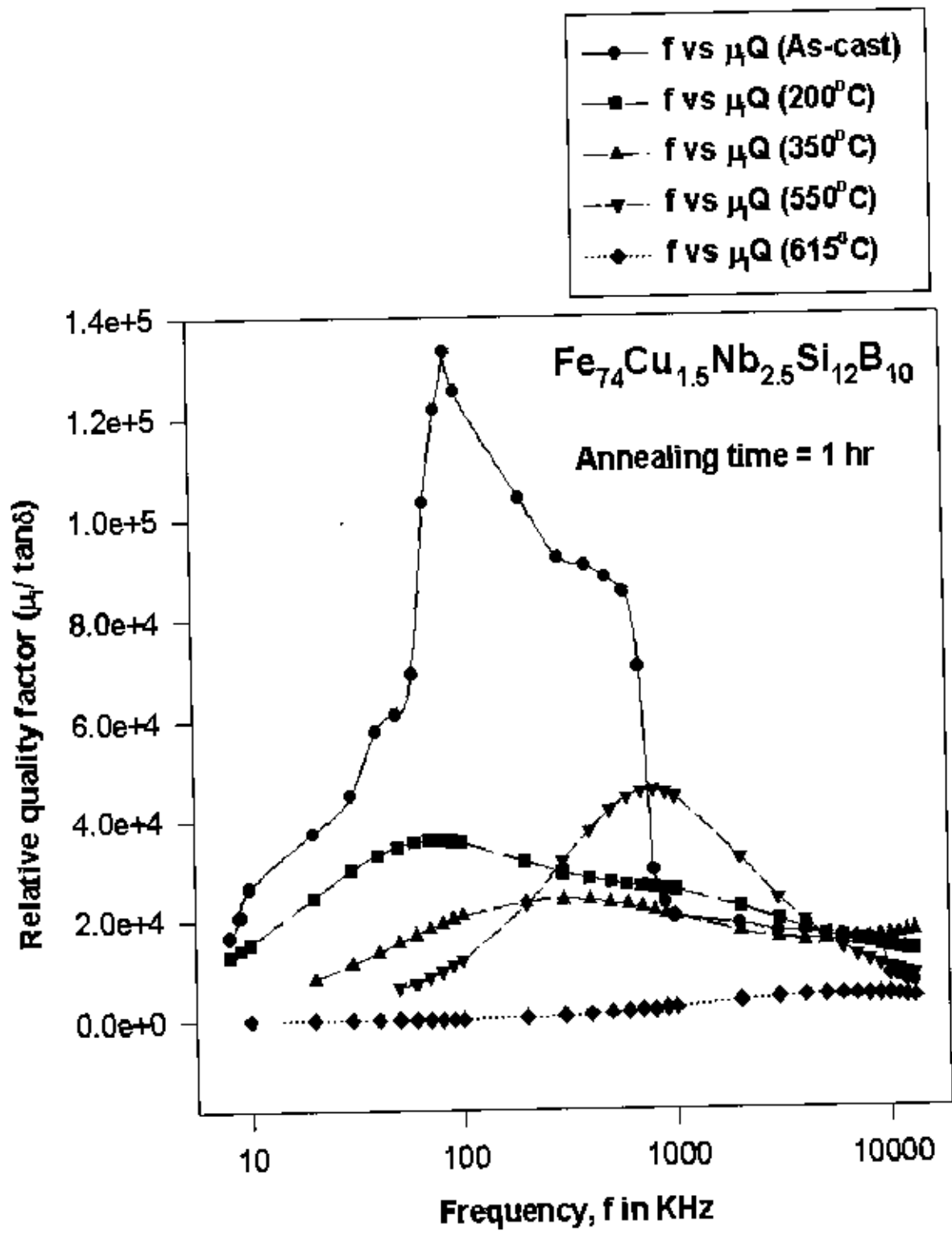


Figure 5.21: The Relative Quality Factor vs. Frequency of Sample 2 For Different Annealing Temperatures for 1 hour.

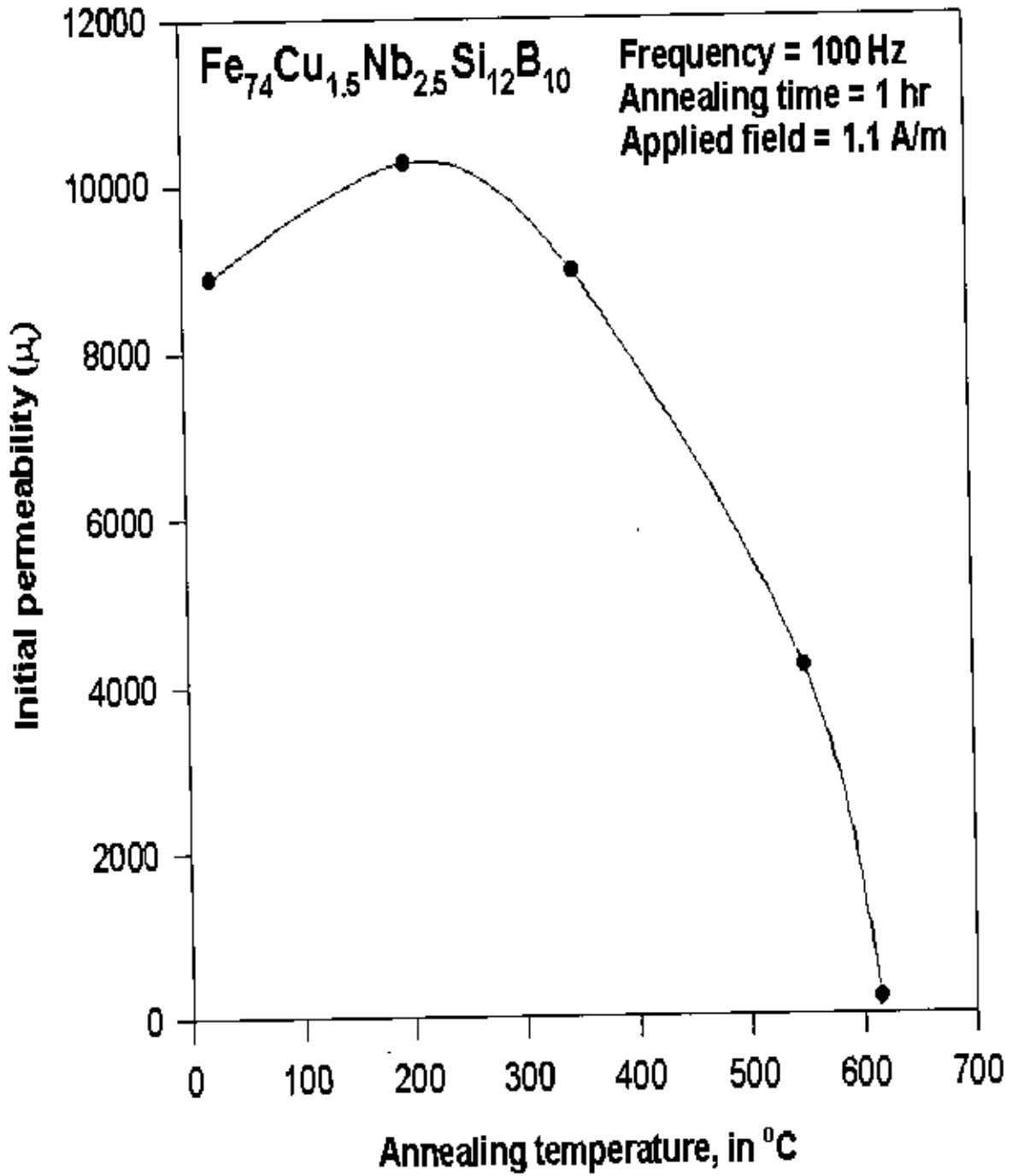
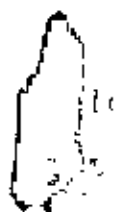


Figure 5.22: Initial Permeability vs. Annealing Temperatures of Sample 2



improvement in the initial permeability is due to the removal of small barriers in the domain wall motion. However, with an increase in the annealing temperature the initial permeability decreases rather drastically, becoming very small when the annealing temperature is above  $600^{\circ} C$ . This is explained as due to the growth of crystallites whose boundaries create obstacles to the domain wall motion. For annealing temperatures which are above or near the Curie temperature, the absence of domain walls leads to a random distribution of the short range order configuration and hence, to a significant decrease in domain wall spinning.



## Chapter 6

# CONCLUSION

Nanocrystalline alloy as thin as 20-22 nm of amorphous state can be prepared by melt spinning technique. The nanocrystalline alloys with high quality soft magnetic properties have been prepared by annealing amorphous ribbons. The compositions of the starting alloys were Fe-Cu-Nb-B-Si and FeCo-Cu-Nb-B-Si. The suitable concentrations are 1% of Cu and 2-3% of Nb. In the technique we have used amorphous ribbons are prepared by melt-spinning technique and the amorphous system is then heat-treated to produce nanocrystals within the amorphous matrix. By this method, even within a single sample one can produce soft or hard ferromagnet or super paramagnet. The guiding factors are the ratio of the structural co-relation and the distribution of length and size of the embedded nanocrystals. The chemical composition of the starting material contains magnetic elements like Fe, Co and Ni; Si and B as glass forming material; Cu as crystallizing component and Nb for stabilizing the crystallites. Nanostructured materials have some features common with the amorphous such as magnetic softness, high electrical resistivity and low dimensionality. This is because nanostructured materials have amorphous matrix. However, there are special advantages of nanostructured materials in respect of high magnetic moment, high Curie temperature and high operational temperature. By heat-treating the nanocrystalline material a favorable frequency dependence of permeability and low eddy current losses can be obtained. The highest permeability in our sample with composition  $(Fe_{0.9}Co_{0.1})_{73.5}Cu_{1.5}Nb_3Si_{13.5}B_0$  is 12595 and for the material with composition  $Fe_{74}Cu_{1.5}Nb_{2.5}Si_{12}B_{10}$  is 8870. The maximum frequency for which the samples 1 and 2 can be used is quite high, being closed to 13 KHz. The frequency response was controlled by heat treatment, which in its turn controlled the grain size distribution. The greatest advantage of nanostructured magnetic material lies in the freedom of tailoring its magnetic softness and hardness as also its frequency response. The nanocrystalline alloy after heat-treatment between  $530^{\circ}C$  -  $600^{\circ}C$  has a structure of  $\alpha - Fe(Si)$ . The grain size is about nanometer scale, which grows slowly while the annealing temperature increases. This nanocrystalline alloy is suitable for magnetic core in the pulse transformer, which works well at frequencies of 50-100 KHz.

The saturation magnetization for nanocrystalline samples has slightly higher value for higher

percentage of iron. The Curie temperature,  $T_c$  of the main phase is extremely high and indicates that the sample is not in the amorphous state. It can be expected that nanocrystalline material can be applied to many kinds of high frequency uses, because of its high saturation flux density, low magnetostriction and excellent soft magnetic properties in a high frequency range.

The crystallization phase separation has been measured by DTA method. First crystallization phase  $T_L$ , indicates stability of amorphous state in respect of structural stability and magnetic ordering.  $T_L$ , of value  $553^{\circ}C$  is observed for  $Fe_{74}Cu_{15}Nb_{25}Si_{12}B_{10}$ , when Co-atoms replace iron-atoms in the Fe-Co-Nb-Si-B system, highest  $T_{\tau_1}$  value of  $635^{\circ}C$  is observed. The magnetic properties of nanocrystalline materials are superior to those of Co-based alloys. The advantages realized are higher saturation induction and better thermal stability with soft magnetic properties at application temperatures.

Nanocrystalline materials are becoming increasingly important for their potentials as a new magnetic materials both for theoretical understanding and technological applications. The possible applications are as inductors, recording media, high-density information storage, magnetic heads, and high frequency transformer etc. These possibilities have drawn the attention of the developed countries like America, Japan and countries of Europe to this material.

There is much scope for further research on this material in respect of controlling the magnetic characteristics by changing composition and heat treatment. The magnetic permeability, saturation magnetization, Curie temperature, magnetic anisotropy, magnetostriction and coercivity are all controllable by choosing appropriate composition, altering preparation technique, selecting the temperature and duration of the heat treatment. Certain important parameters like magnetic anisotropy and magnetostriction need to be studied in detail for their variations with the preparation techniques, composition and heat treatment. Mossbauer study will provide information regarding the distribution of the iron atoms and the hyperfine fields.

# Bibliography

- [1] Herzer. G., "Grain structure and magnetism of nanocrystalline ferromagnets", IEEE Trans. Magn., vol. 26, pp. 1397-1402, 1990.
- [2] Schuler. R. Hubert. A and Herzer. G, "Domain observation on nanocrystalline materials", J. App. Phys. vol. 69: pp. 5325-7, 1991.
- [3] Suzuki. K., Kataoka. N, Enoue A., Makino A and Masumoto T., "High saturation magnetization and soft magnetic properties of bcc Fe-Zr-B alloys with ultrafine grain structure", Matter Trans. Jem, pp. 31743-6, 1990.
- [4] Alben R, Becker. J. J and Chi M C, "Random anisotropy in amorphous Ferro magnets", J. Appl. phys. vol., 49, pp. 1653-8, 1978.
- [5] Luboskey Fe, "High coercive material", J. Appl. Phys., vol. 32, pp. 5171-83, 1961.
- [6] Yoshizawa Y, Yamauchi K, "Iron based soft magnetic alloys composed of ultra fine grain structure", Matter. Trans. JIM, pp. 307-14 1990.
- [7] E. C Stoner and E. P. Wohlfarth, Phil. Trans. Roy. Soc. (London), vol. A-240, pp. 599, 1948.
- [8] "Effect of magnetic field annealing on magnetic properties in ultrafine crystalline Fe-Cu-Nb-Si-B alloys", IEEE Trans. Magn , vol. 25 pp. 3324-6, 1989.
- [9] "Soft magnetic properties and structure of Fe-Co-Nb-Zr multilayers". Appl. Phys. Lett., vol. 53, pp. 2386. 1989.

- [10] S. S. Sikder, M. A. Asgar, "The Kinetics of atomic and magnetic ordering of Co-based amorphous ribbons as affected by iron substitution", *Thermochica Acta.*, vol. 326, pp. 119-126, 1999.
- [11] M.A.Asgar, S.S.Sikder, "Influence of Glass forming material on atomic and magnetic ordering of Fe-based metallic glass", *Indian J. Phys.*, vol. 73a(4), pp. 1-10; 1999.
- [12] W. Klement Jr., R.H. Willens and P. Dewez, *Nature*, vol. 187 pp. 809, 1960.
- [13] Gubanov, A.I. 1960. *Fiz Tver*, vol. 2, pp. 502. 1960.
- [14] Pond, R. Jr and R. Maddin, *Trans. Met. Soc. ALME*, vol. 245, pp 2475, 1969.
- [15] Mader, S. and A.S. Nowick, " ", *Appl. Phys. Lett.*, vol. 7, pp. 57, 1965.
- [16] Tsuei, C. C. and P. Dewez. " ", *J. Appl. Phys.*, vol. 37, pp. 435, 1967.
- [17] T Mizoguchi, " ", *IBM Research Report*, RC 6054. 1976.
- [18] R. Alben, J. J. Budnick, G.S. Gargill, "III Metallic Glasses". *American Soc. for Metals*. pp. 304, 1978.
- [19] A. R. Javari, R. Barrue, M. Harmelin and J. C. Perron, *J. Magn. Magn. Mater.*, vol. 69, pp. 43. 1987.
- [20] P. Gorria, I. Orue, F. Plazaola and J. M. Barandiaran, *J. Appl Phys.*, vol. 73, pp. 6600, 1993.
- [21] P. Allia, P. Tiberto, M. Baricco and F. Vinai, *Rev. Sci. Instrum.*, vol. 64, pp. 1053. 1993.
- [22] Hernando. " ", *IEEE Trans. Magn* , vol. 26, pp. 1397-1402. 1990.
- [23] Turnbull, " ", *IEEE Trans. Magn.*, vol. 26. pp. 1397-1402, 1990.
- [24] Duwez, " ", *IEEE Trans. Magn.*, vol. 26, pp. 1397-1402, 1990.
- [25] Turnbull, D., *J de Physique*, vol. 35, C4-1, 1974.
- [26] Takayama, S. " *J. Materials Sci.*, vol. 11, pp. 164, 1976.

- [27] Cohen, M. H. and D. Turnbull, *Nature*, vol. 189, pp. 131, 1961.
- [28] Felsch W., *Z. Phys.*, pp. 219 & 280, 1969
- [29] Luborsky F. E., *J Magn & Magn Matter*, vol. 7, pp. 143, 1987.
- [30] Kaul. S.N., *Phys.Rev. B24*, pp. 6550, 1981
- [31] Pan D., and D. Turnbull, *J. Appl.Phys.*, vol. 45, pp. 1406, 1974
- [32] J. T. S. Irvine, E. Amano, A. Huanosta, R. Valenzuela and A. R. West, *Solid state Ionics*, vol. 40/41, pp. 220, 1990
- [33] E.Amano, R. Valenzuela, J.T.S. Irvine and A. R. west, *J. Appl. Phys.*, vol. 67, pp. 5589, 1990.
- [34] J.T.S. Irvine, E Amano and, R. Valenzuela, *Matewel, Sci, ENG.*, vol. A133, pp. 140, 1991
- [35] R. M. Jones, *IEEE Trans. Mag. MAG*, vol. 18, pp. 1559,1982.
- [36] M.R.J.Gibbs, *Proc. Conf. Metallic Glasses Science and Technology, Budapest 1980*, vol. 2c., Hargitai, J. Bakonyi and T. kemeny. (Kultura, Budapest) p.37.
- [37] Harris, R., M. Phischke and M.J. Zucherman, *Phys. Rev. Lett.*, vol. 31, pp. 160, 1973.
- [38] Handrich, K., *Phys. Stat. Sol. (b)*, vol. 53, pp. k17, 1972.
- [39] Keffer, F., In *Ferromagnetism* ed. H.P J. Wijn (Springer, Berlin), vol. XVIII.2, pp.1, 1966.
- [40] Harris, R., M. plischke and M.J. Zuckerman, *Phys. Rev. Lett.*, vol. 31, pp. 160, 1973.
- [41] Chatclier, H.Le., *Bull SOC Franc. Mineral*, vol. 10, pp. 204, 1887.
- [42] M. A. Mazid and M. A. Chowdhury, "Design and construction of a former type vibration sample magnetometer", *AECD/MMD/1*, June 1986(Bangladesh).
- [43] S. Forner, *Rev. Sci. Instr.* vol. 27, pp. 548, 1956.
- [44] C. L. Chen and R S. Hasegwa, *ibid.* vol. 49, pp.1721, 1978.

- [45] K. Moorjani, S. K. Chatak, K. V. Rao, B. Kramer and H. S. Chen, Int. Conf. on Liquid and Amorphous Metals, Grenoble, France, 1980.
- [46] M. A. Willard et. al. J. Appl. Phys., vol. 85. No. 8. April 1999.
- [47] R. M. Bozorth. Ferromagnetism (D. Van Nostrand Co.), Princeton, N. J., 1951.

